Geochemistry and petrogenesis of Late Permian basalts from the Sichuan Basin, SW China: Implications for the geodynamics of the Emeishan mantle plume

Fanchao Meng[a,b,c*], Yulu Tian[a,b,c], Andrew C. Kerr[d*], Wei Wang[e], Zhiping Wu[a,b,c], Qiang Xu[f], Qing Du[a,b,c], Yaoqi Zhou[a,b,c], Jiaqi Liu[g]

a. School of Geosciences, China University of Petroleum (East China), Qingdao 266580, China

b. Pilot National Laboratory for Marine Science and Technology (Qingdao), Qingdao 266061, China

c. Shandong Provincial Key Laboratory of Deep Oil and Gas, China University of Petroleum (East China), Qingdao 266580, China

d. School of Earth and Environmental Sciences, Cardiff University, Cardiff, Wales CF10 3AT, United Kingdom

e. Exploration and development Research Institute of Southwest Oil and Gas Field Company, PetroChina, Chengdu 610041, China

f. School of Geoscience and Technology, Southwest Petroleum University, Chengdu 610500, China

g. Institute of Geology and Geophysics, Chinese Academy of Sciences, Beijing 100029, China

Abstract

Plume-lithosphere interactions are significant in the formation of Large Igneous Provinces (LIPs). The Permian Emeishan Large Igneous Province (ELIP) is considered to be the result of a mantle plume. The Emeishan flood basalts comprise a major part of the ELIP and they define three zones: the inner, intermediate and outer zones. Both high-Ti and low-Ti basalts are present in the inner zone, whereas only high-Ti basalts are found in the intermediate zone and outer zone. However, there are only sparse outcrops in the outer zone, and so geochemical data on basalts from the outer zone are

* Corresponding author.
E-mail address: mengfc@upc.edu.cn (Fanchao Meng), kerra@cf.ac.uk (Andrew C. Kerr).

rare and the role of plume-lithosphere interaction in the petrogenesis of volcanic rocks in the outer zone remains poorly understood. In the Sichuan basin, the Basalt Formation is found between the Permian Maokou Formation limestone and the Longtan Formation marl in some drill cores as well as in outcrops in the basin. This relationship demonstrates that the basaltic layer in the basin is part of the Emeishan flood basalts. These basalts have TiO_2 contents of 3.7-4.2 wt.% and Ti/Y ratios of 604-720, being high-Ti sub-alkaline basalts. They display chondrite-normalized rare earth elements (REE) patterns enriched in light rare earth elements (LREE) relative to heavy rare earth elements (HREE) and have elevated large ion lithophile elements (LILE) and high field strength elements (HFSE). Lead isotope ratios are high ($^{206}Pb/^{204}Pb(t)$= 18.102-18.392, $^{207}Pb/^{204}Pb(t)$= 15.578-15.606, $^{208}Pb/^{204}Pb(t)$= 38.410-38.850), and $\varepsilon_{Nd}(t)$ values are -0.38~1.17. Detailed petrology and geochemistry suggest that the high-Ti basalts from the Sichuan Basin did not experience significant contamination of crustal and lithospheric mantle material during the ascent of magma. We infer that these basalts resulted from low-degree melting of the plume mantle source and underwent fractional crystallization of clinopyroxene. The distribution and petrogenesis of the Sichuan Basin basalts in the outer zone are different from those of the basalts in the inner zone and there are clearly different plume-lithosphere interactions in different parts of the ELIP. In the inner zone, the temperature of the lithosphere mantle was markedly elevated due to underplating of the mantle plume, causing a substantial quantity of lithosphere mantle melting and the initial formation of low-Ti basalts. This was followed by melting of the mantle plume and the formation of high-Ti basalts. In the outer zone, lower temperatures further from the plume centre were insufficient to generate extensive melting of the lithospheric mantle. Consequently, only the mantle plume melted in the outer zone, resulting in the formation of high-Ti basalts with minimal lithospheric input.

Keywords: Emeishan mantle plume, outer zone, Sichuan Basin basalts, petrogenesis of high-Ti basalts, plume-lithosphere interaction

1. Introduction

The Emeishan Large Igneous Province (ELIP) in the Upper Yangtze craton, Southwest China is composed mainly of Late Permian flood basalts, mafic-ultramafic intrusions and mafic dykes, along with lesser amounts of felsic volcanic rocks, pyroclastic counterparts, and alkaline rocks. The stratigraphy, chronology, geochemistry and geophysics of the ELIP has been studied in detail for many years and has been proposed to have formed by melting of a mantle plume (Chen et al., 2015; Liu et al., 2017; Shellnutt, 2014; Xiao et al., 2003; Xu et al., 2020; Xu et al., 2021; Zhang et al., 2008; Zhou et al., 2022). The Emeishan continental flood basalts have been broadly divided into two groups: a high-Ti series (TiO_2 > 2.5 wt.% and Ti/Y > 500) and a low-Ti series (He et al., 2007; Song et al., 2008).

Geographically, the ELIP has been divided into inner, intermediate and outer zones based on geochemical, sedimentological, and biostratigraphic characteristics of the rock units (He et al., 2003; Xiao et al., 2004; Xu et al., 2014). The rocks in the inner zone include both the high-Ti and low-Ti series, which are widely distributed in the Binchuan, Jianchuan, Lijiang and Ertan areas, whereas rocks in the intermediate and outer zones are dominated by high-Ti basalts (Li et al., 2017a; Liao, et al., 2012; Xiao et al., 2004; Xu et al., 2001, 2004). Basalts are much more extensively exposed in the intermediate zone (in Zhaotong, Qiaojia and Dongchuan) than in the outer zone (Tian et al., 2021; Xu et al., 2001; Zhang et al., 2011). The outer zone does have some well-developed outcrops in Guangxi and Guizhou provinces (Liao et al., 2012; Xiao et al.,

2004; Xu et al., 2001, 2004).

There are three major petrogenetic models for the Emeishan basalts: 1) High-Ti basalts were derived from low-degree partial melting of the mantle plume (Cheng et al., 2019; Liang et al., 2021; Wang et al., 2007; Xiao et al., 2004; Xu et al., 2001), whereas the low-Ti basalts were generated from the sub-continental lithosphere mantle (SCLM), possibly with assimilation of some upper crust (Fan et al., 2008; Kamenetsky et al., 2012; Li et al., 2010; Song et al., 2008; Wang et al., 2007; Xiao et al., 2004); 2) High-Ti basalts were derived from the SCLM or mixed with lithospheric mantle materials during magma ascent, whereas the low-Ti basalts were generated from the mantle plume (Xu et al., 2007); 3) High-Ti and low-Ti basalts have the same mantle source and may represent different degrees of partial melting, fractional crystallization and/or crustal contamination (Dong et al., 2009; Hou et al., 2011; Ren et al., 2017; Zhang et al., 2019). A common feature of all models is that the lithosphere is most influential at the centre of the Emeishan mantle plume (Li et al., 2015; Song et al., 2001, 2008; Xiao et al., 2004; Xu et al., 2001, 2014; Zhang et al., 2006).

These previous studies, however, have mainly focused on the inner and intermediate zones and although there have been some more recent studies of igneous rocks in the outer zone (Li et al., 2017a; Liu et al., 2017; Liu et al., 2022), there is still a lack of information on the source of the Emeishan high-Ti basalts and comparison between the inner and outer zones. For instance, it is still unclear whether there was plume-lithosphere interaction in the outer zone of the ELIP.

In this paper, we investigate the petrology, major and trace elements, and Sr-Nd-Pb isotope systematics of eighteen samples from three boreholes (twelve samples) and three outcrops (six samples) within and around the Sichuan Basin belonging to the outer zone of the ELIP in order to assess their petrogenesis. This data is combined with

previously published data from the inner and outer zones in order to ascertain the nature of plume-lithosphere interaction and the influence of the Emeishan mantle plume over the whole province, especially the difference between the inner and outer zones.

2. Geological background

The ELIP is located on the western Yangtze Plate and to the east of the Qinghai-Tibet Plateau, and mainly erupted in 260~257 Ma (Fan et al., 2008; Huang et al., 2022; Li et al., 2015; Shellnutt et al., 2012; Zhong et al., 2014). Traditionally, the ELIP has been thought to be bounded on the northeast and southeast by the Baoxing-Yibin fault and the Mile-Shizong fault, respectively. The eastern boundary is situated in the Fuquan-Weng'an areas, eastern Guiyang, China. The northwestern and southwestern boundaries are the Longmenshan belt and the Jinshajiang-Ailaoshan-Red River fault, respectively (Chung et al., 1998; Li et al., 2016a; Xiao et al., 2003). Tectonic movements occur in the region, with a series of well-developed north-trending faults, such as the Anninghe fault, the Longmenshan fault and the Xianshuihe fault (Song et al., 2001; Yan et al., 2018a; Yan et al., 2018b) (Fig. 1). The basement of the ELIP is dominated by Mesoproterozoic metamorphic rocks (Zhai et al., 1986), overlying Pre-Sinian-Cenozoic strata.

The Emeishan volcanic sequence is mainly composed of flood basalts and contemporaneous ultramafic-felsic plutons, layered mafic-ultramafic intrusions and radiating mafic dyke swarms (Li et al., 2015; Liu et al., 2022; Shellnutt, 2014; Xu et al., 2001; Zhou et al., 2022). The Emeishan flood basalts range from a few hundred to five thousand meters in thickness (Xiao et al., 2003; Xu et al., 2001; Zhang et al., 2001) and the areal extent of the basalts may well be larger than 1×10^6 km^2 (Li et al., 2017a; Liu

et al., 2022). The thickness of the basalts gradually decreases from the inner zone to the outer zone (Chung et al., 1998; Xu et al., 2001; Zhu et al., 2018). The inner zone consists of a variety of lavas and pyroclastic rocks, including picrites, basalts, basaltic andesites and basaltic pyroclastic rocks, with trachytic and rhyolite tuff in the uppermost part of the sequence (Xiao et al., 2004; Xu et al., 2001, 2004). A more-restricted range of rocks is found in the intermediate and outer zones and includes tholeiites and alkaline basalts (He et al., 2010).

The Sichuan Basin, located in the northeast (outer zone) of the ELIP in the northwestern Yangtze Craton in the South China Block, is a typical superimposed basin common in southwestern China (Liu et al., 2021a). The Late Permian basalt outcrops of the ELIP have only been found in a few places (Jinding, Huayingshan and Yanghe) in the Sichuan Basin (e.g., Li et al., 2017a; Liang et al., 2021; Liu et al., 2021a). The lack of volcanic outcrops in this region can be attributed to the complex burial history of the Sichuan Basin, and this has made geochemical research difficult on the Emeishan basalts in the basin. However, abundant drill cores from the Sichuan Basin indicate that the Emeishan basalts are widely distributed between the Middle and Upper Permian strata (Liang et al., 2021). Based on seismic and drilling data, it has been proposed that basalts are mainly distributed in the western Sichuan Basin with a thickness of 40-500 m, which thins from the southwest to northeast (Fig. 2) (Liu et al., 2021a; Tian et al., 2017). However, the geochemistry and petrogenesis of the basalts in the Sichuan Basin are still unclear. Therefore, in this study we have sampled the drill cores and available outcrops from the Sichuan Basin.

3. Samples and geochronology

All samples in this study were collected from six areas within and around the southwest of the Sichuan Basin (Fig. 2) , including the borehole samples from ST1 (ST1-2, ST1-5) (Fig. 3a), YT1 (YT1-1, YT1-3, YT1-4, YT1-5, YT1-6, YT1-7) (Fig. 3b) and ZG2 (ZG2-4, ZG2-5, ZG2-7, ZG2-8) (Fig. 3c, d), as well as outcrops Longmendong in Leshan City (20LMD04, 20LMD05) (Fig. 3e, f), Longchi in Emeishan City (20LC04, 20LC06) (Fig. 3g) and Xinlin in Leshan City (20XL01, 20XL02) (Fig. 3h). Boreholes YT1 and ST1 are located around the Longquanshan fault, Longchi outcrop is close to the Longmenshan fault, while outcrops Xinlin and Longmendong, and borehole ZG2 border the Emei-Yibin fault in the western Sichuan Basin (Fig. 2b). All the samples were analysed for whole-rock major and trace elements, and eleven samples were analysed for Sr, Nd and Pb isotopes. All samples were collected from the central part of the massive lava flows with little amygdales and crack fillings. The basalts contain 2% to 15% phenocrysts of clinopyroxene, plagioclase, and minor olivine, set in a matrix comprising mostly plagioclase. The clinopyroxene phenocrysts are generally subhedral, occasionally euhedral, whereas the plagioclase phenocrysts are euhedral grains. The phenocrysts range in size from 700 μm to 1800 μm in samples YT1-6 and YT1-7, while they are about 60~400 μm in size in ZG2 Well, Longchi and Xinlin (Fig. 3b, d).

Stratigraphally, the Sichuan Basin volcanic rocks lie between the Permian Maokou Formation limestone and the Longtan Formation marl (Fig. 4), indicating that the Sichuan Basin basalts erupted in the Mid-Late Permian. This eruption time is consistent with the formation time of the ELIP, which suggests the Sichuan Basin basalts belong to the ELIP (Li et al., 2017a; Liu et al., 2022). Based on chronological data (Table 1), the main duration of the ELIP eruption is 260~257 Ma (e.g., Fan et al., 2008; Lai et al., 2012; Li et al., 2016a; Li et al., 2016b; Zhou et al., 2006; Zi et al., 2010).

4. Analytical methods

Fresh rocks were selected based on the characteristics of rock thin sections. Following the removal of amygdales and minor veins, the samples were crushed to 200 mesh by an agate mortar. The pre-treatment ensures the accuracy of whole-rock geochemical analyses.

The major and trace elements and Sr-Nd-Pb isotopes of the samples were determined at the Wuhan Sample Solution Analytical Technology Co., Ltd., Wuhan, China. International reference material values are listed in the appendix.

Major elements were analysed by a Primus Ⅱ X-ray fluorescence spectrometer (XRF) with wave-length dispersive X-ray fluorescence spectrometry. The major element data are corrected by the theoretical α coefficient method, and relative standard deviations (RSD) for most major element oxides are within ±1-3%. The contents of trace elements were analysed by Agilent 7700e ICP-MS. The analytical precision and accuracy for trace elements are mostly better than 10%. The detailed sample-preparation procedure for ICP-MS analyses can be found in Rudnick et al. (2004) and Liu et al. (2008).

Sr-Nd-Pb isotopic analyses of whole-rock samples were carried out on a Neptune Plus MC-ICP-MS (Thermo Fisher Scientific, Dreieich, Germany). All chemical preparations were performed on class 100 work benches within a class 1000 over-pressured clean laboratory. The sample powders were acid-leached before isotopic analysis (Weis et al., 2005). The data was processed by "Iso-Compass" software (Zhang et al., 2020a). Detailed analytical procedures are described in Chen et al. (2002) and Li et al. (2012).

The analysed $^{87}Sr/^{86}Sr$ of NBS 987 standard solution is 0.710242±14 (2SD, n=345), which is consistent with the published values (0.710248±12, Zhang and Hu, 2020). In addition, analysis of USGS reference materials BCR-2 (basalt) yielded ratios of 0.705012±22 (2SD, n=63) for $^{87}Sr/^{86}Sr$, which are identical within error to their published results (Li et al. 2012). The Sr isotope standard precision (2SE) = 0.000010-0.000020 (0.01‰-0.03‰, 2RSE), and the accuracy is better than 0.000020 (~0.03‰). For standard GSB 04-3258-2015, a $^{143}Nd/^{144}Nd$ of 0.512440±6 (2SD, n=31) was obtained which is identical, within error, to its published value (0.512438±6 (2SD), Li et al., 2017b). In addition, the measurement results of $^{143}Nd/^{144}Nd$ for USGS reference materials BCR-2 (basalt) are 0.512641±11 (2SD, n=82), which are identical, within error, to their published values (Li et al. 2012). The precision of Nd isotope analyses (2SE) = 0.000005-0.000025 (0.01‰-0.05‰, 2RSE), and the analytical accuracy is better than 0.000025 (~0.05‰). The external precision of $^{20x}Pb/^{204}Pb$ ratios for the reference material NBS 981 is 0.03% (2RSD). Furthermore, the USGS reference material BCR-2 (basalt) had analysed ratios of $^{208}Pb/^{204}Pb$=38.736±17, $^{207}Pb/^{204}Pb$=15.628±3, and $^{206}Pb/^{204}Pb$=18.756±10 (2SD, n=22), which are consistent within error of 0.03% with the published results ($^{208}Pb/^{204}Pb$=38.725±22, $^{207}Pb/^{204}Pb$=15.621±4, $^{206}Pb/^{204}Pb$=18.753±8, Zhang and Hu 2020). The internal precision of $^{20x}Pb/^{204}Pb$ ratio is 0.002%-0.025%, and the analytical accuracy is better than 0.03%.

5. Results

5.1 Major elements

The major element compositions of the volcanic rock samples from different

223 regions of the Sichuan Basin are listed in Table 2. The samples have all experienced
224 some degree of hydrothermal alteration, and so the whole-rock raw data has been
225 normalised on a volatile-free basis. Samples ST1-2 and ST1-5 have high LOI values of
226 5.9 wt.% and 6.0 wt.% respectively and so their major element compositions were not
227 used in this study.

228 The samples of the Sichuan Basin show large variations in SiO_2 (45.6-49.2 wt.%)
229 and MgO (4.3-7.1 wt.%). The rocks have total alkalis (Na_2O+K_2O) that range from 3.0
230 to 5.8 wt.% and have K_2O/Na_2O ratios of ~1.7. They have high TiO_2 contents of 3.7 to
231 4.2 wt.% and Ti/Y ratios of 604 to 720, indicating that the basin basalts belong to the
232 high-Ti series (Fig. 5a). The analysed samples mainly plot in the sub-alkaline field on
233 the Ol'-Ne'-Q' diagram (Fig. 5b). The concentrations of the Al_2O_3 and CaO are
234 positively correlated with MgO, whereas K_2O, TiO_2, P_2O_5, $Fe_2O_3^T$, La and Nb are
235 negatively correlated with MgO (Fig. 6). Compared with the outer zone of the ELIP,
236 the inner zone has variable volcanic rock types, ranging from low-Ti series to high-Ti
237 series (Fig. 5a).

238

239 **5.2 Trace elements**

240 The trace element contents of the basalts in the Sichuan Basin are listed in Table
241 2. Chondrite-normalised REE patterns are enriched in the LREE ($(La/Yb)_N$ = 9.8-13.2)
242 and depleted in the HREE ($(Dy/Yb)_N$ = 1.8-2.0), with only slight negative Eu anomalies
243 (δEu = 0.83-0.95) (Fig. 7a). On primitive mantle-normalised trace element diagrams
244 (Fig. 7b), the large ion lithophile elements (LILE) are quite variable, especially the large
245 negative anomalies of Rb and K, as well as positive anomalies of Ba and Pb, which
246 may result from sub-solidus hydrothermal alteration. However, alteration-resistant

immobile high field strength elements (HFSE, e.g., Nb, Ta, Zr, Hf, Th) of the samples are much more consistent, with slightly negative Zr anomalies and positive Th anomalies (Fig. 7b). The trace element compositions of the samples ST1-2 and ST1-5 have not been affected considerably except for some mobile elements, therefore, they are still used in the following discussion. Overall, the Sichuan basalts have OIB (ocean island basalt)-like REE and trace element signatures, which are similar to compositions of the Emeishan high-Ti basalts from other regions.

5.3 Sr-Nd-Pb isotopes

The isotopic data of the basalts in the Sichuan Basin are presented in Table 3. The initial Sr-Nd-Pb isotopic compositions have been age-corrected to 258.5 Ma based on the age range of the Emeishan basalts in this paper. The initial Sr isotopic compositions of the high-Ti basalts in the Sichuan Basin range from 0.705230 to 0.706935 and the $\varepsilon_{Nd}(t)$ values range from -0.38 to 1.17 (Fig. 8a). The Sichuan Basin basalts show a relatively wide range in $^{208}Pb/^{204}Pb(t)$ ratios between 38.403 and 38.845, whereas $^{206}Pb/^{204}Pb(t)$ (18.097-18.388) and $^{207}Pb/^{204}Pb(t)$ (15.578-15.606) compositions are more uniform (Fig. 8c, d). Compared with low-Ti basalts in the inner zone, the compositional range of high-Ti basalts in the ELIP is relatively constant with typical OIB-like Sr-Nd-Pb isotopic characteristics. The Sichuan Basin samples have slightly higher $^{87}Sr/^{86}Sr(t)$ ratios than the high-Ti samples in other areas of the ELIP, and show the characteristics of the EMII end-member. However, in general, the basin samples overlap with the field of high-Ti basalts in the outer zone, which indicates the Sichuan Basin basalts belong to the outer zone of the ELIP.

These data plot above the LoNd (low Nd) array, close to OIB and EMII, in distinct

contrast to the DM (depleted mantle) and MORB (mid-ocean ridge basalt) (Fig. 8a, b). The samples lie above the North Hemisphere Reference Line (NHRL) and overlap with the field of OIB (Fig. 8c, d). In terms of $^{206}Pb/^{204}Pb(t)$ vs. $^{208}Pb/^{204}Pb(t)$, the Sichuan Basin samples data have similar compositions to the high-Ti basalts in the ELIP and overlap with alkaline lavas from the Kerguelen Plateau (Fig. 8d) (Fan et al., 2008). The Kerguelen Plateau in the South Indian Ocean (which comprises a large amount of alkaline basalts, (Zhu et al., 2007)) is one of the largest LIPs in the world, which is related to the Kerguelen plume activity from the Early Cretaceous.

6. Discussion

6.1 Crustal contamination and fractional crystallization

As previously noted fluid-mobile elements (LILE) such as Rb, Ba, K, Pb and Sr show large variations and both positive and negative peaks, which are most likely to be caused by sub-solidus hydrothermal alteration, however, the REE, Th and HFSE (e.g., Hf, Nb and Ta) are relatively alteration-resistant and so are essentially immobile. Therefore, in the following discussion, only immobile elements are used to assess the petrogenesis of these rocks.

It is necessary to evaluate the role of crustal contamination and fractional crystallization during magma ascent before we discuss potential mantle sources of volcanic rocks. Importantly, the proxies for crustal contamination, Th/Nb, La/Nb, Th/Ta and Nb/U ratios are not changed by partial melting or fractional crystallization in magma. Crustal contamination usually results in high Th/Nb (>5), La/Nb (>12) and Th/Ta ratios, and low Nb/U ratios (Neal et al., 2002; Pearce, 2008; Rudnick and Gao, 2003). The basalts in the present study have low La/Nb (1.01-1.23), Th/Nb (0.15-0.22)

and Th/Ta (2.41-3.27), and high Nb/U (21.48-28.00). These characteristics reveal that they were derived from mantle source without significant continental crust contamination. In addition, there is no clear mixing trend between the Sichuan Basin samples and average continental crust on a Ce vs. Nb/Th diagram (Fig. 9a). The analysed samples are broadly similar to primitive mantle (PM) values, and are close to the field of Kerguelen alkaline OIB, as well as plotting far from the values of middle and upper continental crust (MC and UC) (Fig. 9b). Moreover, slightly positive Th anomalies, and slightly negative Nb and Ta anomalies (Fig. 7b) also confirm that the Sichuan Basin basalts have not been significantly contaminated by crustal materials, because continental crust is enriched in Th and strongly depleted in Nb and Ta. Furthermore, $(^{87}Sr/^{86}Sr)_i$ and $\varepsilon_{Nd}(t)$ do not correlate with increasing SiO_2 (Fig. 9c, d), which also suggests little crustal contamination occurred. Therefore, the magmatic evolution of basalts in the Sichuan Basin is dominated by fractional crystallization or partial melting.

Basalts from Sichuan Basin have low MgO values (4.3-7.1 wt.%) and display good correlations between MgO and other major oxides (Al_2O_3, K_2O, $Fe_2O_3^T$) as well as trace elements (La, Nb) (Fig. 6), which indicates the likely occurrence of fractional crystallization. The basalts in the Sichuan Basin have lower Ni, Cr and MgO than primitive magma (Hirajima et al., 1990) (Fig. 6), further suggesting that the magma experienced a substantial amount of fractional crystallization (e.g., olivine, clinopyroxene) during ascent.

The basalts are characterised by a positive correlation between MgO and CaO (Fig. 6b), indicating that the magma underwent the fractional crystallization of clinopyroxene (Wei et al., 2013). A slight negative Eu anomaly (Fig. 7b) suggests the magma also experienced slight fractional crystallization of plagioclase. As illustrated in Fig. 10a,

the Sichuan Basin basalts exhibit a positive correlation between CaO/Al_2O_3 ratios and Mg# values, similar to other Emeishan basalts. The calculated effects of fractional crystallization are shown in mineral vector diagrams in Figs. 10b and c. The data mostly plot near the clinopyroxene crystallization vector (Fig. 10b, c), further suggesting that clinopyroxene is the most significant mineral phase in the fractional crystallization. This is consistent with the petrographic features (Fig. 3), as there are more clinopyroxene phenocrysts than plagioclase in YT1-7 (Fig. 3b) and ZG2-5 (Fig. 3d). Moreover, the Sichuan basalts have enriched Fe and Ti, and MgO vs. $Fe_2O_3^T$ and TiO_2 show negative correlations (Fig. 6d, e). These characteristics may be induced by the early fractional crystallization of Ti and Fe-poor silicate minerals, which indicates little crystallization of titanomagnetite in low oxygen fugacity conditions (Li et al., 2017; Zhang et al., 2011). Furthermore, low oxygen fugacity may also have promoted the fractional crystallization of clinopyroxene and plagioclase in the Sichuan Basin basalts (Fig. 3) (Li et al., 2017).

6.2 Magma Source and Petrogenesis

The Sichuan Basin basalts have high TiO_2 contents (>3.5 wt.%), relative enrichment of alkalis (3.1-5.9 wt.%), LILE and HFSE, and significant REE fractionation with $(La/Yb)_N$ ratios ranging from 9.8 to 13.2. The trace element and Sr-Nd-Pb isotope signatures are OIB-like with $\varepsilon_{Nd}(t)$ values ranging from -0.38 to 1.17, (Fig. 7, 8). However, the origin of the Emeishan basalts with these characteristics is still controversial, and has been variously ascribed to the melting of either a mantle plume (Cheng et al., 2019; Liang et al., 2021; Wang et al., 2007; Xiao et al., 2004; Zhang et al., 2019) or lithospheric mantle (Lai et al., 2012; Xu et al., 2007). Alternatively, some authors propose that these basalts result from the interaction of mantle plume melts with

the lithospheric mantle (Cheng et al., 2019; Fan et al., 2008; He et al., 2010; Xu et al., 2007).

Like the high-Ti basalts in other regions of the ELIP, REEs, trace elements (except some LILEs) and incompatible element ratios of the Sichuan Basin high-Ti basalts are very similar to OIB and Kerguelen alkaline OIB-like basalts (Fig. 7, 11). Furthermore, the Sichuan Basin samples have OIB-like initial Sr-Nd-Pb isotopic characteristics, broadly fall in the field of OIB and Kerguelen basalts (Fig. 8). These geochemical signatures suggest the high-Ti basalts from the Sichuan Basin might have originated from a plume source, compositionally similar to other regions in the ELIP (e.g., Cheng et al., 2019; He et al., 2010; Liu et al., 2017; Song et al., 2008). It is proposed that the high-Ti basaltic magma from the Sichuan Basin is probably the product of partial melting of the head of the mantle plume, because the outer zone is further from the plume centre, and lower temperatures would have resulted in less lithospheric melting (Cheng et al., 2019).

In terms of incompatible trace element ratios, the Sichuan Basin basalts show broadly constant $(La/Yb)_N$ ratios as $\varepsilon_{Nd}(t)$ values increase (Fig. 12a), and La/Yb ratios have a negative correlation with Yb compositions (Fig. 12b). These characteristics reveal that the Emeishan high-Ti basalts did not originate from partial melting of a homogeneous plume source. The samples from the Sichuan Basin define a linear array on Th/La vs. Nb/U (Fig. 12c) and $^{206}Pb/^{204}Pb$ vs. $\varepsilon_{Nd}(t)$ (Fig. 12d) plots similar to other Emeishan high-Ti basalts, which would support this inference. In addition, it is generally argued that metasomatic melts derived from the primitive mantle have La/Nb ratios of ~0.53, whereas those from MORB source have values of ~1.02 (McKenzie and O'Nions, 1995). The Sichuan Basin basalts have high La/Nb ratios of 1.01-1.23, with OIB-like Sr-Nd isotopes signatures significantly different from MORB (Fig. 8a),

indicating that they were likely derived from OIB-like enriched mantle source that was previously metasomatized. Moreover, the Sichuan Basin high-Ti samples plot around the field of OIB (Fig. 8c, d) and have an EMII-type signature (Fig. 8a, b) in terms of Sr-Nd-Pb isotope space. These features indicate the mantle plume may have been metasomatized by enriched materials before the eruption of the Late Permian basalts (Xu et al., 2021).

It is still unclear whether such enriched components originate from the asthenosphere, SCLM, crust, or recycled materials. The asthenosphere is ruled out since the trace elements and Sr-Nd-Pb isotopes of the Emeishan high-Ti basalts have OIB-like rather than MORB-like characteristics (Fig. 8) (Liu et al., 2017; Song et al., 2001; Wang et al., 2007; Xiao et al., 2004). Like the Emeishan high-Ti basalts in other regions, the basalts in the Sichuan Basin have relatively high Ti/Yb ratios, distant from OIB-SCLM and OIB-crust mixing lines. They are also significantly different from the Sangxiu Formation basalts which have a contribution from both continental lithospheric mantle materials and the Kerguelen mantle plume (Fig. 11b) (Zhu et al., 2007). Furthermore, the Sichuan Basin samples have high Ce, unlike continental lithosphere (Fig. 9a), which indicates minimal involvement of SCLM. As shown in Section 6.1, the samples were not significantly contaminated by crust. Therefore, the enriched components are unlikely to be related to either SCLM or crust.

It has been argued that the enriched signature in the OIB-like source is related to ancient recycled oceanic crust (Sobolev et al., 2000, 2007) or subducted terrigenous sediments (Eisele et al., 2002; Hofmann, 1997; Weaver, 1991). The Sichuan Basin basalts display $(Ta/La)_N$ ratios of 0.8-1.1, with an average of 0.94. Ta is depleted relative to La, and Th/Yb and Nb/Yb ratios are high (Fig. 11a), suggesting the involvement of crustal components during ascent or the contribution of subduction

component. The Sichuan Basin basalts have not experienced crustal contamination, so it is more likely that the Emeishan mantle plume has undergone metasomatism, accompanied by mixing of enriched components during subduction. Many studies on volcanic and sedimentary rocks in southwestern China and the Ailaoshan Region propose that the Ailaoshan Ocean crust (Paleotethyan slab) subducted eastward into the upper mantle beneath the western South China Block during the Permian-Middle Triassic (Hou et al., 2017; Qin et al., 2011; Wang et al., 2013; Xu et al., 2019, 2021; Yang et al., 2012; Yang and He, 2012; Zhong et al., 2013).

Based on a study of the Late Permian and Early Triassic A-type granites in the Yuanyang area of Yunnan, South China, Xu et al. (2021) proposed a geodynamic model of the interaction between the Emeishan mantle plume and the subducted Paleotethyan oceanic crust. According to the model, the Ailaoshan Ocean subducted eastward beneath the western South China Block, and the adjacent Emeishan mantle plume rapidly entrained the recycled lithospheric fragments (Xu et al., 2021). This model provides a mechanism for the metasomatism of the Emeishan mantle plume, and further explains why the composition of the Emeishan mantle plume is heterogeneous. In addition, many authors have proposed that the Emeishan mantle plume is likely to be intrinsically related to recycled ancient oceanic materials (Ren et al., 2017; Zhu et al., 2018). Zhu et al. (2018) proposed that the amount of recycled materials may be 10~20% in the Emeishan plume, which is broadly consistent with the view of Ren et al. (2017). In summary, we propose that the high-Ti basalts in the outer zone were derived from an OIB-like Emeishan mantle plume, which was modified by enriched materials derived from a subducted slab before the Late Permian.

The high-Ti basalts in the Sichuan Basin, which are located in the outer zone of the ELIP, are a similar age to the Emeishan basalts. Reconstruction of the thermal

history of the Sichuan Basin with a high paleogeothermal gradient of 23.0-42.6 ℃/km in 259 Ma, indicates that the Sichuan Basin suffered an intensive thermal event related to the Emeishan mantle plume (Zhu et al., 2010, 2016). The basalts in Guangxi and Guizhou provinces that are relevant to the ELIP imply an extension of magmatism at the periphery (the outer zone) of the plume (Fan et al., 2008; Lai et al., 2012; Liu et al., 2017). This evidence indicates that the Sichuan Basin high-Ti basalts are related to the Emeishan mantle plume.

Rare-earth element ratios of the Sichuan Basin basalts (Fig. 13a) suggest they were derived from a mantle source containing garnet. The Emeishan high-Ti basalts lie between the melting curves for garnet and spinel lherzolites, indicating that they are derived from the spinel-garnet transition zone (Fig. 13b). In contrast, the low-Ti basalts in the inner zones have lower La/Sm, Sm/Yb and Dy/Yb ratios, revealing a higher degree of mantle melting at a shallower melting depth (Wang et al., 2007; Xiao et al., 2004). The low-Ti basalts also plot closer to SCLM end members than high-Ti basalts (Fig. 11b) We therefore argue that low-Ti magma might be generated from, or contain, a greater proportion of material from the SCLM (Fan et al., 2008; Xiao et al., 2004).

6.3 Spatial and temporal distribution of the Emeishan basalts and tectonic significance

Chronological data give precise constraints on the duration of the ELIP eruption as 260~257 Ma (Table 1) (e.g., Fan et al., 2008; Lai et al., 2012; Li et al., 2016a; Li et al., 2016b; Zhou et al., 2006; Zi et al., 2010). Magnetostratigraphic studies of the Emeishan basalts indicate that a substantial number of basalts were formed during a period of normal polarity, with the main eruption lasting ~1-2 Ma (Zheng et al., 2010).

It has been proposed that the major eruption phase lasted less than 1 Ma (Xu et al., 2017; Zhu et al., 2018). Therefore, it is difficult to give the exact eruptive ages of high-Ti and low-Ti basalts, although most low-Ti basalts are stratigraphically below high-Ti basalts in most field profiles (Fig.14).

As summarised in Fig. 14, both high-Ti and low-Ti series are exposed in the inner zone (e.g. Binchuan, Ertan, and Miyi areas), with high-Ti basalts overlying low-Ti basalts, whereas only high-Ti basalts erupted in the outer zone, i.e., a greater distance from the centre of the mantle plume (Table 4) (Fan et al., 2008; He et al., 2010; Song et al., 2001, 2008; Xiao et al., 2004; Xu et al., 2001, 2007; Zhang et al., 2006). Overall, the Permian basalts are distributed from northeast (the Sichuan Basin) to southwest (the centre of the mantle plume) in the ELIP, and the thickness of basalts gradually decreases from the inner zone to the outer zone (Fig. 14). This distribution trend not only is consistent with the hotspot track of the Emeishan mantle plume (Fig. 1b) (Liu et al., 2021b), but also overlaps the seismic anomaly trends and residual gravity anomaly (Deng et al., 2014; Liu et al., 2021b; Xie et al., 2013).

Our petrogenetic model is shown in Fig. 15 and builds on previous models (e.g., Feng et al., 2022; Liu et al., 2021b; Liu et al., 2022; Xiao et al., 2004; He et al., 2010). Based on our new data, we further consider the petrology, geochemistry, and distribution characteristics of the Sichuan Basin basalts in the outer zone of the ELIP, and consider the influence of subduction of the paleo-oceanic crust (Hou et al., 2017; Xu et al., 2019, 2021), the movement of the South China block (Liu et al., 2021b; Liu et al., 2022), and the successive eruptions of the late Permian low-Ti and high-Ti basalts (He et al., 2010; Xiao et al., 2004; Xu et al., 2001).

Paleomagnetic studies suggest that the Yangtze Craton moved northward between 300 and ~260 Ma and experienced an overall ~27° clockwise rotation from Permian to

present (Huang et al., 2018; Liu et al., 2021b). The Western Yangtze block experienced Ailaoshan slab eastward subduction from the early-Guadalupian (~269 Ma) (Xu et al., 2021), and the adjacent Emeishan mantle plume was modified by the recycled lithospheric fragments (Fig. 15a) (e.g. Hou et al., 2017; Qin et al., 2011; Wang et al., 2013; Xu et al., 2019, 2021). Paleotethyan subduction resulted in an extensional tectonic setting in the Sichuan Basin during Middle-Late Permian (Xu et al., 2021; Liu et al., 2022). Before the eruption of the Emeishan basalts, mantle upflow reached the lithosphere (Liu et al., 2021b), resulting in plume-lithosphere interactions, and crustal uplift. The magnitude of uplift is greater than 1000 m at its core (the inner zone) (He et al., 2003), and the uplift range of the Sichuan Basin in the outer zone is relatively low. The upper part of the Maokou Formation was exposed at the surface, resulting in different degrees of weathering, denudation, and a paleo-karst landscape (Hu et al., 2012; Xiao et al., 2014; Zhang et al., 2020b). This resulted in variable degrees of uplift in the Sichuan Basin. As the South China block drifted northward, major eruptions including low-Ti and high-Ti series occurred throughout the ELIP during the end-Guadalupian (260~257 Ma) (Fig. 15b, c) (Liu et al., 2021b, Feng et al., 2022).

We propose that from 260 to ~257 Ma, the temperature of the lithosphere mantle in the inner zone rose dramatically due to underplating of the mantle plume, causing partial melting of lithosphere mantle and forming the low-Ti basalts (Fig. 15b). As the lithospheric mantle gradually became refractory, OIB-like high-Ti basalts derived from the plume became the predominant magma type that erupted over the low-Ti basalts (Fig. 14, 15d). In contrast, at the periphery of the plume, the lithospheric mantle was cooler due to the distance from the centre of the mantle plume. As a result, the temperature would have been insufficient to generate extensive melting of the lithospheric mantle (Xu et al., 2001; Xiao et al., 2004; He et al. al., 2010). Therefore,

only the mantle plume melted in the outer zone, forming high-Ti basalts (Fig. 15c). As discussed in Section 6.2, the geochemical evidence also indicates that the source of the high-Ti basalts did not involve melts from SCLM.

The coexistence of high-Ti and low-Ti magma in the inner zone of the Emeishan mantle plume could be attributed to plume-lithosphere interaction. Geochemical modeling suggests that the Emeishan high-Ti basalts are formed at a higher melting pressure than the low-Ti basalts (Liu et al., 2017; Zhang et al., 2019). Continuous polybaric melting of the mantle source might account for compositional variations of the rock types in the inner zone. Furthermore, Dy/Yb and La/Yb ratios of the high-Ti basalts in the outer zone are lower than those in the inner zone, indicating a shallower source and higher melting degree of mantle peridotite for the high-Ti basalts in the outer zone (Tian et al., 2021). It is proposed that melting generally happens beneath thin lithosphere rather than thickened lithosphere, i.e., lid-effect, and the extent of melting beneath the thin lithosphere is likely very low (no more than ~5%) (Fram and Lesher, 1993; Niu et al., 2021). The lithosphere in the outer zone is thicker than that in the inner zone in the ELIP (Tian et al., 2021). The magmatic activity in the outer zone is more limited than that in the inner zone, which is consistent with the “lid effect” model.

Therefore, the high-Ti basalts from the Sichuan Basin are the result of partial melting of the plume in the outer zone of the ELIP. In contrast, relatively few low-Ti basalts derived from the lithosphere mantle have been discovered in the outer zone, because it is more distant from the centre of the mantle plume and so has a cooler lithosphere.

7. Conclusions

Based on petrography and geochemistry of the basalts in the Sichuan Basin, and combined with published data from the inner and outer zones of the Emeishan mantle plume, it is concluded that.

(1) In the outer zone of the ELIP, the volcanic rocks from the Sichuan Basin are part of the Emeishan flood basalts. Based on chronological data, the main duration of the basalt in outer zone eruption is 260~257 Ma.

(2) Unlike the inner zone, the volcanic rocks in Sichuan Basin of the outer zone are predominantly high-Ti sub-alkaline basalts. The Sichuan Basin basalts with OIB-like geochemical signatures originated from the Emeishan mantle plume, which was modified by enriched materials derived from a subducted slab before the Late Permian. The samples have compositions consistent with low degrees of partial mantle melting and fractional crystallization dominated by clinopyroxene during magma evolution.

(3) During the early-Guadalupian (~269 Ma), Western Yangtze Block experienced Ailaoshan slab (Paleotethys Ocean) eastward subduction, and the adjacent Emeishan mantle plume was modified by the recycled lithospheric fragments. During the end-Guadalupian (260~257 Ma), the Emeishan mantle plume underplated the lithosphere mantle in the Yangtze Continent.

(4) In the inner zone, the lithosphere mantle and the mantle plume melted successively, forming low-Ti basalts and overlying high-Ti basalts respectively. However, in the outer zone, only high-Ti basalts derived from the mantle plume were able to form.

Acknowledgements

We are grateful to two anonymous reviewers, handle editor Liang Qiu and chief

editor Meifu Zhou for their constructive comments and suggestions. We thank Hongfang Chen for help with major and trace elements and Sr-Nd-Pb isotopic composition analyses at the Wuhan Sample Solution Analytical Technology Co., Ltd., Wuhan, China. This study was supported by Marine S&T Fund of Shandong Province for Pilot National Laboratory for Marine Science and Technology (Qingdao) (2021QNLM020001-1), National Natural Science Foundation of China Project (42272225; 42072169) and Shandong Provincial Natural Science Foundation, China (ZR2021MD083).

References

Aldanmaz, E., Pearce, J.A., Thirlwall, M.F., Mitchell, J.G., 2000. Petrogenetic evolution of late Cenozoic, post-collision volcanism in western Anatolia, Turkey. J. Volcanol. Geotherm. Res. 102(1-2), 67-95.

Barling, J., Goldstein, S.L., 1990. Extreme isotopic variations in Heard Island lavas and the nature of mantle reservoirs. Nature 348, 59-62.

Carlson, R.W., 1995. Isotopic inferences on the chemical structure of the mantle. J. Geodyn. 20, 365-386.

Chen, F., Satir, M., Ji, J., Zhong, D., 2002. Nd-Sr-Pb isotopes of Tengchong Cenozoic volcanic rocks from western Yunnan, China: evidence for an enriched-mantle source. J. Asian Earth Sci. 21, 39-45.

Chen, J.F., Jahn, B.M., 1998. Crustal evolution of southeastern China: Nd and Sr isotopic evidence. Tectonophysics 284, 101-133.

Chen, Y., Xu, Y.G., Xu, T., Si, S.K., Liang, X.F., Tian, X.B., Deng, Y.F., Chen, L., Wang, P., Xu, Y.H., Lan, H.Q., Xiao, F.H., Li, W., Zhang, X., Yuan, X.H., Badal, J., Teng, J.W., 2015. Magmatic underplating and crustal growth in the Emeishan Large

Igneous Province, SW China, revealed by a passive seismic experiment. Earth Planet. Sci. Lett. 432, 103-114.

Cheng, W.B., Dong, S.Y., Jin, C.H., Zhao, B., Zhang, Y., Wang, C., 2019. Characteristics of elemental geochemistry and petrogenesis discussion of the Emeishan basalts in Muchuan area, Sichuan province. J. Mineral. Petrol. 39(4), 49-60. In Chinese with English abstract.

Chung, S.L., Jahn, B.M., Wu, G.Y., Lo, C.H., Cong, S.L., 1998. The Emeishan flood basalt in SW China: A mantle plume initiation model and its connection with continental breakup and mass extinction at the Permian-Triassic Boundary. Mantle Dynamics and Plate Interactions in East Asia. American Geophysical Union (AGU) 798(12), 47-58.

Deng, Y., Zhang, Z., Mooney, W., Badal, J., Fan, W., Zhong, Q., 2014. Mantle origin of the Emeishan large igneous province (South China) from the analysis of residual gravity anomalies. Lithos 204, 4-13.

Deniel, C., 1998. Geochemical and isotopic (Sr, Nd, Pb) evidence for plume-lithosphere interactions in the genesis of Grande Comore magmas (Indian Ocean). Chem. Geol. 144, 281-303.

Dong, S.Y., Zhang, Z.C., 2009. Geochemical Behavior of Yttrium in Fe-Ti Oxides - An Example Inferred from the Emeishan Large Igneous Province. Geol. Rev. 55(3), 355-360. In Chinese with English abstract.

Eisele, J., Sharma, M., Galer, S.J.G., Blichert-Toft, J., Devey, C.W., Hofmann, A.W., 2002. The role of sediment recycling in EM-1 inferred from Os, Pb, Hf, Nd, Sr isotope and trace element systematics of the Pitcairn hotspot. Earth Planet. Sci. Lett. 196, 197-212.

Fan, W.M., Zhang, C.H., Wang, Y.J., Guo, F., Peng, T.P., 2008. Geochronology and

592 geochemistry of Permian basalts in western Guangxi Province, Southwest China:
593 evidence for plume–lithosphere interaction. Lithos 102 (1-2), 218-236.
594 Feigenson, M.D., Patino, L.C., Carr, M.J., 1996. Constraints on partial melting imposed
595 by rare earth element variations in Mauna Kea basalts. J. Geophys. Res. 101(B5),
596 11815-11829.
597 Feng, Q.Q., Qiu, N.S., Fu, X.D., Li, W.Z., Liu, X., Ji, R.Y., 2022. Maturity evolution of
598 Permian source rocks in the Sichuan Basin, southwestern China: The role of the
599 Emeishan mantle plume. J. Asian Earth Sci. 229, 105180.
600 Fram, M.S., Lesher, C.E., 1993. Geochemical constraints on mantle melting during
601 creation of the North Atlantic basin. Nature 363(6431), 712-715.
602 Gao, S., Ling, W., Qiu, Y., Lian, Z., Hartmann, G., Simon, K., 1999. Contrasting
603 geochemical and Sm-Nd isotopic compositions of Archean metasediments from
604 the Kongling high-grade terrain of the Yangtze craton: evidence for cratonic
605 evolution and redistribution of REE during crustal anatexis. Geochim. Cosmochim.
606 Acta 63(13-14), 2071-2088.
607 Hamelin, B., Allègre, C.J., 1985. Large scale regional units in the depleted upper mantle
608 revealed by an isotopic study of the south-west India ridge. Nature 315, 196-198.
609 Hart, S.R., 1984. The Dupal anomaly: a large-scale isotopic anomaly in the southern
610 hemisphere. Nature 309, 753-756.
611 Hao, Y.L., Zhang, Z.C., Wang, F.S., Mahoney, J.J., 2004. Petrogenesis of high-Ti and
612 low-Ti basalts from the Emeishan large igneous province. Geol. Rev. 50(6), 587-
613 592. In Chinese with English abstract.
614 Hawkesworth, C.J., Rogers, N.W., van Calsteren, P.W.C., Menzies, M.A., 1984. Mantle
615 enrichment processes. Nature 311 (27), 331-335.
616 He, B., Xu, Y.G., Chung, S.L., Xiao, L., Wang, Y.M., 2003. Sedimentary evidence for

617 a rapid, kilometer-scale crustal doming prior to the eruption of the Emeishan flood
618 basalts, Earth Planet. Sci. Lett. 213, 391-405.
619 He, B., Xu, Y.G., Huang, X.L., Luo, Z.Y., Shi, Y.R., Yang, Q.J., Yu, S.Y., 2007. Age
620 and duration of the Emeishan flood volcanism, SW China: Geochemistry and
621 SHRIMP zircon U–Pb dating of silicic ignimbrites, post-volcanic Xuanwei
622 Formation and clay tuff at the Chaotian scetion. Earth Planet. Sci. Lett. 255, 306-
623 323.
624 He, Q., Xiao, L., Balta, B., Gao, R., Chen, J.Y., 2010. Variety and complexity of the
625 Late-Permian Emeishan basalts: Reappraisal of plume-lithosphere interaction
626 processes. Lithos 119, 91-107.
627 Hirajima, T., Ishiwatari, A., Gong, B., Zhang, R.Y., Nozaka, A.T., 1990. Coesite from
628 Mengzhong eclogite at Dhonghai county, northeastern Jiangsu province, China.
629 Mineral. Mag. 54(377), 579-583.
630 Hofmann, A.W., 1997. Mantle geochemistry: The message from oceanic volcanism.
631 Nature 385, 219-229.
632 Hofmann, A.W., Jochum, K.P., Seufert, M., White, W.M., 1986. Nb and Pb in oceanic
633 basalts: new constraints on mantle evolution. Earth Planet. Sci. Lett. 79, 33-45.
634 Hou, T., Zhang, Z.C., Kusky, T., Du, Y.S., Liu, J.L., Zhao, Z.D., 2011. A reappraisal of
635 the high-Ti and low-Ti classification of basalts and petrogenetic linkage between
636 basalts and mafic-ultramafic intrusions in the Emeishan Large Igneous Province,
637 SW China. Ore Geol. Rev. 41, 133-143.
638 Hou, Y.L., Zhong, Y.T., Xu, Y.G., He, B., 2017. The provenance of late Permian karstic
639 bauxite deposits in SW China, constrained by the geochemistry of interbedded
640 clastic rocks, and U-Pb-Hf-O isotopes of detrital zircons. Lithos 278-281, 240-254.
641 Hu, M.Y., Hu, Z.G., Wei, G.Q., Yang, W., Liu, M.C., 2012. Sequence lithofacies

642 paleogeography and reservoir prediction of the Maokou Formation in Sichuan
643 Basin. Petrol. Explor. Dev. 39(1), 45-55. In Chinese with English abstract.
644 Huang, B., Yan, Y., Piper, J.D.A., Zhang, D., Yi, Z., Yu, S., Zhou, T., 2018.
645 Paleomagnetic constraints on the paleogeography of the East Asian blocks during
646 Late Paleozoic and Early Mesozoic times. Earth-Sci. Rev. 186, 8-36.
647 Huang, H., Huyskens, M.H., Yin, Q.Z., Cawood, P.A., Hou, M.C., Yang, J.H., Xiong,
648 F.H., Du, Y.S., Yang, C.C., 2022. Eruptive tempo of Emeishan large igneous
649 province, southwestern China and northern Vietnam: Relations to biotic crises and
650 paleoclimate changes around the Guadalupian-Lopingian boundary. Geology doi:
651 https://doi.org/10.1130/G50183.1.
652 Kamenetsky, V.S., Chung, S.L., Kamenetsky, M., Kuzmin, D.V., 2012. Picrites from
653 the Emeishan Large Igneous Province, SW China: a Compositional Continuum in
654 Primitive Magmas and their Respective Mantle Sources. J. Petrol. 53(10), 2095-
655 2113.
656 LaFlèche, M.R., Camiré, G., Jenner, G.A., 1998. Geochemistry of post-Acadian,
657 Carboniferous continental intraplate basalts from the Maritimes basin, Magdalen
658 islands, Québec, Canada. Chem. Geol. 148, 115-136.
659 Lai, S.C., Qin, J.F., Li, Y.F., Li, S.Z., Santosh, M., 2012. Permian high-Ti/Y basalts
660 from the eastern part of the Emeishan Large Igneous Province, Southwestern
661 China: Petrogenesis and tectonic implications. J. Asian Earth Sci. 47, 216-230.
662 Lassiter J.C., Depaolo, D.J., 1997. Plume/lithosphere interaction in the generation of
663 continental and oceanic flood basalts: Chemical and isotopic constraints. Large
664 igneous provinces: Continental, oceanic, and planetary flood volcanism.
665 Geophysical Monograph 100, 335-355.
666 Li, C., Ripley, E.M., Tao, Y., Hu, R.Z., 2016b. The significance of PGE variations with

667 Sr-Nd isotopes and lithophile elements in the Emeishan flood basalt province from
668 SW China to northern Vietnam. Lithos 248-251, 1-11.
669 Li, C.F., Li, X.H., Li, Q.L., Guo, J.H., Yang, Y.H., 2012. Rapid and precise
670 determination of Sr and Nd isotopic ratios in geological samples from the same
671 filament loading by thermal ionization mass spectrometry employing a single-step
672 separation scheme. Anal. Chim. Acta 727(10), 54-60.
673 Li, H.B., Zhang, Z.C., Ernst, R., Lu, L.S., Santosh, M., Zhang, D.Y., Cheng, Z.G., 2015.
674 Giant radiating mafic dyke swarm of the Emeishan Large Igneous Province,
675 Identifying the mantle plume centre. Terra Nova 27(4), 247-257.
676 Li, H.B., Zhang, Z.C., Santosh, M., Lü, L.S., Han, L., Liu, W., 2017a. Late Permian
677 basalts in the Yanghe area, eastern Sichuan Province, SW China, Implications for
678 the geodynamics of the Emeishan flood basalt province and Permian global mass
679 extinction. J. Asian Earth Sci. 134, 293-308.
680 Li, H.B., Zhang, Z.C., Santosh, M., Lü, L.S., Han, L., Liu, W., Cheng, Z.G., 2016a.
681 Late Permian basalts in the northwestern margin of the Emeishan Large Igneous
682 Province, Implications for the origin of the Songpan-Ganzi terrane. Lithos 256-
683 257, 75-87.
684 Li, J., Zhong, H., Zhu, W.G., Bai, Z.J., Hu, W.J., 2017c. Elemental and Sr–Nd isotopic
685 geochemistry of Permian Emeishan flood basalts in Zhaotong, Yunnan Province,
686 SW China. Int. J. Earth Sci. 106, 617-630.
687 Li, J., Tang, S.H., Zhu, X.K., Pan, C.X., 2017b. Production and Certification of the
688 Reference MaterialGSB 04-3258-2015 as a $^{143}Nd/^{144}Nd$ Isotope Ratio Reference.
689 Geostand. Geoanal. Res. 41, 255-262.
690 Li, J., Xu, J.F., Suzuki, K., He, B., Xu, Y.G., Ren, Z.Y., 2010. Os, Nd and Sr isotope
691 and trace element geochemistry of the Muli picrites: Insights into the mantle

692 source of the Emeishan Large Igneous Province. Lithos 119(1-2), 108-122.
693 Liang, Y.X., Li, H., Zhang, D.D., Yang, K., Zhou, D.W., Zheng, T.Y., Dong, Y.K., Zhai,
694 L.G., 2021. Geochemical characteristics and genetic analysis of Huayingshan
695 Emeishan basalt in Sichuan Basin. Chin. J. Geol. 56(1), 288-302. In Chinese with
696 English abstract.
697 Liao, B.L., Zhang, Z.C., Kou, C.H., Li, H.B., 2012. Geochemistry of the Shuicheng
698 Permian sodium trachybasalts in Guizhou Province and constraints on the mantle
699 sources. Acta Petrol. Sin. 28(4), 1238-1250. In Chinese with English abstract.
700 Liu, R., Luo, B., Li, Y., Qiu, N.S., Wang, W., Zhang, Y., He, Q.L., Pei, S.Q., 2021a.
701 Relationship between Permian volcanic rocks distribution and karst
702 paleogeomorphology of Maokou Formation and its significance for petroleum
703 exploration in western Sichuan Basin, SW China. Petrol. Explor. Dev. 48(3), 575-
704 585. In Chinese with English abstract.
705 Liu, X.J., Liang, Q.D., Li, Z.L., Castillo, P.R., Shi Y., Xu, J.F., Huang, X.L., Liao, S.A.,
706 Huang, W.L., Wu, W.N., 2017. Origin of Permian extremely high-Ti/Y mafic lavas
707 and dykes from Western Guangxi, SW China: Implications for the Emeishan
708 mantle plume magmatism. J. Asian Earth Sci. 141, 97-111.
709 Liu, X.Y., Qiu, N.S., Søager, N., Fu, X.D., Liu, R., 2022. Geochemistry of Late Permian
710 basalts from boreholes in the Sichuan Basin, SW China: Implications for an
711 extension of the Emeishan large igneous province. Chem. Geol. 588, 120636.
712 Liu, Y.D., Li, L., van Wijk, J., Li, A.B., Fu, Y. V., 2021b. Surface-wave tomography of
713 the Emeishan large igneous province (China): Magma storage system, hidden
714 hotspot track, and its impact on the Capitanian mass extinction. Geology 49(9),
715 1032-1037.
716 Liu, Y.S., Zong, K.Q., Kelemen, P.B., Gao, S., 2008. Geochemistry and magmatic

history of eclogites and ultramafic rocks from the Chinese continental scientific drill hole: subduction and ultrahigh-pressure metamorphism of lower crustal cumulates. Chem. Geol. 247, 133-153.

Ma, C.Q., Ehlers, C., Xu, C.H., 2000. The roots of the Dabieshan ultrahigh-pressure metamorphic terrain: constraints from geochemistry and Nd-Sr isotope systematics. Precambrian Res. 102, 279-301.

McDonough, W.F., 1990. Constraints on the composition of the continental lithosphere mantle. Earth Planet. Sci. Lett. 101, 1-18.

McKenzie, D., O'Nions, R.K., 1991. Partial melt distributions from inversion of rare earth element concentrations. J. Petrol. 32, 1021-1091.

McKenzie, D., O'Nions, R.K., 1995. The Source Regions of Ocean Island Basalts. J. Petrol. 36(1), 133-159.

Neal, G.R., Mahoney, J.J., Chazey III, W.J., 2002. Mantle sources and the highly variable role of the continental lithosphere in basalt petrogenesis of the Kerguelen Plateau and the broken ridge LIP: results from ODP Leg 183. J. Petrol. 43, 1177-1205.

Niu, Y.L., 2021. Lithosphere thickness controls the extent of mantle melting, depth of melt extraction and basalt compositions in all tectonic settings on Earth-A review and new perspectives. Earth-Sci. Rev. 217, 103614.

Norman, M.D., 1998. Melting and metasomatism in the continental lithosphere: laser ablation ICPMS analysis of minerals in spinel lherzolites from eastern Australia. Contrib. Mineral. Petrol. 130(3-4), 240-255.

Palacz, Z.A., Saunders, A.D., 1986. Coupled trace element and isotope enrichment in the Cook–Austral– Samoa islands, southwest Pacific. Earth Planet. Sci. Lett. 79, 270-280.

742 Pearce, J.A., 2008. Geochemical fingerprinting of oceanic basalts with applications to
743 ophiolite classification and the search for Archean oceanic crust. Lithos 100(1–4),
744 14-48.
745 Qin, X. F., Wang, Z. Q., Zhang, Y. L., Pan, L. Z., Hu, G. A., Zhou, F. S., 2011.
746 Geochronology and geochemistry of early Mesozoic acid volcanic rocks from
747 Southwest Guangxi: Constraints on tectonic evolution of the southwestern
748 segment of Qinzhou- Hangzhou joint belt. Acta Petrol. Sin. 27(3), 794-808.
749 Ren, Z.Y., Wu, Y.D., Zhang, L., Nichols, A.R.L., Hong, L.B., Zhang, Y.H., Zhang, Y.,
750 Liu, J.Q., Xu, Y.G., 2017. Primary magmas and mantle sources of Emeishan
751 basalts constrained from major element, trace element and Pb isotope
752 compositions of olivine-hosted melt inclusions. Geochim. Cosmochim. Acta
753 208(2), 63-85.
754 Rudnick, R.L., Gao, S., 2003. Composition of the Continental Crust. Treatise Geochem.
755 3, 1-64.
756 Rudnick, R.L., Gao, S., Ling, W.L., Liu, Y.S., McDonough, W.F., 2004. Petrology and
757 geochemistry of spinel peridotite xenoliths from Hannuoba and Qixia, North
758 China Craton. Lithos 77, 609-637.
759 Shellnutt, J. G., 2014. The Emeishan large igneous province: a synthesis. Geosci. Front.
760 5(3), 369-394.
761 Shellnutt, J.G., Denyszyn, S.W., Mundil, R., 2012. Precise age determination of mafic
762 and felsic intrusive rocks from the Permian Emeishan large igneous province (SW
763 China). Gondwana Res. 22, 118-126.
764 Sobolev, A.V., Hofmann, A.W., Kuzmin, D.V., Yaxley, G.M., Arndt, N.T., Chung, S.L.,
765 Danyushevsky, L.V., Elliott, T., Frey, F.A., Garcia, M.O., 2007. The amount of
766 recycled crust in sources of mantle-derived melts. Science 316, 412-417.

767 Sobolev, A.V., Hofmann, A.W., Nikogosian, I.K., 2000. Recycled oceanic crust
768 observed in “ghost plagioclase” within the source of Mauna Loa lavas. Nature 404,
769 986-990.
770 Song, X.Y., Qi, H.W., Robinson, P.T., Zhou, M.F., Cao, Z.M., Chen, L.M., 2008.
771 Melting of the subcontinental lithosphere mantle by the Emeishan mantle plume:
772 evidence from the basal alkaline basalts in Dongchuan, Yunnan, Southwestern
773 China. Lithos 100, 93-111.
774 Song, X.Y., Zhou, M.F., Hou, Z.Q., Cao, Z.M., Wang, Y.L., Li, Y.G., 2001.
775 Geochemical constraints on the mantle source of the Upper Permian Emeishan
776 continental flood basalts, southwestern China. Int. Geol. Rev. 43, 213-225.
777 Stanley, C.R., Russel, J.K., 1989. Petrologic hypothesis testing with Pearce element
778 ration diagrams derivation of diagram axes. Contrib. Mineral. Petrol. 103, 78-89.
779 Sun, S.S., McDonough, W.F., 1989. Chemical and isotopic systematics of oceanic
780 basalt: Implications for mantle composition and processes. Geo. Soc. London
781 Special Pub. 42, 313-345.
782 Tao, Y., Ma, Y., Miao, L., Zhu, F., 2009. SHRIMP U-Pb zircon age of the Jinbaoshan
783 ultramafic intrusion, Yunnan Province, SW China. Chin. Sci. Bull. 54, 168-172.
784 Thirlwall, M.F., Upton, B.G.J., Jenkins, C., 1994. Interaction between continental
785 lithosphere and the Iceland plume—Sr-Nd-Pb isotope geochemistry of Tertiary
786 basalts, NE Greenland. J. Petrol. 35(3), 839-879.
787 Thompson, G.M., Ali, J.R., Song, X.Y., Jolley, D.W., 2001. Emeishan basalts, SW
788 China: Reappraisal of the formation’s type area stratigraphy and a discussion of its
789 significance as a large igneous province. J. Geol. Soc. 158(4), 593-599.
790 Tian, J.C., Lin, X.B., Guo, W., Zhang, X., Huang, P.H., 2017. Geological significance
791 of oil and gas in the Permian basalt eruption event in Sichuan Basin, China. J.

792 Chengdu University Technology (Sci. Technology Edition) 44(1), 14-20. In
793 Chinese with English abstract.
794 Tian, Y.L., Li, Y., Meng, F.C., Zhao, L.K., Wu, Z.P., Du, Q., 2021. A study of the
795 petrogenesis and spatial difference of the Emeishan large igneous province: Based
796 on geochemical analysis and simulation of the high-Ti basalts in the whole region.
797 Acta Petrol. Mineral. 40(4), 687-703. In Chinese with English abstract.
798 Wang, C.Y., Zhou, M.F., 2006. Genesis of the Permian Baimazhai magmatic Ni-Cu-
799 (PGE) sulfide deposit, Yunnan, SW China. Miner. Deposita 41, 771-783.
800 Wang, C.Y., Zhou, M.F., Qi, L., 2007. Permian flood basalts and mafic intrusions in the
801 Jinping (SW China)-Song Da (northern Vietnam) district: Mantle sources, crustal
802 contamination and sulfide segregation. Chem. Geol. 243, 317-343.
803 Wang, Z. L., Xu, D.R., WU, C.J., Fu, W.W., Wang, L., Wu, J., 2013. Discovery of the
804 late Paleozoic ocean island basalts (OIB) in Hainan Island and their geodynamic
805 implications. Acta Petrol. Sin. 29(3), 875-886.
806 Weaver, B.L., 1991. The origin of ocean island basalt end-member compositions: trace
807 element and isotopic constraints. Earth Planet. Sci. Lett. 104, 381-397.
808 Wei, X., Xu, Y.G., 2013. Petrogenesis of the mafic dykes from Bachu and implications
809 for the magma evolution of the Tarim large igneous province, SW China. Acta
810 Petrol. Sin. 29(10), 3323-3335.
811 Weis, D., Kieffer, B., Maerschalk, C., Pretorius, W., Barling, J., 2005. High-precision
812 Pb-Sr-Nd-Hf isotopic characterization of USGS BHVO-1 and BHVO-2 reference
813 materials. Geochem. Geophys. Geosyst. 6(2), 1-10.
814 Xiao, D., Tan, X.C., Shan, S.J., Chen, Y.Q., Xia, J.W., Yang, J., Zhou, T., Cheng, Y.,
815 2014. The restoration of palaeokarst geomorphology of middle Permian Maokou
816 Formation and its petroleum geological significance in southern Sichuan Basin.

817 Acta Geol. Sin. 88(10), 1992-2002. In Chinese with English abstract.
818 Xiao, L., Xu, Y.G., Chung, S.L., He, B., Mei, H.J., 2003. Chemostratigraphic
819 correlation of Upper Permian lavas from Yunnan province, China: extent of the
820 Emeishan large igneous province. Int. Geol. Rev. 45, 753-766.
821 Xiao, L., Xu, Y.G., Mei, H.J., Zheng, Y.F., He, B., Pirajno, F., 2004. Distinct mantle
822 sources of low-Ti and high-Ti basalts from the Eastern Emeishan Large Igneous
823 Province, SW China: implications for plume-lithosphere interaction. Earth Planet.
824 Sci. Lett. 228(3-4), 525-546.
825 Xie, J., Ritzwoller, M.H., Shen, W., Yang, Y., Zheng, Y., Zhou, L., 2013. Crustal radial
826 anisotropy across eastern Tibet and the western Yangtze craton. J. Geophys. Res.
827 - Sol. Ea. 118(8), 4226-4252.
828 Xu, J., Xia, X.P., Lai, C.K., Zhou, M., Ma, P., 2019. First identification of Late Permian
829 Nb- enriched basalts in Ailaoshan region (SW Yunnan, China): Contribution from
830 Emeishan plume to subduction of eastern Paleotethys. Geophys. Res. Lett. 46,
831 2511-2523.
832 Xu, J., Xia, X.P., Wang, Q., Spencer, C.J., He, B., Lai, C.K., 2021. Low-$\delta^{18}O$ A-type
833 granites in SW China: Evidence for the interaction between the subducted
834 Paleotethyan slab and the Emeishan mantle plume. Geol Soc. Am. Bull.
835 https://doi.org/10.1130/B35929.1.
836 Xu, J.F., Suzuki K., Xu Y.G., Mei H.J., Li J., 2007. Os, Pb, and Nd isotope geochemistry
837 of the Permian Emeishan continental flood basalts: Insights into the source of a
838 large igneous province. Geochim. Cosmochim. Acta 71, 2104-2119.
839 Xu, R., Liu, Y., Lambart, S., 2020. Melting of a hydrous peridotite mantle source under
840 the Emeishan large igneous province. Earth-Sci. Rev. 207, 103253.
841 Xu, Y.G., Chung, S.L., Jahn, B.M., Wu, G.Y., 2001. Petrologic and geochemical

842 constraints on the petrogenesis of Permian-Triassic Emeishan flood basalts in
843 southern China. Lithos 58, 145-168.
844 Xu, Y.G., He, B., Chung, S.L., Menzies, M.A., Frey, F.A., 2014. Geologic, geochemical
845 and geophysical consequences of plume involvement in the Emeishan flood-basalt
846 province. Geology 32, 917-920.
847 Xu, Y.G., He, B., Luo, Z.Y., Liu, H.Q., 2013. Study on mantle plume and Large igneous
848 provinces in China: An overview and perspectives. Bull. Mineral. Petrol.
849 Geochem. 32(1), 25-39. In Chinese with English abstract.
850 Xu, Y.G., Luo, Z.Y., Huang, X.L., He, B., Xiao, L., Xie, L.W., Shi, Y.R., 2008. Zircon
851 U-Pb and Hf isotope constraints on crustal melting associated with the Emeishan
852 mantle plume. Geochim. Cosmochim. Acta 72(13), 3084-3104.
853 Xu, Y.G., Zhong, Y.T., Wei, X., Chen, J., Liu, H.Q., Xie, W., Luo, Z.Y., Li, H.Y., He,
854 B., Huang, X.L., Wang, Y., Chen, Y., 2017. Permian Mantle Plumes and Earth's
855 Surface System Evolution. Bull. Mineral. Petrol. Geochem. 36(3), 359-373+358.
856 In Chinese with English abstract.
857 Yan, D.P., Qiu, L., Wells, M.L., Zhou, M.F., Meng, X., Lu, S., Zhang, S., Wang, Y., Li,
858 S.B., 2018a. Structural and Geochronological constraints on the early Mesozoic
859 North Longmen Shan Thrust Belt: Foreland fold- thrust propagation of the SW
860 Qinling Orogenic Belt, Northeastern Tibetan plateau. Tectonics 37(12), 4595-4624.
861 Yan, D.P., Zhou, Y., Qiu, L., Wells, M.L., Mu, H., Xu, C.G., 2018b. The Longmenshan
862 tectonic complex and adjacent tectonic units in the eastern margin of the Tibetan
863 Plateau: a review. J. Asian Earth Sci. 164, 33-57.
864 Yang, J., Cawood, P. A., Du, Y., Huang, H., Hu, L., 2012. Detrital record of Indosinian
865 mountain building in SW China: Provenance of the middle Triassic turbidites in
866 the Youjiang Basin. Tectonophysics 574- 575, 105-117.

867 Yang, Z., He, B., 2012. Geochronology of detrital zircons from the middle Triassic
868 sedimentary rocks in the Nanpanjiang Basin: Provenance and its geological
869 significance. Geotectonica et Metallogenia 36(4), 581-596. In Chinese with
870 English abstract.
871 Zhai, M.G., Yang, R.Y., 1986. Early Precambrian gneiss basement in the Panxi area,
872 Southwest China. Acta Petrol. Sin. 2(3), 22-37. In Chinese with English abstract.
873 Zhang, J., Cao, X.M., Wang, J.L., Zhang, Z.C., 2011. Petrology of the Permian
874 Langmao Basaltic Porphyry, Luquan County, Yunnan Province: Implications for
875 the Petrogenesis of High-Ti Basalts. Geoscience 25(4), 692-702. In Chinese with
876 English abstract.
877 Zhang, L., Ren, Z.Y., Handler, M.R., Wu, Y.D., Xu, Y.G., 2019. The origins of high-Ti
878 and low-Ti magmas in large igneous provinces, insights from melt inclusion trace
879 elements and Sr-Pb isotopes in the Emeishan large Igneous Province. Lithos 344-
880 345, 122-133.
881 Zhang, L., Ren, Z.Y., Zhang, L., Wu, Y.D., Qian, S.P., Xia, X.P., Xu, Y.G., 2021. Nature
882 of the mantle plume under the Emeishan large igneous province: Constraints from
883 olivine-hosted melt inclusions of the Lijiang picrites. J. Geophys. Res. Sol. Ea.
884 126, e2020JB021022.
885 Zhang, W., Hu Z.C., 2020. Estimation of isotopic reference values for pure materials
886 and geological reference materials. At. Spectrosc. 41(3), 93-102.
887 Zhang, W., Hu, Z.C., Liu, Y.S., 2020a. Iso-Compass: new freeware software for isotopic
888 data reduction of LA-MC-ICP-MS. J. Anal. At. Spectrom. 35, 1087-1096.
889 Zhang, Y., Chen, S.L., Zhang, X.L., Zhang, X.H., Xie, C., Chen, C., Yang, Y.R., Gao,
890 Y.L., 2020b. Restoration of paleokarst geomorphology of Lower Permian Maokou
891 Formation and its petroleum exploration implication in Sichuan Basin. Lithologic

892 Reservoirs 32(3), 44-55. In Chinese with English abstract.
893 Zhang, Y.X. 1988. Panxi rift. Beijing: Geological Press.
894 Zhang, Z.C., Mahoney, J.J., Mao, J.W., Wang, F.S., 2006. Geochemistry of picritic and
895 associated basalt flows of the western Emeishan flood basalt province, China. J.
896 Petrol. 47, 1997-2019.
897 Zhang, Z.C., Wang, F.S., 2003. Sr, Nd and Pb Isotopic Characteristics of Emeishan
898 Baslat Province and Discussion on Their Source Region. Earth Sci.- J. China
899 University of Geosciences 28(4), 431-439. In Chinese with English abstract.
900 Zhang, Z.C., Wang, F.S., Fan, W.M., Deng, H.L., Xu, Y.G., Xu, J.F., Wang, Y.J., 2001.
901 A Discussion on Some Problems Concerning the Study of the Emeishan Basalts.
902 Acta Petrol. Mineral. 20(3), 239-246. In Chinese with English abstract.
903 Zhang, Z.C., Zhi, X.C., Chen, L., Saunders, A.D., Reichow, M.K., 2008. Re-Os isotopic
904 compositions of picrites from the Emeishan flood basalt province, China. Earth
905 Planet. Sci. Lett. 276, 30-39.
906 Zheng, L.D., Yang, Z.Y., Tong, Y.B., Yuan, W., 2010. Magnetostratigraphic constraints
907 on two-stage eruptions of the Emeishan continental flood basalts. Geochem.
908 Geophy. Geosy. 11(12), 1-19.
909 Zhong, H., Zhu, W.G., 2006. Geochronology of layered mafic intrusions from the Pan-
910 Xi area in the Emeishan large igneous province, SW China. Miner. Deposita 41,
911 599-606.
912 Zhong, Y.T., He, B., Mundil, R., Xu, Y.G., 2014. CA-TIMS zircon U-Pb dating of felsic
913 ignimbrite from the Binchuan section: implications for the termination age of
914 Emeishan large igneous province. Lithos 204, 14-19.
915 Zhong, Y.T., He, B., Xu, Y.G., 2013. Mineralogy and geochemistry of claystones from
916 the Guadalupian– Lopingian boundary at Penglaitan, South China: Insights into

the pre- Lopingian geological events. J. Asian Earth Sci. 62, 438-462.

Zhou, M.F., Chen, W.T., Wang, C.Y., Prevec, S.A., Liu, P.P., Howarth, G.H., 2013. Two stages of immiscible liquid separation in the formation of Panzhihua-type Fe-Ti-V oxide deposits, SW China. Geosci. Front. 4, 481-502.

Zhou, M.F., Malpas, J.G., Song, X.Y., Robinson, P.T., Sun, M., Kennedy, A., Lesher, M., Keays, R.R., 2002. A temporal link between the Emeishan large igneous province (SW China) and the end-Guadalupian mass extinction. Earth Planet. Sci. Lett. 196(3-4), 113-122.

Zhou, M.F., Wang, Z.C., Zhao, W.W., Qi, L., Zhao, Z., Zhou, J.X., Huang, Z.L., Chen, W.T., 2022. A reconnaissance study of potentially important scandium deposits associated with carbonatite and alkaline igneous complexes of the Permian Emeishan Large Igneous Province, SW China. J. Asian Earth Sci. 236, 105309.

Zhou, M.F., Zhao, J.H., Qi, L., Su, W.C., Hu, R.Z., 2006. Zircon U-Pb geochronology and elemental and Sr-Nd isotope geochemistry of Permian mafic rocks in the Funing area, SW China. Contrib. Mineral. Petrol. 151, 1-19.

Zhu, C.Q., Hu, S.B., Qiu, N.S., Rao, S., Yuan, Y.S., 2016. The thermal history of the Sichuan Basin, SW China: evidence from the deep boreholes. Sci. China, Ser. D: Earth Sci. 59, 70-82.

Zhu, C.Q., Xu, M., Yuan, Y.S., Zhao, Y.Q., Shan, J.N., He, Z.G., Tian, Y.T., Hu, S.B., 2010. Palaeogeothermal response and record of the effusing of Emeishan basalts in the Sichuan basin. Chin. Sci. B 55, 949-956.

Zhu, D.C., Mo, X.X., Wang, L.Q., Zhao, Z.D., Liao, Z.L., 2008. Hotspot-ridge interaction of the evolution of Neo-Tethys: insights from the Late Jurassic-Early Cretaceous magmatism in southern Tibet. Acta Petrol. Sin. 24(2), 225-237.

Zhu, D.C., Pan, G.T., Mo, X.X., Liao, Z.L., Jiang, X.S., Wang, L.Q., Zhao, Z.D., 2007.

Petrogenesis of volcanic rocks in the sangxiu formation, central segment of Tethyan Himalaya: a probable example of plume-lithosphere interaction. J. Asian Earth Sci. 29(2-3), 320-335.

Zhu, J., 2019. A study of mantle plume dynamics and its environmental effect in the Emeishan large igneous province. Beijing: China University of Geosciences (Beijing). In Chinese with English abstract.

Zhu, J., Zhang, Z.C., Reichow, M.K., Li, H.B., Cai, W.C., Pan, R.H., 2018. Weak vertical surface movement caused by the ascent of the Emeishan mantle anomaly. J. Geophys. Res. Sol. Ea. 123(2), 1018-1034.

Zi, J.W., Fan, W.M., Wang, Y.J., Cawood, P.A., Peng, T.P., Sun, L.H., Xu, Z.Q., 2010. U-Pb geochronology and geochemistry of the Dashibao Basalts in the Songpan-Ganzi Terrane, SW China, with implications for the age of Emeishan volcanism. Am. J. Sci. 310(9), 1054-1080.

Fig. 1. Simplified geological map showing the inner, intermediate and outer zones of the ELIP and sampling locations (modified after He et al., 2003; Zi et al., 2010).

The inner, intermediate, and outer zones in the ELIP area were defined by He et al., 2003. The hotspot track was obtained from Liu et al., 2021b. The ELIP eruption centre was obtained from He et al., 2010.

CAO = Central Asia Orogen; TM = Tarim Block; AHO = Alpine–Himalaya Orogen; QKO = Qinling-Qilian-Kunlun Orogen; NCC = North China Craton; YC = Yangtze Craton; CC = Cathaysia Craton.

Fig. 2. Schematic map of southwestern China showing the distribution of volcanic rocks in the Late Permian (a), and geological map of the Sichuan Basin showing the distribution of the Late Permian volcanic rocks (b) (modified after Liu et al., 2021a).

Fig. 3. Representative photos of field geology and petrographic features of the volcanic rocks from the drill cores and outcrops in and around the Sichuan Basin.

a. ST1-2, stomata almond basalt; b. YT1-7, massive basalt (cross-polarised light); c. ZG2-5, massive basalt; d. ZG2-5, massive basalt (cross-polarised light); e. Longmendong section; f. Longmendong basalt outcrop; g. Longchi basalt outcrop; h. Xinlin basalt outcrop.

Pl-plagioclase, Cpx-clinopyroxene.

Fig. 4. The connecting well section of boreholes ZG2-YT1-TF2-ZJ2-ST1 in the Sichuan Basin (based on logging data from Southwest Oil and Gas Field Company,

978 PetroChina).

979 The location of the connecting well section is shown in Fig. 2

980

981 Fig. 5. TiO_2 vs. Ti/Y (a), and Ol'-Ne'-Q' (b) classification diagrams for the basalts in
982 Sichuan Basin (LT and HT data from the inner zone in the ELIP were obtained from
983 Song et al., 2001; Xiao et al., 2004; Xu et al., 2001; Zhang et al., 2006; data of HT from
984 the outer zone were obtained from Fan et al., 2008; Lai et al., 2012; Li et al., 2016b;
985 Wang et al., 2007; Xu et al., 2007).

986 (a) LT-low Ti series, HT-high low series. (b). A-Alkaline, S-Sub-alkaline.

987

988 Fig. 6. Selected elements plotted vs. MgO for the basalts from the Sichuan Basin

989

990 Fig. 7. Chondrite-normalised REE (a), and primitive mantle-normalised trace element
991 (b) for the basalts in the Sichuan Basin (data for chondrite, primitive mantle and OIB
992 are from Sun and McDonough, 1989; sources of geochemical data from other regions
993 in the ELIP as for Fig. 5).

994

995 Fig. 8. Plots of $^{87}Sr/^{86}Sr(t)$ vs. $\varepsilon_{Nd}(t)$ (a), $^{206}Pb/^{204}Pb(t)$ vs. $^{87}Sr/^{86}Sr(t)$ (b), $^{206}Pb/^{204}Pb(t)$
996 vs. $^{207}Pb/^{204}Pb(t)$ (c), and $^{206}Pb/^{204}Pb(t)$ vs. $^{208}Pb/^{204}Pb(t)$ (d) for the basalts in the
997 Sichuan Basin (Sources of geochemical data from other regions in the ELIP as for Fig.
998 5. The fields of DM, MORB, Atlantic-Pacific MORB, Indian Ocean MORB, FOZO
999 (focal zone), OIB, Dupal OIB, BSE (bulk silicate earth), HIMU (mantle with high U/Pb
1000 ratios), EMI and EMII (enriched mantle), Kerguelen are from Barling and Goldstein,
1001 1990; Deniel, 1998; Hamelin and Allègre, 1985; Hart, 1984; Hawkesworth et al., 1984;

and Weaver, 1991. The LoNd (low Nd) array and NHRL (Northern Hemisphere Reference Line) are from Hart, 1984. The Yangtze Block crustal compositions are from Chen and Jahn, 1998; Gao et al., 1999; Ma et al.,2000 and Zhang et al., 2008.)

Fig. 9. Plots of Ce vs. Nb/Th (a), $(Th/Ta)_P$ vs. $(La/Nb)_P$ (b), SiO_2 vs. $^{87}Sr/^{86}Sr(t)$ (c), and SiO_2 vs. $\varepsilon_{Nd}(t)$ (d) for the basalts in the Sichuan Basin (The fields of PM, N-MORB and E-MORB are from Sun and McDonough, 1989; SCLM are from McDonough, 1990; UC (upper crust), MC (middle crust) and LC (lower crust) are from Rudnick and Gao, 2003; Kerguelen alkaline basalts are from http://georoc.mpch-mainz.gwdg.de/georoc/Entry.html.)

Fig. 10. Plots of Mg# vs. CaO/Al_2O_3 (a), Eu_N/Eu^* vs. Th+U (b), and Eu_N/Eu^* vs. $\sum REE$ (c) for the basalts in the Sichuan Basin (sources of geochemical data from other regions in the ELIP as for Fig. 5; the sample 20LMD05 is assumed as the initial melt of fractional crystallization, mineral fractionation vectors are calculated using Rayleigh fractionation law, and partition coefficients are from McKenzie and O'Nions, 1991).

Pl-plagioclase, Cpx-clinopyroxene and Opx-orthopyroxene.

Fig. 11. Diagrams of Nb/Yb vs. Th/Yb (a), and Ti/Yb vs. Nb/Th (b) for the basalts in the Sichuan Basin (sources of geochemical data from other regions in the ELIP as for Fig. 5. (a) MORB-OIB array, subduction component adding models are from Pearce, 2008. The arrow in the Figure represents the trend of adding subduction component. (b) SCLM are from McDonough, 1990; UC, MC and LC are from Rudnick et al., 2003; Hawaiian OIB mean was obtained from Feigenson et al., 1996; Kerguelen alkaline

basalts are from http://georoc.mpch-mainz.gwdg.de/georoc/Entry.html; Sangxiu Formation basalts were obtained from Zhu et al., 2007).

Fig. 12. Plots of $\varepsilon_{Nd}(t)$ vs. $(La/Yb)_N$ (a), Yb vs. La/Yb (b), Th/La vs. Nb/U (c), and $^{206}Pb/^{204}Pb$ vs. $\varepsilon_{Nd}(t)$ (d) for the basalts in the Sichuan Basin (sources of geochemical data from other regions in the ELIP as for Fig. 5).

Fig. 13. Diagrams of $(La/Sm)_N$ vs. $(Tb/Yb)_N$ (a), and Sm/Yb vs. La/Sm (b) for the basalts in the Sichuan Basin (sources of geochemical data from other regions in the ELIP as for Fig. 5; (b) batch melting trends for garnet and spinel lherzolite were obtained from Lassiter and Depaolo, 1997).

Fig. 14. Stratigraphic variation of the representative lava successions in the ELIP (modified after Xiao et al., 2004; Xu et al., 2001, 2014).

Fig. 15. Evolution model of EILP during the Middle Permian. (The framework for the plumbing system of ELIP associated with the Emeishan mantle plume was modified from Feng et al. (2022) and Liu et al. (2021b). The boundaries of the inner-intermediate-outer zones in the ELIP was defined by He et al. (2003) and Xiao et al. (2004). LQF, HYF and QYF represent the Longquanshan fault, Huayingshan fault and Longquanshan fault, respectively. LT and HT represent low-Ti basalts and high-Ti basalts, respectively. The NE (northeastward) arrows show the direction of movement of the South China Block (Liu et al., 2021b).)

a. During the early-Guadalupian (~269 Ma), Western Yangtze Block experienced Ailaoshan slab (Paleotethys Ocean) eastward subduction, and the adjacent Emeishan mantle plume was modified by the recycled lithospheric fragments. b. In the first stage of end-Guadalupian (260~257 Ma), lithosphere mantle melted and formed the low-Ti basalts (LT) in the inner zone. c. In the second stage of end-Guadalupian (260~257 Ma), the mantle plume melted and formed the high-Ti basalts (HT) in the inner-intermediate-outer zones, with high-Ti basalts overlying low-Ti basalts in the inner zone.

1056 Table 1 Zircon U-Pb dating results of the Emeishan large igneous province

Locality		Rock type	Analytical method	Age/Ma	Reference
Inner Zone	Dali-Jiangwei	acid volcanic rock	ID-TIMS zircon U-Pb	258.9±0.5	Xu et al. (2013)
	Midu-Jinbaoshan	wehrlite	Shrimp zircon U-Pb	260.6±3.5	Tao et al. (2009)
		hornblendite	Shrimp zircon U-Pb	260.7±5.6	
	Binchuan	acid tuff	ID-TIMS zircon U-Pb	259.1±0.5	Zhong et al. (2014)
		basalt	Shrimp zircon U-Pb	256.2±1.4	Li et al. (2016a)
	Panxi-Daheishan	syenite	ID-TIMS zircon U-Pb	259.1±0.5	Shellnutt et al. (2012)
	Panxi-Baima	granite	ID-TIMS zircon U-Pb	259.2±0.4	
	Panxi-Huangcao	syenite	ID-TIMS zircon U-Pb	258.9±0.7	
	Panxi-Cida	granite	ID-TIMS zircon U-Pb	258.4±0.6	
	Panxi-Maomaogou	syenite	Shrimp zircon U-Pb	261.6 ± 4.4	Xu et al. (2008)
	Panxi-Miyi	syenite	Shrimp zircon U-Pb	259.8 ± 3.5	
	Panxi-Salian	diorite	Shrimp zircon U-Pb	260.4 ± 3.6	
	Panxi-Taihe	granite	Shrimp zircon U-Pb	261.4 ± 2.3	
	Panxi-Hongge	gabbro	Shrimp zircon U-Pb	259.3±1.3	Zhong and Zhu (2006)
		gabbro	Shrimp zircon U-Pb	259.3 ± 1.3	
	Panxi-Binggu	gabbro	Shrimp zircon U-Pb	260.7 ± 0.8	
	Xinjie	gabbro	Shrimp zircon U-Pb	259±3	Zhou et al. (2002)
Intermediate Zone	Guizhou-Weining	boundary clay rock	ID-TIMS zircon U-Pb	258.1±0.6	Xu et al. (2013)
	Panxian-Zhudong	ignimbrite	ID-TIMS zircon U-Pb	258.3±1.4	Zhu (2019)
	Xingyi-Xiongwu	tuff	ID-TIMS zircon U-Pb	258.5±0.9	
	Puan-Louxia	tuff	ID-TIMS zircon U-Pb	258.1±1.1	
	Baimazhai	pyroxenite	Shrimp zircon U-Pb	258.5±3.5	Wang et al. (2006)
Outer Zone	Tubagou	basalt	Shrimp zircon U-Pb	257.3±2.0	Li et al. (2016b)
	Baise-Yangxu	basalt	Shrimp zircon U-Pb	259.1±4.0	Fan et al. (2008)
	Bama-Minan	basalt	Shrimp zircon U-Pb	259.6±5.9	
	Nayong-Xilin-Tianyang Area	basalt	LA-ICP-MS zircon U-Pb	257.0±9.0	Lai et al. (2012)

	Guangyuan-Chaotian	boundary clay rock	ID-TIMS zircon U-Pb	258.6±1.4	Xu et al. (2013)
				259.2±0.3	Zhong et al. (2014)
	Funing	diabase	Shrimp zircon U-Pb	260±3	Zhou et al. (2006)
		diorite	Shrimp zircon U-Pb	258±3	
	Mianhuadi	metagabbro	MC-ICP-MS zircon U-Pb	259.6±0.8	Zhou et al. (2013)

1057

1058 Table 2 Major elements (wt.%) and trace elements ($\times 10^{-6}$) contents for the analysed volcanic rocks in the Sichuan Basin

Samples	ST1-2	ST1-5	YT1-1	YT1-3	YT1-4	YT1-5	YT1-6	YT1-7	ZG2-4	ZG2-5	ZG2-7	ZG2-8	20LMD04	20LMD05	20LC04	20LC06	20XL01	20XL02	20XL02 (replicate)
Locality	ST1 Well		YT1 Well						ZG2 Well				Longmendong		Longchi		Xinlin		
SiO_2	49.64	48.78	48.62	47.55	46.69	47.67	48.67	48.96	46.59	47.64	48.74	45.59	45.99	48.99	45.94	49.08	49.21	48.12	48.32
TiO_2	4.01	3.87	4.06	3.91	4.17	4.19	3.83	3.71	4.01	3.98	4.05	4.14	3.69	3.73	4.08	3.69	4.24	3.82	3.84
Al_2O_3	13.75	13.66	13.69	13.66	13.64	13.82	14.99	14.96	13.07	12.98	13.30	13.70	13.44	13.90	13.91	13.88	13.57	13.08	13.06
$Fe_2O_3^T$	12.92	13.82	13.86	15.65	16.91	16.10	13.41	13.60	18.43	17.46	14.02	16.27	15.44	12.75	15.75	12.40	14.32	14.16	14.23
MnO	0.21	0.17	0.18	0.16	0.17	0.17	0.16	0.16	0.20	0.19	0.20	0.19	0.21	0.16	0.17	0.17	0.18	0.17	0.17
MgO	3.43	3.68	4.92	4.81	4.38	4.47	4.99	5.08	4.69	4.33	4.69	4.89	7.12	5.28	5.24	5.41	4.65	5.06	5.10
CaO	4.88	4.27	6.53	8.26	6.03	7.39	7.22	7.21	6.99	7.87	7.01	7.40	6.79	9.09	7.20	6.75	9.15	8.08	8.13
Na_2O	4.38	3.91	3.82	2.29	3.44	2.39	2.78	2.75	4.32	2.14	2.38	2.34	2.81	1.97	2.47	3.52	2.05	2.78	2.76
K_2O	0.22	0.56	1.96	1.73	2.36	1.98	1.92	1.93	0.85	1.94	2.21	2.03	1.51	1.42	1.17	2.15	0.99	1.83	1.85
P_2O_5	0.45	0.45	0.40	0.40	0.42	0.42	0.40	0.43	0.44	0.43	0.43	0.43	0.37	0.39	0.43	0.39	0.45	0.40	0.40
LOI	5.87	6.04	1.89	1.70	1.33	1.12	1.15	1.21	0.54	0.77	2.59	2.68	2.89	2.03	3.03	1.99	1.38	2.25	2.24
Total	99.76	99.20	99.94	100.1	99.56	99.70	99.51	99.99	100.1	99.71	99.61	99.66	100.2	99.71	99.37	99.41	100.1	99.75	100.12
Mg#	34.45	34.49	41.29	37.85	33.92	35.47	42.42	42.53	33.53	32.93	39.85	37.33	47.74	45.09	39.72	46.36	39.15	41.42	39.12
La	45.2	45.1	47.9	46.8	47.1	49.4	45.2	45.8	49.5	48.7	44.2	44.8	37.4	47.2	43.3	44.3	48.4	42.0	41.9
Ce	96.3	95.6	98.3	97.5	99.4	103	93.6	95.6	99.1	101	95.0	97.6	85.9	104	98.0	101	106	94.9	93.4
Pr	12.4	12.2	12.8	12.7	12.9	13.0	11.8	12.4	12.9	13.4	12.8	12.8	11.3	13.2	12.8	13.1	13.8	12.5	12.3
Nd	52.6	51.9	52.1	52.0	52.9	52.7	49.5	50.4	51.4	56.0	52.8	54.0	48.7	54.3	53.4	53.7	56.8	52.8	51.5
Sm	11.7	11.0	11.0	10.6	10.6	10.6	9.41	9.91	9.99	11.6	10.6	11.4	10.8	11.5	11.4	11.6	12.0	11.3	10.7
Eu	3.00	2.82	2.97	3.06	3.01	2.98	2.87	2.95	2.94	3.01	2.96	3.04	2.84	3.08	3.06	3.02	3.30	3.11	3.03
Gd	9.72	9.91	9.55	9.83	9.58	9.51	9.05	9.25	9.67	10.3	9.80	10.3	9.48	10.0	9.69	9.69	10.4	9.64	9.46
Tb	1.36	1.31	1.26	1.28	1.26	1.27	1.13	1.22	1.29	1.33	1.33	1.39	1.32	1.41	1.35	1.41	1.43	1.34	1.31
Dy	8.07	7.36	7.47	7.50	7.80	7.51	6.90	7.02	7.90	8.13	7.83	8.02	7.28	7.65	7.47	7.79	7.91	7.64	7.38
Ho	1.45	1.26	1.29	1.26	1.30	1.35	1.16	1.15	1.37	1.35	1.29	1.39	1.31	1.40	1.33	1.44	1.42	1.35	1.28

Er	3.61	3.36	3.45	3.41	3.42	3.38	3.12	3.08	3.51	3.59	3.51	3.61	3.36	3.61	3.49	3.70	3.55	3.47	3.44
Tm	0.47	0.46	0.44	0.45	0.46	0.46	0.41	0.44	0.50	0.49	0.50	0.51	0.45	0.47	0.46	0.48	0.47	0.47	0.45
Yb	2.93	2.73	2.73	2.70	2.77	2.69	2.48	2.53	2.93	2.75	2.86	2.98	2.74	2.91	2.80	2.97	2.84	2.81	2.73
Lu	0.38	0.36	0.36	0.37	0.37	0.35	0.35	0.36	0.40	0.40	0.39	0.41	0.39	0.40	0.40	0.42	0.40	0.39	0.38
V	355	346	369	366	351	342	307	298	403	388	379	389	382	348	382	329	388	389	375
Cr	345	437	406	76.1	81.6	73.0	346	332	123	111	459	543	197	302	222	271	337	184	166
Co	48.4	45.6	47.5	45.8	46.1	45.3	49.9	50.6	43.3	46.7	49.9	57.8	48.1	41.4	48.7	40.1	46.6	44.9	43.6
Ni	226	265	257	139	158	131	247	246	302	257	255	293	136	172	132	163	195	120	107
Cu	254	284	284	249	304	266	259	267	364	541	193	412	257	241	234	64.4	247	332	326
Zn	128	124	141	133	134	131	116	118	150	123	140	146	136	120	145	120	142	136	132
Ga	25.8	23.1	26.2	25.8	25.2	25.7	25.4	25.5	24.5	25.7	25.4	26.5	27.9	25.5	27.3	23.5	26.0	26.6	25.7
Rb	3.82	13.3	43.4	38.5	52.1	45.7	53.5	53.1	22.6	65.1	70.6	68.9	58.5	38.8	46.9	70.3	23.1	59.7	58.6
Sr	882	870	830	580	1027	639	661	672	457	484	742	785	451	511	448	569	586	546	539
Y	38.3	36.9	36.5	36.0	36.2	35.4	32.7	33.6	37.1	37.0	36.7	37.7	34.4	36.9	35.4	37.6	37.2	36.1	35.0
Zr	365	350	350	348	360	349	327	324	366	352	356	377	304	349	352	353	370	341	335
Nb	40.8	40.4	42.0	42.2	41.8	43.3	42.0	40.2	43.0	39.4	41.8	44.3	33.3	39.0	39.9	38.7	41.9	37.1	36.3
Ba	239	424	1306	405	1621	524	472	498	239	741	1065	1003	627	479	578	697	407	510	490
Hf	9.47	8.78	8.81	8.56	8.79	8.66	7.74	7.91	8.65	8.50	8.55	9.19	7.74	8.96	8.96	9.22	9.51	8.76	8.67
Ta	2.38	2.38	2.54	2.52	2.55	2.58	2.48	2.52	2.56	2.34	2.57	2.83	2.20	2.57	2.62	2.57	2.69	2.46	2.38
Pb	8.48	8.92	7.42	7.74	12.4	8.94	6.61	5.97	5.63	7.64	6.95	8.15	6.54	11.9	7.80	7.64	6.64	8.62	8.95
Th	7.12	6.90	6.84	6.77	7.03	6.97	6.70	6.63	6.58	6.61	6.57	6.81	7.21	8.12	6.49	8.35	6.97	6.47	6.25
U	1.60	1.58	1.69	1.60	1.74	1.69	1.52	1.58	1.55	1.48	1.49	1.68	1.52	1.82	1.50	1.76	1.65	1.47	1.46

LOI: weight loss on ignition to 1000 ℃. Mg# = $Mg^{2+}/(Mg^{2+}+Fe^{2+})$ in atomic ratio, assuming 15% of total iron oxide is ferric.

Table 3 Sr-Nd-Pb isotope ratios for the analysed volcanic rocks in the Sichuan Basin

Sample	ST1-5	YT1-1	YT1-3	YT1-6	YT1-7	ZG2-5	ZG2-7	ZG2-8	20LMD05	20LC06	20XL01
Locality	ST1 Well	YT1 Well				ZG2 Well			Longmendong	Longchi	Xinlin
Rb($\times10^{-6}$)	13.3	43.4	38.5	53.5	53.1	65.1	70.6	68.9	38.8	70.3	23.1
Sr($\times10^{-6}$)	870	830	580	661	672	484	742	785	511	569	586
$^{87}Rb/^{86}Sr$	0.044372	0.151194	0.192215	0.234105	0.228342	0.389072	0.275352	0.254148	0.219834	0.357378	0.113896
$^{87}Sr/^{86}Sr$	0.706884	0.707491	0.707355	0.706681	0.706694	0.706661	0.707085	0.707075	0.706865	0.707546	0.705942
$^{2}\sigma$	0.000008	0.000007	0.00001	0.000008	0.000008	0.000008	0.000006	0.000007	0.000007	0.00001	0.000009
$^{87}Sr/^{86}Sr(t)$	0.706721	0.706935	0.706648	0.705820	0.705854	0.705230	0.706072	0.706140	0.706057	0.706232	0.705523
Sm($\times10^{-6}$)	11.0	11.0	10.6	9.41	9.91	11.6	10.6	11.4	11.5	11.6	12.0
Nd($\times10^{-6}$)	51.9	52.1	52.0	49.5	50.4	56.0	52.8	54.0	54.3	53.7	56.8
$^{147}Sm/^{144}Nd$	0.128166	0.127908	0.123307	0.114987	0.118988	0.125756	0.121209	0.128019	0.128721	0.130854	0.127975
$^{143}Nd/^{144}Nd$	0.512530	0.512533	0.512526	0.512528	0.512528	0.512567	0.512570	0.512573	0.512507	0.512507	0.512561
$^{2}\sigma$	0.000005	0.000008	0.000005	0.000006	0.000005	0.000004	0.000006	0.000013	0.000004	0.000004	0.000008
$^{143}Nd/^{144}Nd(t)$	0.512313	0.512317	0.512317	0.512333	0.512327	0.512354	0.512365	0.512356	0.512289	0.512286	0.512344
$\varepsilon_{Nd}(t)$	0.16	0.22	0.24	0.55	0.42	0.96	1.17	1.00	-0.31	-0.38	0.77
T_{DM}(Ma)	1106	1098	1054	962	1002	1012	958	1028	1154	1184	1049
$f_{Sm/Nd}$	-0.35	-0.35	-0.37	-0.42	-0.40	-0.36	-0.38	-0.35	-0.35	-0.33	-0.35
$^{206}Pb/^{204}Pb$	18.715	18.751	18.728	18.757	18.789	18.800	18.888	18.867	18.789	18.881	18.899
$^{2}\sigma$	0.001	0.001	0.001	0.001	0.001	0.001	0.001	0.001	0.000	0.001	0.000
$^{207}Pb/^{204}Pb$	15.609	15.613	15.612	15.611	15.613	15.617	15.620	15.621	15.626	15.629	15.614
$^{2}\sigma$	0.001	0.001	0.001	0.001	0.001	0.001	0.001	0.001	0.000	0.001	0.000
$^{208}Pb/^{204}Pb$	39.236	39.292	39.271	39.310	39.357	39.276	39.356	39.316	39.432	39.628	39.349
$^{2}\sigma$	0.002	0.002	0.002	0.002	0.002	0.002	0.001	0.002	0.001	0.002	0.001
$^{206}Pb/^{204}Pb(t)$	18.251	18.154	18.185	18.156	18.097	18.293	18.323	18.325	18.388	18.272	18.245
$^{207}Pb/^{204}Pb(t)$	15.585	15.582	15.584	15.580	15.578	15.592	15.591	15.593	15.606	15.598	15.581
$^{208}Pb/^{204}Pb(t)$	38.572	38.500	38.520	38.440	38.403	38.533	38.542	38.597	38.845	38.685	38.446

Notes:

1. $^{87}Rb/^{86}Sr$ and $^{147}Sm/^{144}Nd$ ratios are calculated using Rb, Sr, Sm and Nd contents by ICP-MS and measured $^{87}Sr/^{86}Sr$ and $^{143}Nd/^{144}Nd$ ratios by MC-ICP-MS.
2. In T_{DM} calculation, ratios of $(^{143}Nd/^{144}Nd)_{DM}$ and $(^{147}Sm/^{144}Nd)_{DM}$ took values of 0.51315 and 0.225, respectively.
3. In $\varepsilon_{Nd}(t)$ calculations, ratios of $(^{87}Sr/^{86}Sr)_{CHUR}$, $(^{87}Rb/^{86}Sr)_{CHUR}$, $(^{143}Nd/^{144}Nd)_{CHUR}$ and $(^{147}Sm/^{144}Nd)_{CHUR}$ are 0.7045, 0.0847, 0.512638 and 0.1967, respectively, while t = 258.5 Ma.

Table 4 Distribution of the Emeishan basalts in the ELIP

Zone	Locality	Rock type	Reference
Inner zone	Dali	High-Ti basalts, low Ti basalts	Hanski et al. (2010)
	Lijiang	High-Ti basalts, low Ti basalts	Song et al. (2001), Zhang et al. (2006)
	Binchuan	High-Ti basalts, low Ti basalts	Song et al. (2001), Xiao et al. (2004), Xu et al. (2007), Xu et al. (2001)
	Ertan	High-Ti basalts, low Ti basalts	Song et al. (2001), Xu et al. (2001)
	Jianchuan	High-Ti basalts, low Ti basalts	Song et al. (2001)
	Pingchuan	Low Ti basalts	Xu et al. (2014)
	Miyi	High-Ti basalts	Xu et al. (2014)
	Kangsi	High-Ti basalts	He et al. (2010)
	Wanmachang	High-Ti basalts	He et al. (2010)
	Shuidiqiao	High-Ti basalts	He et al. (2010)
	Longzhoushan	High-Ti basalts	Xu et al. (2007)
	Yongsheng	High-Ti basalts, low Ti basalts	Hao et al. (2004)
Intermediate zone	Dongchuan	High-Ti basalts	Song et al. (2008), Xu et al. (2001)
	Qingyin	High-Ti basalts	Xu et al. (2014)
	Qiaojia	High-Ti basalts	Xu et al. (2014)
	Weining	High-Ti basalts	Xu et al. (2014)
	Duge	High-Ti basalts	Xu et al. (2014)
	Zhaotong	High-Ti basalts	Li et al. (2017c)
Outer zone	Zhijin	High-Ti basalts	Lai et al. (2012), Xu et al. (2007)
	Jinding	High-Ti basalts	Xu et al. (2007)
	Tubagou	High-Ti basalts	Li et al. (2016b)
	Baise	High-Ti basalts	Fan et al. (2008)
	Bama	High-Ti basalts	Fan et al. (2008), Lai et al. (2012), Liu et al. (2017)
	Tianyang	High-Ti basalts	Fan et al. (2008), Liu et al. (2017)
	Sichuan Basin	High-Ti basalts	This study

Geochemistry and petrogenesis of Late Permian basalts from the Sichuan Basin, SW China: Implications for the geodynamics of the Emeishan mantle plume

Fanchao Meng[a,b,c*], Yulu Tian[a,b,c], Andrew C. Kerr[d*], Wei Wang[e], Zhiping Wu[a,b,c], Qiang Xu[f], Qing Du[a,b,c], Yaoqi Zhou[a,b,c], Jiaqi Liu[g]

a. School of Geosciences, China University of Petroleum (East China), Qingdao 266580, China

b. Pilot National Laboratory for Marine Science and Technology (Qingdao), Qingdao 266061, China

c. Shandong Provincial Key Laboratory of Deep Oil and Gas, China University of Petroleum (East China), Qingdao 266580, China

d. School of Earth and Environmental Sciences, Cardiff University, Cardiff, Wales CF10 3AT, United Kingdom

e. Exploration and development Research Institute of Southwest Oil and Gas Field Company, PetroChina, Chengdu 610041, China

f. School of Geoscience and Technology, Southwest Petroleum University, Chengdu 610500, China

g. Institute of Geology and Geophysics, Chinese Academy of Sciences, Beijing 100029, China

Abstract

Plume-lithosphere interactions are significant in the formation of Large Igneous Provinces (LIPs). The Permian Emeishan Large Igneous Province (ELIP) is considered to be the result of a mantle plume. The Emeishan flood basalts comprise a major part of the ELIP and they define three zones: the inner, intermediate and outer zones. Both high-Ti and low-Ti basalts are present in the inner zone, whereas only high-Ti basalts are found in the intermediate zone and outer zone. However, there are only sparse outcrops in the outer zone, and so geochemical data on basalts from the outer zone are

* Corresponding author.
E-mail address: mengfc@upc.edu.cn (Fanchao Meng), kerra@cf.ac.uk (Andrew C. Kerr).

rare and the role of plume-lithosphere interaction in the petrogenesis of volcanic rocks in the outer zone remains poorly understood. In the Sichuan basin, the Basalt Formation is found between the Permian Maokou Formation limestone and the Longtan Formation marl in some drill cores as well as in outcrops in the basin. This relationship demonstrates that the basaltic layer in the basin is part of the Emeishan flood basalts. These basalts have TiO_2 contents of 3.7-4.2 wt.% and Ti/Y ratios of 604-720, being high-Ti sub-alkaline basalts. They display chondrite-normalized rare earth elements (REE) patterns enriched in light rare earth elements (LREE) relative to heavy rare earth elements (HREE) and have elevated large ion lithophile elements (LILE) and high field strength elements (HFSE). Lead isotope ratios are high ($^{206}Pb/^{204}Pb(t)$= 18.102-18.392, $^{207}Pb/^{204}Pb(t)$= 15.578-15.606, $^{208}Pb/^{204}Pb(t)$= 38.410-38.850), and $\varepsilon_{Nd}(t)$ values are -0.38~1.17. Detailed petrology and geochemistry suggest that the high-Ti basalts from the Sichuan Basin did not experience significant contamination of crustal and lithospheric mantle material during the ascent of magma. We infer that these basalts resulted from low-degree melting of the plume mantle source and underwent fractional crystallization of clinopyroxene. The distribution and petrogenesis of the Sichuan Basin basalts in the outer zone are different from those of the basalts in the inner zone and there are clearly different plume-lithosphere interactions in different parts of the ELIP. In the inner zone, the temperature of the lithosphere mantle was markedly elevated due to underplating of the mantle plume, causing a substantial quantity of lithosphere mantle melting and the initial formation of low-Ti basalts. This was followed by melting of the mantle plume and the formation of high-Ti basalts. In the outer zone, lower temperatures further from the plume centre were insufficient to generate extensive melting of the lithospheric mantle. Consequently, only the mantle plume melted in the outer zone, resulting in the formation of high-Ti basalts with minimal lithospheric input.

Keywords: Emeishan mantle plume, outer zone, Sichuan Basin basalts, petrogenesis of high-Ti basalts, plume-lithosphere interaction

1. Introduction

The Emeishan Large Igneous Province (ELIP) in the Upper Yangtze craton, Southwest China is composed mainly of Late Permian flood basalts, mafic-ultramafic intrusions and mafic dykes, along with lesser amounts of felsic volcanic rocks, pyroclastic counterparts, and alkaline rocks. The stratigraphy, chronology, geochemistry and geophysics of the ELIP has been studied in detail for many years and has been proposed to have formed by melting of a mantle plume (Chen et al., 2015; Liu et al., 2017; Shellnutt, 2014; Xiao et al., 2003; Xu et al., 2020; Xu et al., 2021; Zhang et al., 2008; Zhou et al., 2022). The Emeishan continental flood basalts have been broadly divided into two groups: a high-Ti series (TiO_2 > 2.5 wt.% and Ti/Y > 500) and a low-Ti series (He et al., 2007; Song et al., 2008).

Geographically, the ELIP has been divided into inner, intermediate and outer zones based on geochemical, sedimentological, and biostratigraphic characteristics of the rock units (He et al., 2003; Xiao et al., 2004; Xu et al., 2014). The rocks in the inner zone include both the high-Ti and low-Ti series, which are widely distributed in the Binchuan, Jianchuan, Lijiang and Ertan areas, whereas rocks in the intermediate and outer zones are dominated by high-Ti basalts (Li et al., 2017a; Liao, et al., 2012; Xiao et al., 2004; Xu et al., 2001, 2004). Basalts are much more extensively exposed in the intermediate zone (in Zhaotong, Qiaojia and Dongchuan) than in the outer zone (Tian et al., 2021; Xu et al., 2001; Zhang et al., 2011). The outer zone does have some well-developed outcrops in Guangxi and Guizhou provinces (Liao et al., 2012; Xiao et al.,

2004; Xu et al., 2001, 2004).

There are three major petrogenetic models for the Emeishan basalts: 1) High-Ti basalts were derived from low-degree partial melting of the mantle plume (Cheng et al., 2019; Liang et al., 2021; Wang et al., 2007; Xiao et al., 2004; Xu et al., 2001), whereas the low-Ti basalts were generated from the sub-continental lithosphere mantle (SCLM), possibly with assimilation of some upper crust (Fan et al., 2008; Kamenetsky et al., 2012; Li et al., 2010; Song et al., 2008; Wang et al., 2007; Xiao et al., 2004); 2) High-Ti basalts were derived from the SCLM or mixed with lithospheric mantle materials during magma ascent, whereas the low-Ti basalts were generated from the mantle plume (Xu et al., 2007); 3) High-Ti and low-Ti basalts have the same mantle source and may represent different degrees of partial melting, fractional crystallization and/or crustal contamination (Dong et al., 2009; Hou et al., 2011; Ren et al., 2017; Zhang et al., 2019). A common feature of all models is that the lithosphere is most influential at the centre of the Emeishan mantle plume (Li et al., 2015; Song et al., 2001, 2008; Xiao et al., 2004; Xu et al., 2001, 2014; Zhang et al., 2006).

These previous studies, however, have mainly focused on the inner and intermediate zones and although there have been some more recent studies of igneous rocks in the outer zone (Li et al., 2017a; Liu et al., 2017; Liu et al., 2022), there is still a lack of information on the source of the Emeishan high-Ti basalts and comparison between the inner and outer zones. For instance, it is still unclear whether there was plume-lithosphere interaction in the outer zone of the ELIP.

In this paper, we investigate the petrology, major and trace elements, and Sr-Nd-Pb isotope systematics of eighteen samples from three boreholes (twelve samples) and three outcrops (six samples) within and around the Sichuan Basin belonging to the outer zone of the ELIP in order to assess their petrogenesis. This data is combined with

previously published data from the inner and outer zones in order to ascertain the nature of plume-lithosphere interaction and the influence of the Emeishan mantle plume over the whole province, especially the difference between the inner and outer zones.

2. Geological background

The ELIP is located on the western Yangtze Plate and to the east of the Qinghai-Tibet Plateau, and mainly erupted in 260~257 Ma (Fan et al., 2008; Huang et al., 2022; Li et al., 2015; Shellnutt et al., 2012; Zhong et al., 2014). Traditionally, the ELIP has been thought to be bounded on the northeast and southeast by the Baoxing-Yibin fault and the Mile-Shizong fault, respectively. The eastern boundary is situated in the Fuquan-Weng'an areas, eastern Guiyang, China. The northwestern and southwestern boundaries are the Longmenshan belt and the Jinshajiang-Ailaoshan-Red River fault, respectively (Chung et al., 1998; Li et al., 2016a; Xiao et al., 2003). Tectonic movements occur in the region, with a series of well-developed north-trending faults, such as the Anninghe fault, the Longmenshan fault and the Xianshuihe fault (Song et al., 2001; Yan et al., 2018a; Yan et al., 2018b) (Fig. 1). The basement of the ELIP is dominated by Mesoproterozoic metamorphic rocks (Zhai et al., 1986), overlying Pre-Sinian-Cenozoic strata.

The Emeishan volcanic sequence is mainly composed of flood basalts and contemporaneous ultramafic-felsic plutons, layered mafic-ultramafic intrusions and radiating mafic dyke swarms (Li et al., 2015; Liu et al., 2022; Shellnutt, 2014; Xu et al., 2001; Zhou et al., 2022). The Emeishan flood basalts range from a few hundred to five thousand meters in thickness (Xiao et al., 2003; Xu et al., 2001; Zhang et al., 2001) and the areal extent of the basalts may well be larger than 1×10^6 km^2 (Li et al., 2017a; Liu

et al., 2022). The thickness of the basalts gradually decreases from the inner zone to the outer zone (Chung et al., 1998; Xu et al., 2001; Zhu et al., 2018). The inner zone consists of a variety of lavas and pyroclastic rocks, including picrites, basalts, basaltic andesites and basaltic pyroclastic rocks, with trachytic and rhyolite tuff in the uppermost part of the sequence (Xiao et al., 2004; Xu et al., 2001, 2004). A more-restricted range of rocks is found in the intermediate and outer zones and includes tholeiites and alkaline basalts (He et al., 2010).

The Sichuan Basin, located in the northeast (outer zone) of the ELIP in the northwestern Yangtze Craton in the South China Block, is a typical superimposed basin common in southwestern China (Liu et al., 2021a). The Late Permian basalt outcrops of the ELIP have only been found in a few places (Jinding, Huayingshan and Yanghe) in the Sichuan Basin (e.g., Li et al., 2017a; Liang et al., 2021; Liu et al., 2021a). The lack of volcanic outcrops in this region can be attributed to the complex burial history of the Sichuan Basin, and this has made geochemical research difficult on the Emeishan basalts in the basin. However, abundant drill cores from the Sichuan Basin indicate that the Emeishan basalts are widely distributed between the Middle and Upper Permian strata (Liang et al., 2021). Based on seismic and drilling data, it has been proposed that basalts are mainly distributed in the western Sichuan Basin with a thickness of 40-500 m, which thins from the southwest to northeast (Fig. 2) (Liu et al., 2021a; Tian et al., 2017). However, the geochemistry and petrogenesis of the basalts in the Sichuan Basin are still unclear. Therefore, in this study we have sampled the drill cores and available outcrops from the Sichuan Basin.

3. Samples and geochronology

All samples in this study were collected from six areas within and around the southwest of the Sichuan Basin (Fig. 2) , including the borehole samples from ST1 (ST1-2, ST1-5) (Fig. 3a), YT1 (YT1-1, YT1-3, YT1-4, YT1-5, YT1-6, YT1-7) (Fig. 3b) and ZG2 (ZG2-4, ZG2-5, ZG2-7, ZG2-8) (Fig. 3c, d), as well as outcrops Longmendong in Leshan City (20LMD04, 20LMD05) (Fig. 3e, f), Longchi in Emeishan City (20LC04, 20LC06) (Fig. 3g) and Xinlin in Leshan City (20XL01, 20XL02) (Fig. 3h). Boreholes YT1 and ST1 are located around the Longquanshan fault, Longchi outcrop is close to the Longmenshan fault, while outcrops Xinlin and Longmendong, and borehole ZG2 border the Emei-Yibin fault in the western Sichuan Basin (Fig. 2b). All the samples were analysed for whole-rock major and trace elements, and eleven samples were analysed for Sr, Nd and Pb isotopes. All samples were collected from the central part of the massive lava flows with little amygdales and crack fillings. The basalts contain 2% to 15% phenocrysts of clinopyroxene, plagioclase, and minor olivine, set in a matrix comprising mostly plagioclase. The clinopyroxene phenocrysts are generally subhedral, occasionally euhedral, whereas the plagioclase phenocrysts are euhedral grains. The phenocrysts range in size from 700 μm to 1800 μm in samples YT1-6 and YT1-7, while they are about 60~400 μm in size in ZG2 Well, Longchi and Xinlin (Fig. 3b, d).

Stratigraphally, the Sichuan Basin volcanic rocks lie between the Permian Maokou Formation limestone and the Longtan Formation marl (Fig. 4), indicating that the Sichuan Basin basalts erupted in the Mid-Late Permian. This eruption time is consistent with the formation time of the ELIP, which suggests the Sichuan Basin basalts belong to the ELIP (Li et al., 2017a; Liu et al., 2022). Based on chronological data (Table 1), the main duration of the ELIP eruption is 260~257 Ma (e.g., Fan et al., 2008; Lai et al., 2012; Li et al., 2016a; Li et al., 2016b; Zhou et al., 2006; Zi et al., 2010).

4. Analytical methods

Fresh rocks were selected based on the characteristics of rock thin sections. Following the removal of amygdales and minor veins, the samples were crushed to 200 mesh by an agate mortar. The pre-treatment ensures the accuracy of whole-rock geochemical analyses.

The major and trace elements and Sr-Nd-Pb isotopes of the samples were determined at the Wuhan Sample Solution Analytical Technology Co., Ltd., Wuhan, China. International reference material values are listed in the appendix.

Major elements were analysed by a Primus Ⅱ X-ray fluorescence spectrometer (XRF) with wave-length dispersive X-ray fluorescence spectrometry. The major element data are corrected by the theoretical α coefficient method, and relative standard deviations (RSD) for most major element oxides are within ±1-3%. The contents of trace elements were analysed by Agilent 7700e ICP-MS. The analytical precision and accuracy for trace elements are mostly better than 10%. The detailed sample-preparation procedure for ICP-MS analyses can be found in Rudnick et al. (2004) and Liu et al. (2008).

Sr-Nd-Pb isotopic analyses of whole-rock samples were carried out on a Neptune Plus MC-ICP-MS (Thermo Fisher Scientific, Dreieich, Germany). All chemical preparations were performed on class 100 work benches within a class 1000 over-pressured clean laboratory. The sample powders were acid-leached before isotopic analysis (Weis et al., 2005). The data was processed by "Iso-Compass" software (Zhang et al., 2020a). Detailed analytical procedures are described in Chen et al. (2002) and Li et al. (2012).

The analysed $^{87}Sr/^{86}Sr$ of NBS 987 standard solution is 0.710242±14 (2SD, n=345), which is consistent with the published values (0.710248±12, Zhang and Hu, 2020). In addition, analysis of USGS reference materials BCR-2 (basalt) yielded ratios of 0.705012±22 (2SD, n=63) for $^{87}Sr/^{86}Sr$, which are identical within error to their published results (Li et al. 2012). The Sr isotope standard precision (2SE) = 0.000010-0.000020 (0.01‰-0.03‰, 2RSE), and the accuracy is better than 0.000020 (~0.03‰). For standard GSB 04-3258-2015, a $^{143}Nd/^{144}Nd$ of 0.512440±6 (2SD, n=31) was obtained which is identical, within error, to its published value (0.512438±6 (2SD), Li et al., 2017b). In addition, the measurement results of $^{143}Nd/^{144}Nd$ for USGS reference materials BCR-2 (basalt) are 0.512641±11 (2SD, n=82), which are identical, within error, to their published values (Li et al. 2012). The precision of Nd isotope analyses (2SE) = 0.000005-0.000025 (0.01‰-0.05‰, 2RSE), and the analytical accuracy is better than 0.000025 (~0.05‰). The external precision of $^{20x}Pb/^{204}Pb$ ratios for the reference material NBS 981 is 0.03% (2RSD). Furthermore, the USGS reference material BCR-2 (basalt) had analysed ratios of $^{208}Pb/^{204}Pb$=38.736±17, $^{207}Pb/^{204}Pb$=15.628±3, and $^{206}Pb/^{204}Pb$=18.756±10 (2SD, n=22), which are consistent within error of 0.03% with the published results ($^{208}Pb/^{204}Pb$=38.725±22, $^{207}Pb/^{204}Pb$=15.621±4, $^{206}Pb/^{204}Pb$=18.753±8, Zhang and Hu 2020). The internal precision of $^{20x}Pb/^{204}Pb$ ratio is 0.002%-0.025%, and the analytical accuracy is better than 0.03%.

5. Results

5.1 Major elements

The major element compositions of the volcanic rock samples from different

223 regions of the Sichuan Basin are listed in Table 2. The samples have all experienced
224 some degree of hydrothermal alteration, and so the whole-rock raw data has been
225 normalised on a volatile-free basis. Samples ST1-2 and ST1-5 have high LOI values of
226 5.9 wt.% and 6.0 wt.% respectively and so their major element compositions were not
227 used in this study.

228 The samples of the Sichuan Basin show large variations in SiO_2 (45.6-49.2 wt.%)
229 and MgO (4.3-7.1 wt.%). The rocks have total alkalis (Na_2O+K_2O) that range from 3.0
230 to 5.8 wt.% and have K_2O/Na_2O ratios of ~1.7. They have high TiO_2 contents of 3.7 to
231 4.2 wt.% and Ti/Y ratios of 604 to 720, indicating that the basin basalts belong to the
232 high-Ti series (Fig. 5a). The analysed samples mainly plot in the sub-alkaline field on
233 the Ol'-Ne'-Q' diagram (Fig. 5b). The concentrations of the Al_2O_3 and CaO are
234 positively correlated with MgO, whereas K_2O, TiO_2, P_2O_5, $Fe_2O_3^T$, La and Nb are
235 negatively correlated with MgO (Fig. 6). Compared with the outer zone of the ELIP,
236 the inner zone has variable volcanic rock types, ranging from low-Ti series to high-Ti
237 series (Fig. 5a).

238

239 **5.2 Trace elements**

240 The trace element contents of the basalts in the Sichuan Basin are listed in Table
241 2. Chondrite-normalised REE patterns are enriched in the LREE ($(La/Yb)_N$ = 9.8-13.2)
242 and depleted in the HREE ($(Dy/Yb)_N$ = 1.8-2.0), with only slight negative Eu anomalies
243 (δEu = 0.83-0.95) (Fig. 7a). On primitive mantle-normalised trace element diagrams
244 (Fig. 7b), the large ion lithophile elements (LILE) are quite variable, especially the large
245 negative anomalies of Rb and K, as well as positive anomalies of Ba and Pb, which
246 may result from sub-solidus hydrothermal alteration. However, alteration-resistant

immobile high field strength elements (HFSE, e.g., Nb, Ta, Zr, Hf, Th) of the samples are much more consistent, with slightly negative Zr anomalies and positive Th anomalies (Fig. 7b). The trace element compositions of the samples ST1-2 and ST1-5 have not been affected considerably except for some mobile elements, therefore, they are still used in the following discussion. Overall, the Sichuan basalts have OIB (ocean island basalt)-like REE and trace element signatures, which are similar to compositions of the Emeishan high-Ti basalts from other regions.

5.3 Sr-Nd-Pb isotopes

The isotopic data of the basalts in the Sichuan Basin are presented in Table 3. The initial Sr-Nd-Pb isotopic compositions have been age-corrected to 258.5 Ma based on the age range of the Emeishan basalts in this paper. The initial Sr isotopic compositions of the high-Ti basalts in the Sichuan Basin range from 0.705230 to 0.706935 and the $\varepsilon_{Nd}(t)$ values range from -0.38 to 1.17 (Fig. 8a). The Sichuan Basin basalts show a relatively wide range in $^{208}Pb/^{204}Pb(t)$ ratios between 38.403 and 38.845, whereas $^{206}Pb/^{204}Pb(t)$ (18.097-18.388) and $^{207}Pb/^{204}Pb(t)$ (15.578-15.606) compositions are more uniform (Fig. 8c, d). Compared with low-Ti basalts in the inner zone, the compositional range of high-Ti basalts in the ELIP is relatively constant with typical OIB-like Sr-Nd-Pb isotopic characteristics. The Sichuan Basin samples have slightly higher $^{87}Sr/^{86}Sr(t)$ ratios than the high-Ti samples in other areas of the ELIP, and show the characteristics of the EMII end-member. However, in general, the basin samples overlap with the field of high-Ti basalts in the outer zone, which indicates the Sichuan Basin basalts belong to the outer zone of the ELIP.

These data plot above the LoNd (low Nd) array, close to OIB and EMII, in distinct

contrast to the DM (depleted mantle) and MORB (mid-ocean ridge basalt) (Fig. 8a, b). The samples lie above the North Hemisphere Reference Line (NHRL) and overlap with the field of OIB (Fig. 8c, d). In terms of $^{206}Pb/^{204}Pb(t)$ vs. $^{208}Pb/^{204}Pb(t)$, the Sichuan Basin samples data have similar compositions to the high-Ti basalts in the ELIP and overlap with alkaline lavas from the Kerguelen Plateau (Fig. 8d) (Fan et al., 2008). The Kerguelen Plateau in the South Indian Ocean (which comprises a large amount of alkaline basalts, (Zhu et al., 2007)) is one of the largest LIPs in the world, which is related to the Kerguelen plume activity from the Early Cretaceous.

6. Discussion

6.1 Crustal contamination and fractional crystallization

As previously noted fluid-mobile elements (LILE) such as Rb, Ba, K, Pb and Sr show large variations and both positive and negative peaks, which are most likely to be caused by sub-solidus hydrothermal alteration, however, the REE, Th and HFSE (e.g., Hf, Nb and Ta) are relatively alteration-resistant and so are essentially immobile. Therefore, in the following discussion, only immobile elements are used to assess the petrogenesis of these rocks.

It is necessary to evaluate the role of crustal contamination and fractional crystallization during magma ascent before we discuss potential mantle sources of volcanic rocks. Importantly, the proxies for crustal contamination, Th/Nb, La/Nb, Th/Ta and Nb/U ratios are not changed by partial melting or fractional crystallization in magma. Crustal contamination usually results in high Th/Nb (>5), La/Nb (>12) and Th/Ta ratios, and low Nb/U ratios (Neal et al., 2002; Pearce, 2008; Rudnick and Gao, 2003). The basalts in the present study have low La/Nb (1.01-1.23), Th/Nb (0.15-0.22)

and Th/Ta (2.41-3.27), and high Nb/U (21.48-28.00). These characteristics reveal that they were derived from mantle source without significant continental crust contamination. In addition, there is no clear mixing trend between the Sichuan Basin samples and average continental crust on a Ce vs. Nb/Th diagram (Fig. 9a). The analysed samples are broadly similar to primitive mantle (PM) values, and are close to the field of Kerguelen alkaline OIB, as well as plotting far from the values of middle and upper continental crust (MC and UC) (Fig. 9b). Moreover, slightly positive Th anomalies, and slightly negative Nb and Ta anomalies (Fig. 7b) also confirm that the Sichuan Basin basalts have not been significantly contaminated by crustal materials, because continental crust is enriched in Th and strongly depleted in Nb and Ta. Furthermore, $(^{87}Sr/^{86}Sr)_i$ and $\varepsilon_{Nd}(t)$ do not correlate with increasing SiO_2 (Fig. 9c, d), which also suggests little crustal contamination occurred. Therefore, the magmatic evolution of basalts in the Sichuan Basin is dominated by fractional crystallization or partial melting.

Basalts from Sichuan Basin have low MgO values (4.3-7.1 wt.%) and display good correlations between MgO and other major oxides (Al_2O_3, K_2O, $Fe_2O_3^T$) as well as trace elements (La, Nb) (Fig. 6), which indicates the likely occurrence of fractional crystallization. The basalts in the Sichuan Basin have lower Ni, Cr and MgO than primitive magma (Hirajima et al., 1990) (Fig. 6), further suggesting that the magma experienced a substantial amount of fractional crystallization (e.g., olivine, clinopyroxene) during ascent.

The basalts are characterised by a positive correlation between MgO and CaO (Fig. 6b), indicating that the magma underwent the fractional crystallization of clinopyroxene (Wei et al., 2013). A slight negative Eu anomaly (Fig. 7b) suggests the magma also experienced slight fractional crystallization of plagioclase. As illustrated in Fig. 10a,

the Sichuan Basin basalts exhibit a positive correlation between CaO/Al_2O_3 ratios and Mg# values, similar to other Emeishan basalts. The calculated effects of fractional crystallization are shown in mineral vector diagrams in Figs. 10b and c. The data mostly plot near the clinopyroxene crystallization vector (Fig. 10b, c), further suggesting that clinopyroxene is the most significant mineral phase in the fractional crystallization. This is consistent with the petrographic features (Fig. 3), as there are more clinopyroxene phenocrysts than plagioclase in YT1-7 (Fig. 3b) and ZG2-5 (Fig. 3d). Moreover, the Sichuan basalts have enriched Fe and Ti, and MgO vs. $Fe_2O_3^T$ and TiO_2 show negative correlations (Fig. 6d, e). These characteristics may be induced by the early fractional crystallization of Ti and Fe-poor silicate minerals, which indicates little crystallization of titanomagnetite in low oxygen fugacity conditions (Li et al., 2017; Zhang et al., 2011). Furthermore, low oxygen fugacity may also have promoted the fractional crystallization of clinopyroxene and plagioclase in the Sichuan Basin basalts (Fig. 3) (Li et al., 2017).

6.2 Magma Source and Petrogenesis

The Sichuan Basin basalts have high TiO_2 contents (>3.5 wt.%), relative enrichment of alkalis (3.1-5.9 wt.%), LILE and HFSE, and significant REE fractionation with $(La/Yb)_N$ ratios ranging from 9.8 to 13.2. The trace element and Sr-Nd-Pb isotope signatures are OIB-like with $\varepsilon_{Nd}(t)$ values ranging from -0.38 to 1.17, (Fig. 7, 8). However, the origin of the Emeishan basalts with these characteristics is still controversial, and has been variously ascribed to the melting of either a mantle plume (Cheng et al., 2019; Liang et al., 2021; Wang et al., 2007; Xiao et al., 2004; Zhang et al., 2019) or lithospheric mantle (Lai et al., 2012; Xu et al., 2007). Alternatively, some authors propose that these basalts result from the interaction of mantle plume melts with

the lithospheric mantle (Cheng et al., 2019; Fan et al., 2008; He et al., 2010; Xu et al., 2007).

Like the high-Ti basalts in other regions of the ELIP, REEs, trace elements (except some LILEs) and incompatible element ratios of the Sichuan Basin high-Ti basalts are very similar to OIB and Kerguelen alkaline OIB-like basalts (Fig. 7, 11). Furthermore, the Sichuan Basin samples have OIB-like initial Sr-Nd-Pb isotopic characteristics, broadly fall in the field of OIB and Kerguelen basalts (Fig. 8). These geochemical signatures suggest the high-Ti basalts from the Sichuan Basin might have originated from a plume source, compositionally similar to other regions in the ELIP (e.g., Cheng et al., 2019; He et al., 2010; Liu et al., 2017; Song et al., 2008). It is proposed that the high-Ti basaltic magma from the Sichuan Basin is probably the product of partial melting of the head of the mantle plume, because the outer zone is further from the plume centre, and lower temperatures would have resulted in less lithospheric melting (Cheng et al., 2019).

In terms of incompatible trace element ratios, the Sichuan Basin basalts show broadly constant $(La/Yb)_N$ ratios as $\varepsilon_{Nd}(t)$ values increase (Fig. 12a), and La/Yb ratios have a negative correlation with Yb compositions (Fig. 12b). These characteristics reveal that the Emeishan high-Ti basalts did not originate from partial melting of a homogeneous plume source. The samples from the Sichuan Basin define a linear array on Th/La vs. Nb/U (Fig. 12c) and $^{206}Pb/^{204}Pb$ vs. $\varepsilon_{Nd}(t)$ (Fig. 12d) plots similar to other Emeishan high-Ti basalts, which would support this inference. In addition, it is generally argued that metasomatic melts derived from the primitive mantle have La/Nb ratios of ~0.53, whereas those from MORB source have values of ~1.02 (McKenzie and O'Nions, 1995). The Sichuan Basin basalts have high La/Nb ratios of 1.01-1.23, with OIB-like Sr-Nd isotopes signatures significantly different from MORB (Fig. 8a),

indicating that they were likely derived from OIB-like enriched mantle source that was previously metasomatized. Moreover, the Sichuan Basin high-Ti samples plot around the field of OIB (Fig. 8c, d) and have an EMII-type signature (Fig. 8a, b) in terms of Sr-Nd-Pb isotope space. These features indicate the mantle plume may have been metasomatized by enriched materials before the eruption of the Late Permian basalts (Xu et al., 2021).

It is still unclear whether such enriched components originate from the asthenosphere, SCLM, crust, or recycled materials. The asthenosphere is ruled out since the trace elements and Sr-Nd-Pb isotopes of the Emeishan high-Ti basalts have OIB-like rather than MORB-like characteristics (Fig. 8) (Liu et al., 2017; Song et al., 2001; Wang et al., 2007; Xiao et al., 2004). Like the Emeishan high-Ti basalts in other regions, the basalts in the Sichuan Basin have relatively high Ti/Yb ratios, distant from OIB-SCLM and OIB-crust mixing lines. They are also significantly different from the Sangxiu Formation basalts which have a contribution from both continental lithospheric mantle materials and the Kerguelen mantle plume (Fig. 11b) (Zhu et al., 2007). Furthermore, the Sichuan Basin samples have high Ce, unlike continental lithosphere (Fig. 9a), which indicates minimal involvement of SCLM. As shown in Section 6.1, the samples were not significantly contaminated by crust. Therefore, the enriched components are unlikely to be related to either SCLM or crust.

It has been argued that the enriched signature in the OIB-like source is related to ancient recycled oceanic crust (Sobolev et al., 2000, 2007) or subducted terrigenous sediments (Eisele et al., 2002; Hofmann, 1997; Weaver, 1991). The Sichuan Basin basalts display $(Ta/La)_N$ ratios of 0.8-1.1, with an average of 0.94. Ta is depleted relative to La, and Th/Yb and Nb/Yb ratios are high (Fig. 11a), suggesting the involvement of crustal components during ascent or the contribution of subduction

component. The Sichuan Basin basalts have not experienced crustal contamination, so it is more likely that the Emeishan mantle plume has undergone metasomatism, accompanied by mixing of enriched components during subduction. Many studies on volcanic and sedimentary rocks in southwestern China and the Ailaoshan Region propose that the Ailaoshan Ocean crust (Paleotethyan slab) subducted eastward into the upper mantle beneath the western South China Block during the Permian-Middle Triassic (Hou et al., 2017; Qin et al., 2011; Wang et al., 2013; Xu et al., 2019, 2021; Yang et al., 2012; Yang and He, 2012; Zhong et al., 2013).

Based on a study of the Late Permian and Early Triassic A-type granites in the Yuanyang area of Yunnan, South China, Xu et al. (2021) proposed a geodynamic model of the interaction between the Emeishan mantle plume and the subducted Paleotethyan oceanic crust. According to the model, the Ailaoshan Ocean subducted eastward beneath the western South China Block, and the adjacent Emeishan mantle plume rapidly entrained the recycled lithospheric fragments (Xu et al., 2021). This model provides a mechanism for the metasomatism of the Emeishan mantle plume, and further explains why the composition of the Emeishan mantle plume is heterogeneous. In addition, many authors have proposed that the Emeishan mantle plume is likely to be intrinsically related to recycled ancient oceanic materials (Ren et al., 2017; Zhu et al., 2018). Zhu et al. (2018) proposed that the amount of recycled materials may be 10~20% in the Emeishan plume, which is broadly consistent with the view of Ren et al. (2017). In summary, we propose that the high-Ti basalts in the outer zone were derived from an OIB-like Emeishan mantle plume, which was modified by enriched materials derived from a subducted slab before the Late Permian.

The high-Ti basalts in the Sichuan Basin, which are located in the outer zone of the ELIP, are a similar age to the Emeishan basalts. Reconstruction of the thermal

history of the Sichuan Basin with a high paleogeothermal gradient of 23.0-42.6 ℃/km in 259 Ma, indicates that the Sichuan Basin suffered an intensive thermal event related to the Emeishan mantle plume (Zhu et al., 2010, 2016). The basalts in Guangxi and Guizhou provinces that are relevant to the ELIP imply an extension of magmatism at the periphery (the outer zone) of the plume (Fan et al., 2008; Lai et al., 2012; Liu et al., 2017). This evidence indicates that the Sichuan Basin high-Ti basalts are related to the Emeishan mantle plume.

Rare-earth element ratios of the Sichuan Basin basalts (Fig. 13a) suggest they were derived from a mantle source containing garnet. The Emeishan high-Ti basalts lie between the melting curves for garnet and spinel lherzolites, indicating that they are derived from the spinel-garnet transition zone (Fig. 13b). In contrast, the low-Ti basalts in the inner zones have lower La/Sm, Sm/Yb and Dy/Yb ratios, revealing a higher degree of mantle melting at a shallower melting depth (Wang et al., 2007; Xiao et al., 2004). The low-Ti basalts also plot closer to SCLM end members than high-Ti basalts (Fig. 11b) We therefore argue that low-Ti magma might be generated from, or contain, a greater proportion of material from the SCLM (Fan et al., 2008; Xiao et al., 2004).

6.3 Spatial and temporal distribution of the Emeishan basalts and tectonic significance

Chronological data give precise constraints on the duration of the ELIP eruption as 260~257 Ma (Table 1) (e.g., Fan et al., 2008; Lai et al., 2012; Li et al., 2016a; Li et al., 2016b; Zhou et al., 2006; Zi et al., 2010). Magnetostratigraphic studies of the Emeishan basalts indicate that a substantial number of basalts were formed during a period of normal polarity, with the main eruption lasting ~1-2 Ma (Zheng et al., 2010).

444 It has been proposed that the major eruption phase lasted less than 1 Ma (Xu et al., 2017;
445 Zhu et al., 2018). Therefore, it is difficult to give the exact eruptive ages of high-Ti and
446 low-Ti basalts, although most low-Ti basalts are stratigraphically below high-Ti basalts
447 in most field profiles (Fig.14).

448 As summarised in Fig. 14, both high-Ti and low-Ti series are exposed in the inner
449 zone (e.g. Binchuan, Ertan, and Miyi areas), with high-Ti basalts overlying low-Ti
450 basalts, whereas only high-Ti basalts erupted in the outer zone, i.e., a greater distance
451 from the centre of the mantle plume (Table 4) (Fan et al., 2008; He et al., 2010; Song
452 et al., 2001, 2008; Xiao et al., 2004; Xu et al., 2001, 2007; Zhang et al., 2006). Overall,
453 the Permian basalts are distributed from northeast (the Sichuan Basin) to southwest (the
454 centre of the mantle plume) in the ELIP, and the thickness of basalts gradually decreases
455 from the inner zone to the outer zone (Fig. 14). This distribution trend not only is
456 consistent with the hotspot track of the Emeishan mantle plume (Fig. 1b) (Liu et al.,
457 2021b), but also overlaps the seismic anomaly trends and residual gravity anomaly
458 (Deng et al., 2014; Liu et al., 2021b; Xie et al., 2013).

459 Our petrogenetic model is shown in Fig. 15 and builds on previous models (e.g.,
460 Feng et al., 2022; Liu et al., 2021b; Liu et al., 2022; Xiao et al., 2004; He et al., 2010).
461 Based on our new data, we further consider the petrology, geochemistry, and
462 distribution characteristics of the Sichuan Basin basalts in the outer zone of the ELIP,
463 and consider the influence of subduction of the paleo-oceanic crust (Hou et al., 2017;
464 Xu et al., 2019, 2021), the movement of the South China block (Liu et al., 2021b; Liu
465 et al., 2022), and the successive eruptions of the late Permian low-Ti and high-Ti basalts
466 (He et al., 2010; Xiao et al., 2004; Xu et al., 2001).

467 Paleomagnetic studies suggest that the Yangtze Craton moved northward between
468 300 and ~260 Ma and experienced an overall ~27° clockwise rotation from Permian to

present (Huang et al., 2018; Liu et al., 2021b). The Western Yangtze block experienced Ailaoshan slab eastward subduction from the early-Guadalupian (~269 Ma) (Xu et al., 2021), and the adjacent Emeishan mantle plume was modified by the recycled lithospheric fragments (Fig. 15a) (e.g. Hou et al., 2017; Qin et al., 2011; Wang et al., 2013; Xu et al., 2019, 2021). Paleotethyan subduction resulted in an extensional tectonic setting in the Sichuan Basin during Middle-Late Permian (Xu et al., 2021; Liu et al., 2022). Before the eruption of the Emeishan basalts, mantle upflow reached the lithosphere (Liu et al., 2021b), resulting in plume-lithosphere interactions, and crustal uplift. The magnitude of uplift is greater than 1000 m at its core (the inner zone) (He et al., 2003), and the uplift range of the Sichuan Basin in the outer zone is relatively low. The upper part of the Maokou Formation was exposed at the surface, resulting in different degrees of weathering, denudation, and a paleo-karst landscape (Hu et al., 2012; Xiao et al., 2014; Zhang et al., 2020b). This resulted in variable degrees of uplift in the Sichuan Basin. As the South China block drifted northward, major eruptions including low-Ti and high-Ti series occurred throughout the ELIP during the end-Guadalupian (260~257 Ma) (Fig. 15b, c) (Liu et al., 2021b, Feng et al., 2022).

We propose that from 260 to ~257 Ma, the temperature of the lithosphere mantle in the inner zone rose dramatically due to underplating of the mantle plume, causing partial melting of lithosphere mantle and forming the low-Ti basalts (Fig. 15b). As the lithospheric mantle gradually became refractory, OIB-like high-Ti basalts derived from the plume became the predominant magma type that erupted over the low-Ti basalts (Fig. 14, 15d). In contrast, at the periphery of the plume, the lithospheric mantle was cooler due to the distance from the centre of the mantle plume. As a result, the temperature would have been insufficient to generate extensive melting of the lithospheric mantle (Xu et al., 2001; Xiao et al., 2004; He et al. al., 2010). Therefore,

only the mantle plume melted in the outer zone, forming high-Ti basalts (Fig. 15c). As discussed in Section 6.2, the geochemical evidence also indicates that the source of the high-Ti basalts did not involve melts from SCLM.

The coexistence of high-Ti and low-Ti magma in the inner zone of the Emeishan mantle plume could be attributed to plume-lithosphere interaction. Geochemical modeling suggests that the Emeishan high-Ti basalts are formed at a higher melting pressure than the low-Ti basalts (Liu et al., 2017; Zhang et al., 2019). Continuous polybaric melting of the mantle source might account for compositional variations of the rock types in the inner zone. Furthermore, Dy/Yb and La/Yb ratios of the high-Ti basalts in the outer zone are lower than those in the inner zone, indicating a shallower source and higher melting degree of mantle peridotite for the high-Ti basalts in the outer zone (Tian et al., 2021). It is proposed that melting generally happens beneath thin lithosphere rather than thickened lithosphere, i.e., lid-effect, and the extent of melting beneath the thin lithosphere is likely very low (no more than ~5%) (Fram and Lesher, 1993; Niu et al., 2021). The lithosphere in the outer zone is thicker than that in the inner zone in the ELIP (Tian et al., 2021). The magmatic activity in the outer zone is more limited than that in the inner zone, which is consistent with the “lid effect” model.

Therefore, the high-Ti basalts from the Sichuan Basin are the result of partial melting of the plume in the outer zone of the ELIP. In contrast, relatively few low-Ti basalts derived from the lithosphere mantle have been discovered in the outer zone, because it is more distant from the centre of the mantle plume and so has a cooler lithosphere.

7. Conclusions

Based on petrography and geochemistry of the basalts in the Sichuan Basin, and combined with published data from the inner and outer zones of the Emeishan mantle plume, it is concluded that.

(1) In the outer zone of the ELIP, the volcanic rocks from the Sichuan Basin are part of the Emeishan flood basalts. Based on chronological data, the main duration of the basalt in outer zone eruption is 260~257 Ma.

(2) Unlike the inner zone, the volcanic rocks in Sichuan Basin of the outer zone are predominantly high-Ti sub-alkaline basalts. The Sichuan Basin basalts with OIB-like geochemical signatures originated from the Emeishan mantle plume, which was modified by enriched materials derived from a subducted slab before the Late Permian. The samples have compositions consistent with low degrees of partial mantle melting and fractional crystallization dominated by clinopyroxene during magma evolution.

(3) During the early-Guadalupian (~269 Ma), Western Yangtze Block experienced Ailaoshan slab (Paleotethys Ocean) eastward subduction, and the adjacent Emeishan mantle plume was modified by the recycled lithospheric fragments. During the end-Guadalupian (260~257 Ma), the Emeishan mantle plume underplated the lithosphere mantle in the Yangtze Continent.

(4) In the inner zone, the lithosphere mantle and the mantle plume melted successively, forming low-Ti basalts and overlying high-Ti basalts respectively. However, in the outer zone, only high-Ti basalts derived from the mantle plume were able to form.

Acknowledgements

We are grateful to two anonymous reviewers, handle editor Liang Qiu and chief

editor Meifu Zhou for their constructive comments and suggestions. We thank Hongfang Chen for help with major and trace elements and Sr-Nd-Pb isotopic composition analyses at the Wuhan Sample Solution Analytical Technology Co., Ltd., Wuhan, China. This study was supported by Marine S&T Fund of Shandong Province for Pilot National Laboratory for Marine Science and Technology (Qingdao) (2021QNLM020001-1), National Natural Science Foundation of China Project (42272225; 42072169) and Shandong Provincial Natural Science Foundation, China (ZR2021MD083).

References

Aldanmaz, E., Pearce, J.A., Thirlwall, M.F., Mitchell, J.G., 2000. Petrogenetic evolution of late Cenozoic, post-collision volcanism in western Anatolia, Turkey. J. Volcanol. Geotherm. Res. 102(1-2), 67-95.

Barling, J., Goldstein, S.L., 1990. Extreme isotopic variations in Heard Island lavas and the nature of mantle reservoirs. Nature 348, 59-62.

Carlson, R.W., 1995. Isotopic inferences on the chemical structure of the mantle. J. Geodyn. 20, 365-386.

Chen, F., Satir, M., Ji, J., Zhong, D., 2002. Nd-Sr-Pb isotopes of Tengchong Cenozoic volcanic rocks from western Yunnan, China: evidence for an enriched-mantle source. J. Asian Earth Sci. 21, 39-45.

Chen, J.F., Jahn, B.M., 1998. Crustal evolution of southeastern China: Nd and Sr isotopic evidence. Tectonophysics 284, 101-133.

Chen, Y., Xu, Y.G., Xu, T., Si, S.K., Liang, X.F., Tian, X.B., Deng, Y.F., Chen, L., Wang, P., Xu, Y.H., Lan, H.Q., Xiao, F.H., Li, W., Zhang, X., Yuan, X.H., Badal, J., Teng, J.W., 2015. Magmatic underplating and crustal growth in the Emeishan Large

Igneous Province, SW China, revealed by a passive seismic experiment. Earth Planet. Sci. Lett. 432, 103-114.

Cheng, W.B., Dong, S.Y., Jin, C.H., Zhao, B., Zhang, Y., Wang, C., 2019. Characteristics of elemental geochemistry and petrogenesis discussion of the Emeishan basalts in Muchuan area, Sichuan province. J. Mineral. Petrol. 39(4), 49-60. In Chinese with English abstract.

Chung, S.L., Jahn, B.M., Wu, G.Y., Lo, C.H., Cong, S.L., 1998. The Emeishan flood basalt in SW China: A mantle plume initiation model and its connection with continental breakup and mass extinction at the Permian-Triassic Boundary. Mantle Dynamics and Plate Interactions in East Asia. American Geophysical Union (AGU) 798(12), 47-58.

Deng, Y., Zhang, Z., Mooney, W., Badal, J., Fan, W., Zhong, Q., 2014. Mantle origin of the Emeishan large igneous province (South China) from the analysis of residual gravity anomalies. Lithos 204, 4-13.

Deniel, C., 1998. Geochemical and isotopic (Sr, Nd, Pb) evidence for plume-lithosphere interactions in the genesis of Grande Comore magmas (Indian Ocean). Chem. Geol. 144, 281-303.

Dong, S.Y., Zhang, Z.C., 2009. Geochemical Behavior of Yttrium in Fe-Ti Oxides - An Example Inferred from the Emeishan Large Igneous Province. Geol. Rev. 55(3), 355-360. In Chinese with English abstract.

Eisele, J., Sharma, M., Galer, S.J.G., Blichert-Toft, J., Devey, C.W., Hofmann, A.W., 2002. The role of sediment recycling in EM-1 inferred from Os, Pb, Hf, Nd, Sr isotope and trace element systematics of the Pitcairn hotspot. Earth Planet. Sci. Lett. 196, 197-212.

Fan, W.M., Zhang, C.H., Wang, Y.J., Guo, F., Peng, T.P., 2008. Geochronology and

592 geochemistry of Permian basalts in western Guangxi Province, Southwest China:
593 evidence for plume–lithosphere interaction. Lithos 102 (1-2), 218-236.
594 Feigenson, M.D., Patino, L.C., Carr, M.J., 1996. Constraints on partial melting imposed
595 by rare earth element variations in Mauna Kea basalts. J. Geophys. Res. 101(B5),
596 11815-11829.
597 Feng, Q.Q., Qiu, N.S., Fu, X.D., Li, W.Z., Liu, X., Ji, R.Y., 2022. Maturity evolution of
598 Permian source rocks in the Sichuan Basin, southwestern China: The role of the
599 Emeishan mantle plume. J. Asian Earth Sci. 229, 105180.
600 Fram, M.S., Lesher, C.E., 1993. Geochemical constraints on mantle melting during
601 creation of the North Atlantic basin. Nature 363(6431), 712-715.
602 Gao, S., Ling, W., Qiu, Y., Lian, Z., Hartmann, G., Simon, K., 1999. Contrasting
603 geochemical and Sm-Nd isotopic compositions of Archean metasediments from
604 the Kongling high-grade terrain of the Yangtze craton: evidence for cratonic
605 evolution and redistribution of REE during crustal anatexis. Geochim. Cosmochim.
606 Acta 63(13-14), 2071-2088.
607 Hamelin, B., Allègre, C.J., 1985. Large scale regional units in the depleted upper mantle
608 revealed by an isotopic study of the south-west India ridge. Nature 315, 196-198.
609 Hart, S.R., 1984. The Dupal anomaly: a large-scale isotopic anomaly in the southern
610 hemisphere. Nature 309, 753-756.
611 Hao, Y.L., Zhang, Z.C., Wang, F.S., Mahoney, J.J., 2004. Petrogenesis of high-Ti and
612 low-Ti basalts from the Emeishan large igneous province. Geol. Rev. 50(6), 587-
613 592. In Chinese with English abstract.
614 Hawkesworth, C.J., Rogers, N.W., van Calsteren, P.W.C., Menzies, M.A., 1984. Mantle
615 enrichment processes. Nature 311 (27), 331-335.
616 He, B., Xu, Y.G., Chung, S.L., Xiao, L., Wang, Y.M., 2003. Sedimentary evidence for

617 a rapid, kilometer-scale crustal doming prior to the eruption of the Emeishan flood
618 basalts, Earth Planet. Sci. Lett. 213, 391-405.
619 He, B., Xu, Y.G., Huang, X.L., Luo, Z.Y., Shi, Y.R., Yang, Q.J., Yu, S.Y., 2007. Age
620 and duration of the Emeishan flood volcanism, SW China: Geochemistry and
621 SHRIMP zircon U–Pb dating of silicic ignimbrites, post-volcanic Xuanwei
622 Formation and clay tuff at the Chaotian scetion. Earth Planet. Sci. Lett. 255, 306-
623 323.
624 He, Q., Xiao, L., Balta, B., Gao, R., Chen, J.Y., 2010. Variety and complexity of the
625 Late-Permian Emeishan basalts: Reappraisal of plume-lithosphere interaction
626 processes. Lithos 119, 91-107.
627 Hirajima, T., Ishiwatari, A., Gong, B., Zhang, R.Y., Nozaka, A.T., 1990. Coesite from
628 Mengzhong eclogite at Dhonghai county, northeastern Jiangsu province, China.
629 Mineral. Mag. 54(377), 579-583.
630 Hofmann, A.W., 1997. Mantle geochemistry: The message from oceanic volcanism.
631 Nature 385, 219-229.
632 Hofmann, A.W., Jochum, K.P., Seufert, M., White, W.M., 1986. Nb and Pb in oceanic
633 basalts: new constraints on mantle evolution. Earth Planet. Sci. Lett. 79, 33-45.
634 Hou, T., Zhang, Z.C., Kusky, T., Du, Y.S., Liu, J.L., Zhao, Z.D., 2011. A reappraisal of
635 the high-Ti and low-Ti classification of basalts and petrogenetic linkage between
636 basalts and mafic-ultramafic intrusions in the Emeishan Large Igneous Province,
637 SW China. Ore Geol. Rev. 41, 133-143.
638 Hou, Y.L., Zhong, Y.T., Xu, Y.G., He, B., 2017. The provenance of late Permian karstic
639 bauxite deposits in SW China, constrained by the geochemistry of interbedded
640 clastic rocks, and U-Pb-Hf-O isotopes of detrital zircons. Lithos 278-281, 240-254.
641 Hu, M.Y., Hu, Z.G., Wei, G.Q., Yang, W., Liu, M.C., 2012. Sequence lithofacies

642 paleogeography and reservoir prediction of the Maokou Formation in Sichuan
643 Basin. Petrol. Explor. Dev. 39(1), 45-55. In Chinese with English abstract.
644 Huang, B., Yan, Y., Piper, J.D.A., Zhang, D., Yi, Z., Yu, S., Zhou, T., 2018.
645 Paleomagnetic constraints on the paleogeography of the East Asian blocks during
646 Late Paleozoic and Early Mesozoic times. Earth-Sci. Rev. 186, 8-36.
647 Huang, H., Huyskens, M.H., Yin, Q.Z., Cawood, P.A., Hou, M.C., Yang, J.H., Xiong,
648 F.H., Du, Y.S., Yang, C.C., 2022. Eruptive tempo of Emeishan large igneous
649 province, southwestern China and northern Vietnam: Relations to biotic crises and
650 paleoclimate changes around the Guadalupian-Lopingian boundary. Geology doi:
651 https://doi.org/10.1130/G50183.1.
652 Kamenetsky, V.S., Chung, S.L., Kamenetsky, M., Kuzmin, D.V., 2012. Picrites from
653 the Emeishan Large Igneous Province, SW China: a Compositional Continuum in
654 Primitive Magmas and their Respective Mantle Sources. J. Petrol. 53(10), 2095-
655 2113.
656 LaFlèche, M.R., Camiré, G., Jenner, G.A., 1998. Geochemistry of post-Acadian,
657 Carboniferous continental intraplate basalts from the Maritimes basin, Magdalen
658 islands, Québec, Canada. Chem. Geol. 148, 115-136.
659 Lai, S.C., Qin, J.F., Li, Y.F., Li, S.Z., Santosh, M., 2012. Permian high-Ti/Y basalts
660 from the eastern part of the Emeishan Large Igneous Province, Southwestern
661 China: Petrogenesis and tectonic implications. J. Asian Earth Sci. 47, 216-230.
662 Lassiter J.C., Depaolo, D.J., 1997. Plume/lithosphere interaction in the generation of
663 continental and oceanic flood basalts: Chemical and isotopic constraints. Large
664 igneous provinces: Continental, oceanic, and planetary flood volcanism.
665 Geophysical Monograph 100, 335-355.
666 Li, C., Ripley, E.M., Tao, Y., Hu, R.Z., 2016b. The significance of PGE variations with

667 Sr-Nd isotopes and lithophile elements in the Emeishan flood basalt province from
668 SW China to northern Vietnam. Lithos 248-251, 1-11.
669 Li, C.F., Li, X.H., Li, Q.L., Guo, J.H., Yang, Y.H., 2012. Rapid and precise
670 determination of Sr and Nd isotopic ratios in geological samples from the same
671 filament loading by thermal ionization mass spectrometry employing a single-step
672 separation scheme. Anal. Chim. Acta 727(10), 54-60.
673 Li, H.B., Zhang, Z.C., Ernst, R., Lu, L.S., Santosh, M., Zhang, D.Y., Cheng, Z.G., 2015.
674 Giant radiating mafic dyke swarm of the Emeishan Large Igneous Province,
675 Identifying the mantle plume centre. Terra Nova 27(4), 247-257.
676 Li, H.B., Zhang, Z.C., Santosh, M., Lü, L.S., Han, L., Liu, W., 2017a. Late Permian
677 basalts in the Yanghe area, eastern Sichuan Province, SW China, Implications for
678 the geodynamics of the Emeishan flood basalt province and Permian global mass
679 extinction. J. Asian Earth Sci. 134, 293-308.
680 Li, H.B., Zhang, Z.C., Santosh, M., Lü, L.S., Han, L., Liu, W., Cheng, Z.G., 2016a.
681 Late Permian basalts in the northwestern margin of the Emeishan Large Igneous
682 Province, Implications for the origin of the Songpan-Ganzi terrane. Lithos 256-
683 257, 75-87.
684 Li, J., Zhong, H., Zhu, W.G., Bai, Z.J., Hu, W.J., 2017c. Elemental and Sr–Nd isotopic
685 geochemistry of Permian Emeishan flood basalts in Zhaotong, Yunnan Province,
686 SW China. Int. J. Earth Sci. 106, 617-630.
687 Li, J., Tang, S.H., Zhu, X.K., Pan, C.X., 2017b. Production and Certification of the
688 Reference MaterialGSB 04-3258-2015 as a $^{143}Nd/^{144}Nd$ Isotope Ratio Reference.
689 Geostand. Geoanal. Res. 41, 255-262.
690 Li, J., Xu, J.F., Suzuki, K., He, B., Xu, Y.G., Ren, Z.Y., 2010. Os, Nd and Sr isotope
691 and trace element geochemistry of the Muli picrites: Insights into the mantle

692 source of the Emeishan Large Igneous Province. Lithos 119(1-2), 108-122.
693 Liang, Y.X., Li, H., Zhang, D.D., Yang, K., Zhou, D.W., Zheng, T.Y., Dong, Y.K., Zhai,
694 L.G., 2021. Geochemical characteristics and genetic analysis of Huayingshan
695 Emeishan basalt in Sichuan Basin. Chin. J. Geol. 56(1), 288-302. In Chinese with
696 English abstract.
697 Liao, B.L., Zhang, Z.C., Kou, C.H., Li, H.B., 2012. Geochemistry of the Shuicheng
698 Permian sodium trachybasalts in Guizhou Province and constraints on the mantle
699 sources. Acta Petrol. Sin. 28(4), 1238-1250. In Chinese with English abstract.
700 Liu, R., Luo, B., Li, Y., Qiu, N.S., Wang, W., Zhang, Y., He, Q.L., Pei, S.Q., 2021a.
701 Relationship between Permian volcanic rocks distribution and karst
702 paleogeomorphology of Maokou Formation and its significance for petroleum
703 exploration in western Sichuan Basin, SW China. Petrol. Explor. Dev. 48(3), 575-
704 585. In Chinese with English abstract.
705 Liu, X.J., Liang, Q.D., Li, Z.L., Castillo, P.R., Shi Y., Xu, J.F., Huang, X.L., Liao, S.A.,
706 Huang, W.L., Wu, W.N., 2017. Origin of Permian extremely high-Ti/Y mafic lavas
707 and dykes from Western Guangxi, SW China: Implications for the Emeishan
708 mantle plume magmatism. J. Asian Earth Sci. 141, 97-111.
709 Liu, X.Y., Qiu, N.S., Søager, N., Fu, X.D., Liu, R., 2022. Geochemistry of Late Permian
710 basalts from boreholes in the Sichuan Basin, SW China: Implications for an
711 extension of the Emeishan large igneous province. Chem. Geol. 588, 120636.
712 Liu, Y.D., Li, L., van Wijk, J., Li, A.B., Fu, Y. V., 2021b. Surface-wave tomography of
713 the Emeishan large igneous province (China): Magma storage system, hidden
714 hotspot track, and its impact on the Capitanian mass extinction. Geology 49(9),
715 1032-1037.
716 Liu, Y.S., Zong, K.Q., Kelemen, P.B., Gao, S., 2008. Geochemistry and magmatic

history of eclogites and ultramafic rocks from the Chinese continental scientific drill hole: subduction and ultrahigh-pressure metamorphism of lower crustal cumulates. Chem. Geol. 247, 133-153.

Ma, C.Q., Ehlers, C., Xu, C.H., 2000. The roots of the Dabieshan ultrahigh-pressure metamorphic terrain: constraints from geochemistry and Nd-Sr isotope systematics. Precambrian Res. 102, 279-301.

McDonough, W.F., 1990. Constraints on the composition of the continental lithosphere mantle. Earth Planet. Sci. Lett. 101, 1-18.

McKenzie, D., O'Nions, R.K., 1991. Partial melt distributions from inversion of rare earth element concentrations. J. Petrol. 32, 1021-1091.

McKenzie, D., O'Nions, R.K., 1995. The Source Regions of Ocean Island Basalts. J. Petrol. 36(1), 133-159.

Neal, G.R., Mahoney, J.J., Chazey III, W.J., 2002. Mantle sources and the highly variable role of the continental lithosphere in basalt petrogenesis of the Kerguelen Plateau and the broken ridge LIP: results from ODP Leg 183. J. Petrol. 43, 1177-1205.

Niu, Y.L., 2021. Lithosphere thickness controls the extent of mantle melting, depth of melt extraction and basalt compositions in all tectonic settings on Earth-A review and new perspectives. Earth-Sci. Rev. 217, 103614.

Norman, M.D., 1998. Melting and metasomatism in the continental lithosphere: laser ablation ICPMS analysis of minerals in spinel lherzolites from eastern Australia. Contrib. Mineral. Petrol. 130(3-4), 240-255.

Palacz, Z.A., Saunders, A.D., 1986. Coupled trace element and isotope enrichment in the Cook–Austral– Samoa islands, southwest Pacific. Earth Planet. Sci. Lett. 79, 270-280.

742 Pearce, J.A., 2008. Geochemical fingerprinting of oceanic basalts with applications to
743 ophiolite classification and the search for Archean oceanic crust. Lithos 100(1–4),
744 14-48.
745 Qin, X. F., Wang, Z. Q., Zhang, Y. L., Pan, L. Z., Hu, G. A., Zhou, F. S., 2011.
746 Geochronology and geochemistry of early Mesozoic acid volcanic rocks from
747 Southwest Guangxi: Constraints on tectonic evolution of the southwestern
748 segment of Qinzhou- Hangzhou joint belt. Acta Petrol. Sin. 27(3), 794-808.
749 Ren, Z.Y., Wu, Y.D., Zhang, L., Nichols, A.R.L., Hong, L.B., Zhang, Y.H., Zhang, Y.,
750 Liu, J.Q., Xu, Y.G., 2017. Primary magmas and mantle sources of Emeishan
751 basalts constrained from major element, trace element and Pb isotope
752 compositions of olivine-hosted melt inclusions. Geochim. Cosmochim. Acta
753 208(2), 63-85.
754 Rudnick, R.L., Gao, S., 2003. Composition of the Continental Crust. Treatise Geochem.
755 3, 1-64.
756 Rudnick, R.L., Gao, S., Ling, W.L., Liu, Y.S., McDonough, W.F., 2004. Petrology and
757 geochemistry of spinel peridotite xenoliths from Hannuoba and Qixia, North
758 China Craton. Lithos 77, 609-637.
759 Shellnutt, J. G., 2014. The Emeishan large igneous province: a synthesis. Geosci. Front.
760 5(3), 369-394.
761 Shellnutt, J.G., Denyszyn, S.W., Mundil, R., 2012. Precise age determination of mafic
762 and felsic intrusive rocks from the Permian Emeishan large igneous province (SW
763 China). Gondwana Res. 22, 118-126.
764 Sobolev, A.V., Hofmann, A.W., Kuzmin, D.V., Yaxley, G.M., Arndt, N.T., Chung, S.L.,
765 Danyushevsky, L.V., Elliott, T., Frey, F.A., Garcia, M.O., 2007. The amount of
766 recycled crust in sources of mantle-derived melts. Science 316, 412-417.

767 Sobolev, A.V., Hofmann, A.W., Nikogosian, I.K., 2000. Recycled oceanic crust
768 observed in “ghost plagioclase” within the source of Mauna Loa lavas. Nature 404,
769 986-990.
770 Song, X.Y., Qi, H.W., Robinson, P.T., Zhou, M.F., Cao, Z.M., Chen, L.M., 2008.
771 Melting of the subcontinental lithosphere mantle by the Emeishan mantle plume:
772 evidence from the basal alkaline basalts in Dongchuan, Yunnan, Southwestern
773 China. Lithos 100, 93-111.
774 Song, X.Y., Zhou, M.F., Hou, Z.Q., Cao, Z.M., Wang, Y.L., Li, Y.G., 2001.
775 Geochemical constraints on the mantle source of the Upper Permian Emeishan
776 continental flood basalts, southwestern China. Int. Geol. Rev. 43, 213-225.
777 Stanley, C.R., Russel, J.K., 1989. Petrologic hypothesis testing with Pearce element
778 ration diagrams derivation of diagram axes. Contrib. Mineral. Petrol. 103, 78-89.
779 Sun, S.S., McDonough, W.F., 1989. Chemical and isotopic systematics of oceanic
780 basalt: Implications for mantle composition and processes. Geo. Soc. London
781 Special Pub. 42, 313-345.
782 Tao, Y., Ma, Y., Miao, L., Zhu, F., 2009. SHRIMP U-Pb zircon age of the Jinbaoshan
783 ultramafic intrusion, Yunnan Province, SW China. Chin. Sci. Bull. 54, 168-172.
784 Thirlwall, M.F., Upton, B.G.J., Jenkins, C., 1994. Interaction between continental
785 lithosphere and the Iceland plume—Sr-Nd-Pb isotope geochemistry of Tertiary
786 basalts, NE Greenland. J. Petrol. 35(3), 839-879.
787 Thompson, G.M., Ali, J.R., Song, X.Y., Jolley, D.W., 2001. Emeishan basalts, SW
788 China: Reappraisal of the formation’s type area stratigraphy and a discussion of its
789 significance as a large igneous province. J. Geol. Soc. 158(4), 593-599.
790 Tian, J.C., Lin, X.B., Guo, W., Zhang, X., Huang, P.H., 2017. Geological significance
791 of oil and gas in the Permian basalt eruption event in Sichuan Basin, China. J.

792 Chengdu University Technology (Sci. Technology Edition) 44(1), 14-20. In
793 Chinese with English abstract.
794 Tian, Y.L., Li, Y., Meng, F.C., Zhao, L.K., Wu, Z.P., Du, Q., 2021. A study of the
795 petrogenesis and spatial difference of the Emeishan large igneous province: Based
796 on geochemical analysis and simulation of the high-Ti basalts in the whole region.
797 Acta Petrol. Mineral. 40(4), 687-703. In Chinese with English abstract.
798 Wang, C.Y., Zhou, M.F., 2006. Genesis of the Permian Baimazhai magmatic Ni-Cu-
799 (PGE) sulfide deposit, Yunnan, SW China. Miner. Deposita 41, 771-783.
800 Wang, C.Y., Zhou, M.F., Qi, L., 2007. Permian flood basalts and mafic intrusions in the
801 Jinping (SW China)-Song Da (northern Vietnam) district: Mantle sources, crustal
802 contamination and sulfide segregation. Chem. Geol. 243, 317-343.
803 Wang, Z. L., Xu, D.R., WU, C.J., Fu, W.W., Wang, L., Wu, J., 2013. Discovery of the
804 late Paleozoic ocean island basalts (OIB) in Hainan Island and their geodynamic
805 implications. Acta Petrol. Sin. 29(3), 875-886.
806 Weaver, B.L., 1991. The origin of ocean island basalt end-member compositions: trace
807 element and isotopic constraints. Earth Planet. Sci. Lett. 104, 381-397.
808 Wei, X., Xu, Y.G., 2013. Petrogenesis of the mafic dykes from Bachu and implications
809 for the magma evolution of the Tarim large igneous province, SW China. Acta
810 Petrol. Sin. 29(10), 3323-3335.
811 Weis, D., Kieffer, B., Maerschalk, C., Pretorius, W., Barling, J., 2005. High-precision
812 Pb-Sr-Nd-Hf isotopic characterization of USGS BHVO-1 and BHVO-2 reference
813 materials. Geochem. Geophys. Geosyst. 6(2), 1-10.
814 Xiao, D., Tan, X.C., Shan, S.J., Chen, Y.Q., Xia, J.W., Yang, J., Zhou, T., Cheng, Y.,
815 2014. The restoration of palaeokarst geomorphology of middle Permian Maokou
816 Formation and its petroleum geological significance in southern Sichuan Basin.

817 Acta Geol. Sin. 88(10), 1992-2002. In Chinese with English abstract.
818 Xiao, L., Xu, Y.G., Chung, S.L., He, B., Mei, H.J., 2003. Chemostratigraphic
819 correlation of Upper Permian lavas from Yunnan province, China: extent of the
820 Emeishan large igneous province. Int. Geol. Rev. 45, 753-766.
821 Xiao, L., Xu, Y.G., Mei, H.J., Zheng, Y.F., He, B., Pirajno, F., 2004. Distinct mantle
822 sources of low-Ti and high-Ti basalts from the Eastern Emeishan Large Igneous
823 Province, SW China: implications for plume-lithosphere interaction. Earth Planet.
824 Sci. Lett. 228(3-4), 525-546.
825 Xie, J., Ritzwoller, M.H., Shen, W., Yang, Y., Zheng, Y., Zhou, L., 2013. Crustal radial
826 anisotropy across eastern Tibet and the western Yangtze craton. J. Geophys. Res.
827 - Sol. Ea. 118(8), 4226-4252.
828 Xu, J., Xia, X.P., Lai, C.K., Zhou, M., Ma, P., 2019. First identification of Late Permian
829 Nb- enriched basalts in Ailaoshan region (SW Yunnan, China): Contribution from
830 Emeishan plume to subduction of eastern Paleotethys. Geophys. Res. Lett. 46,
831 2511-2523.
832 Xu, J., Xia, X.P., Wang, Q., Spencer, C.J., He, B., Lai, C.K., 2021. Low-$\delta^{18}O$ A-type
833 granites in SW China: Evidence for the interaction between the subducted
834 Paleotethyan slab and the Emeishan mantle plume. Geol Soc. Am. Bull.
835 https://doi.org/10.1130/B35929.1.
836 Xu, J.F., Suzuki K., Xu Y.G., Mei H.J., Li J., 2007. Os, Pb, and Nd isotope geochemistry
837 of the Permian Emeishan continental flood basalts: Insights into the source of a
838 large igneous province. Geochim. Cosmochim. Acta 71, 2104-2119.
839 Xu, R., Liu, Y., Lambart, S., 2020. Melting of a hydrous peridotite mantle source under
840 the Emeishan large igneous province. Earth-Sci. Rev. 207, 103253.
841 Xu, Y.G., Chung, S.L., Jahn, B.M., Wu, G.Y., 2001. Petrologic and geochemical

842 constraints on the petrogenesis of Permian-Triassic Emeishan flood basalts in
843 southern China. Lithos 58, 145-168.
844 Xu, Y.G., He, B., Chung, S.L., Menzies, M.A., Frey, F.A., 2014. Geologic, geochemical
845 and geophysical consequences of plume involvement in the Emeishan flood-basalt
846 province. Geology 32, 917-920.
847 Xu, Y.G., He, B., Luo, Z.Y., Liu, H.Q., 2013. Study on mantle plume and Large igneous
848 provinces in China: An overview and perspectives. Bull. Mineral. Petrol.
849 Geochem. 32(1), 25-39. In Chinese with English abstract.
850 Xu, Y.G., Luo, Z.Y., Huang, X.L., He, B., Xiao, L., Xie, L.W., Shi, Y.R., 2008. Zircon
851 U-Pb and Hf isotope constraints on crustal melting associated with the Emeishan
852 mantle plume. Geochim. Cosmochim. Acta 72(13), 3084-3104.
853 Xu, Y.G., Zhong, Y.T., Wei, X., Chen, J., Liu, H.Q., Xie, W., Luo, Z.Y., Li, H.Y., He,
854 B., Huang, X.L., Wang, Y., Chen, Y., 2017. Permian Mantle Plumes and Earth's
855 Surface System Evolution. Bull. Mineral. Petrol. Geochem. 36(3), 359-373+358.
856 In Chinese with English abstract.
857 Yan, D.P., Qiu, L., Wells, M.L., Zhou, M.F., Meng, X., Lu, S., Zhang, S., Wang, Y., Li,
858 S.B., 2018a. Structural and Geochronological constraints on the early Mesozoic
859 North Longmen Shan Thrust Belt: Foreland fold- thrust propagation of the SW
860 Qinling Orogenic Belt, Northeastern Tibetan plateau. Tectonics 37(12), 4595-4624.
861 Yan, D.P., Zhou, Y., Qiu, L., Wells, M.L., Mu, H., Xu, C.G., 2018b. The Longmenshan
862 tectonic complex and adjacent tectonic units in the eastern margin of the Tibetan
863 Plateau: a review. J. Asian Earth Sci. 164, 33-57.
864 Yang, J., Cawood, P. A., Du, Y., Huang, H., Hu, L., 2012. Detrital record of Indosinian
865 mountain building in SW China: Provenance of the middle Triassic turbidites in
866 the Youjiang Basin. Tectonophysics 574- 575, 105-117.

867 Yang, Z., He, B., 2012. Geochronology of detrital zircons from the middle Triassic
868 sedimentary rocks in the Nanpanjiang Basin: Provenance and its geological
869 significance. Geotectonica et Metallogenia 36(4), 581-596. In Chinese with
870 English abstract.
871 Zhai, M.G., Yang, R.Y., 1986. Early Precambrian gneiss basement in the Panxi area,
872 Southwest China. Acta Petrol. Sin. 2(3), 22-37. In Chinese with English abstract.
873 Zhang, J., Cao, X.M., Wang, J.L., Zhang, Z.C., 2011. Petrology of the Permian
874 Langmao Basaltic Porphyry, Luquan County, Yunnan Province: Implications for
875 the Petrogenesis of High-Ti Basalts. Geoscience 25(4), 692-702. In Chinese with
876 English abstract.
877 Zhang, L., Ren, Z.Y., Handler, M.R., Wu, Y.D., Xu, Y.G., 2019. The origins of high-Ti
878 and low-Ti magmas in large igneous provinces, insights from melt inclusion trace
879 elements and Sr-Pb isotopes in the Emeishan large Igneous Province. Lithos 344-
880 345, 122-133.
881 Zhang, L., Ren, Z.Y., Zhang, L., Wu, Y.D., Qian, S.P., Xia, X.P., Xu, Y.G., 2021. Nature
882 of the mantle plume under the Emeishan large igneous province: Constraints from
883 olivine-hosted melt inclusions of the Lijiang picrites. J. Geophys. Res. Sol. Ea.
884 126, e2020JB021022.
885 Zhang, W., Hu Z.C., 2020. Estimation of isotopic reference values for pure materials
886 and geological reference materials. At. Spectrosc. 41(3), 93-102.
887 Zhang, W., Hu, Z.C., Liu, Y.S., 2020a. Iso-Compass: new freeware software for isotopic
888 data reduction of LA-MC-ICP-MS. J. Anal. At. Spectrom. 35, 1087-1096.
889 Zhang, Y., Chen, S.L., Zhang, X.L., Zhang, X.H., Xie, C., Chen, C., Yang, Y.R., Gao,
890 Y.L., 2020b. Restoration of paleokarst geomorphology of Lower Permian Maokou
891 Formation and its petroleum exploration implication in Sichuan Basin. Lithologic

892 Reservoirs 32(3), 44-55. In Chinese with English abstract.
893 Zhang, Y.X. 1988. Panxi rift. Beijing: Geological Press.
894 Zhang, Z.C., Mahoney, J.J., Mao, J.W., Wang, F.S., 2006. Geochemistry of picritic and
895 associated basalt flows of the western Emeishan flood basalt province, China. J.
896 Petrol. 47, 1997-2019.
897 Zhang, Z.C., Wang, F.S., 2003. Sr, Nd and Pb Isotopic Characteristics of Emeishan
898 Baslat Province and Discussion on Their Source Region. Earth Sci.- J. China
899 University of Geosciences 28(4), 431-439. In Chinese with English abstract.
900 Zhang, Z.C., Wang, F.S., Fan, W.M., Deng, H.L., Xu, Y.G., Xu, J.F., Wang, Y.J., 2001.
901 A Discussion on Some Problems Concerning the Study of the Emeishan Basalts.
902 Acta Petrol. Mineral. 20(3), 239-246. In Chinese with English abstract.
903 Zhang, Z.C., Zhi, X.C., Chen, L., Saunders, A.D., Reichow, M.K., 2008. Re-Os isotopic
904 compositions of picrites from the Emeishan flood basalt province, China. Earth
905 Planet. Sci. Lett. 276, 30-39.
906 Zheng, L.D., Yang, Z.Y., Tong, Y.B., Yuan, W., 2010. Magnetostratigraphic constraints
907 on two-stage eruptions of the Emeishan continental flood basalts. Geochem.
908 Geophy. Geosy. 11(12), 1-19.
909 Zhong, H., Zhu, W.G., 2006. Geochronology of layered mafic intrusions from the Pan-
910 Xi area in the Emeishan large igneous province, SW China. Miner. Deposita 41,
911 599-606.
912 Zhong, Y.T., He, B., Mundil, R., Xu, Y.G., 2014. CA-TIMS zircon U-Pb dating of felsic
913 ignimbrite from the Binchuan section: implications for the termination age of
914 Emeishan large igneous province. Lithos 204, 14-19.
915 Zhong, Y.T., He, B., Xu, Y.G., 2013. Mineralogy and geochemistry of claystones from
916 the Guadalupian– Lopingian boundary at Penglaitan, South China: Insights into

the pre- Lopingian geological events. J. Asian Earth Sci. 62, 438-462.

Zhou, M.F., Chen, W.T., Wang, C.Y., Prevec, S.A., Liu, P.P., Howarth, G.H., 2013. Two stages of immiscible liquid separation in the formation of Panzhihua-type Fe-Ti-V oxide deposits, SW China. Geosci. Front. 4, 481-502.

Zhou, M.F., Malpas, J.G., Song, X.Y., Robinson, P.T., Sun, M., Kennedy, A., Lesher, M., Keays, R.R., 2002. A temporal link between the Emeishan large igneous province (SW China) and the end-Guadalupian mass extinction. Earth Planet. Sci. Lett. 196(3-4), 113-122.

Zhou, M.F., Wang, Z.C., Zhao, W.W., Qi, L., Zhao, Z., Zhou, J.X., Huang, Z.L., Chen, W.T., 2022. A reconnaissance study of potentially important scandium deposits associated with carbonatite and alkaline igneous complexes of the Permian Emeishan Large Igneous Province, SW China. J. Asian Earth Sci. 236, 105309.

Zhou, M.F., Zhao, J.H., Qi, L., Su, W.C., Hu, R.Z., 2006. Zircon U-Pb geochronology and elemental and Sr-Nd isotope geochemistry of Permian mafic rocks in the Funing area, SW China. Contrib. Mineral. Petrol. 151, 1-19.

Zhu, C.Q., Hu, S.B., Qiu, N.S., Rao, S., Yuan, Y.S., 2016. The thermal history of the Sichuan Basin, SW China: evidence from the deep boreholes. Sci. China, Ser. D: Earth Sci. 59, 70-82.

Zhu, C.Q., Xu, M., Yuan, Y.S., Zhao, Y.Q., Shan, J.N., He, Z.G., Tian, Y.T., Hu, S.B., 2010. Palaeogeothermal response and record of the effusing of Emeishan basalts in the Sichuan basin. Chin. Sci. B 55, 949-956.

Zhu, D.C., Mo, X.X., Wang, L.Q., Zhao, Z.D., Liao, Z.L., 2008. Hotspot-ridge interaction of the evolution of Neo-Tethys: insights from the Late Jurassic-Early Cretaceous magmatism in southern Tibet. Acta Petrol. Sin. 24(2), 225-237.

Zhu, D.C., Pan, G.T., Mo, X.X., Liao, Z.L., Jiang, X.S., Wang, L.Q., Zhao, Z.D., 2007.

Petrogenesis of volcanic rocks in the sangxiu formation, central segment of Tethyan Himalaya: a probable example of plume-lithosphere interaction. J. Asian Earth Sci. 29(2-3), 320-335.

Zhu, J., 2019. A study of mantle plume dynamics and its environmental effect in the Emeishan large igneous province. Beijing: China University of Geosciences (Beijing). In Chinese with English abstract.

Zhu, J., Zhang, Z.C., Reichow, M.K., Li, H.B., Cai, W.C., Pan, R.H., 2018. Weak vertical surface movement caused by the ascent of the Emeishan mantle anomaly. J. Geophys. Res. Sol. Ea. 123(2), 1018-1034.

Zi, J.W., Fan, W.M., Wang, Y.J., Cawood, P.A., Peng, T.P., Sun, L.H., Xu, Z.Q., 2010. U-Pb geochronology and geochemistry of the Dashibao Basalts in the Songpan-Ganzi Terrane, SW China, with implications for the age of Emeishan volcanism. Am. J. Sci. 310(9), 1054-1080.

Fig. 1. Simplified geological map showing the inner, intermediate and outer zones of the ELIP and sampling locations (modified after He et al., 2003; Zi et al., 2010).

The inner, intermediate, and outer zones in the ELIP area were defined by He et al., 2003. The hotspot track was obtained from Liu et al., 2021b. The ELIP eruption centre was obtained from He et al., 2010.

CAO = Central Asia Orogen; TM = Tarim Block; AHO = Alpine–Himalaya Orogen; QKO = Qinling-Qilian-Kunlun Orogen; NCC = North China Craton; YC = Yangtze Craton; CC = Cathaysia Craton.

Fig. 2. Schematic map of southwestern China showing the distribution of volcanic rocks in the Late Permian (a), and geological map of the Sichuan Basin showing the distribution of the Late Permian volcanic rocks (b) (modified after Liu et al., 2021a).

Fig. 3. Representative photos of field geology and petrographic features of the volcanic rocks from the drill cores and outcrops in and around the Sichuan Basin.

a. ST1-2, stomata almond basalt; b. YT1-7, massive basalt (cross-polarised light); c. ZG2-5, massive basalt; d. ZG2-5, massive basalt (cross-polarised light); e. Longmendong section; f. Longmendong basalt outcrop; g. Longchi basalt outcrop; h. Xinlin basalt outcrop.

Pl-plagioclase, Cpx-clinopyroxene.

Fig. 4. The connecting well section of boreholes ZG2-YT1-TF2-ZJ2-ST1 in the Sichuan Basin (based on logging data from Southwest Oil and Gas Field Company,

978 PetroChina).

979 The location of the connecting well section is shown in Fig. 2

980

981 Fig. 5. TiO_2 vs. Ti/Y (a), and Ol'-Ne'-Q' (b) classification diagrams for the basalts in
982 Sichuan Basin (LT and HT data from the inner zone in the ELIP were obtained from
983 Song et al., 2001; Xiao et al., 2004; Xu et al., 2001; Zhang et al., 2006; data of HT from
984 the outer zone were obtained from Fan et al., 2008; Lai et al., 2012; Li et al., 2016b;
985 Wang et al., 2007; Xu et al., 2007).

986 (a) LT-low Ti series, HT-high low series. (b). A-Alkaline, S-Sub-alkaline.

987

988 Fig. 6. Selected elements plotted vs. MgO for the basalts from the Sichuan Basin

989

990 Fig. 7. Chondrite-normalised REE (a), and primitive mantle-normalised trace element
991 (b) for the basalts in the Sichuan Basin (data for chondrite, primitive mantle and OIB
992 are from Sun and McDonough, 1989; sources of geochemical data from other regions
993 in the ELIP as for Fig. 5).

994

995 Fig. 8. Plots of $^{87}Sr/^{86}Sr(t)$ vs. $\varepsilon_{Nd}(t)$ (a), $^{206}Pb/^{204}Pb(t)$ vs. $^{87}Sr/^{86}Sr(t)$ (b), $^{206}Pb/^{204}Pb(t)$
996 vs. $^{207}Pb/^{204}Pb(t)$ (c), and $^{206}Pb/^{204}Pb(t)$ vs. $^{208}Pb/^{204}Pb(t)$ (d) for the basalts in the
997 Sichuan Basin (Sources of geochemical data from other regions in the ELIP as for Fig.
998 5. The fields of DM, MORB, Atlantic-Pacific MORB, Indian Ocean MORB, FOZO
999 (focal zone), OIB, Dupal OIB, BSE (bulk silicate earth), HIMU (mantle with high U/Pb
1000 ratios), EMI and EMII (enriched mantle), Kerguelen are from Barling and Goldstein,
1001 1990; Deniel, 1998; Hamelin and Allègre, 1985; Hart, 1984; Hawkesworth et al., 1984;

and Weaver, 1991. The LoNd (low Nd) array and NHRL (Northern Hemisphere Reference Line) are from Hart, 1984. The Yangtze Block crustal compositions are from Chen and Jahn, 1998; Gao et al., 1999; Ma et al.,2000 and Zhang et al., 2008.)

Fig. 9. Plots of Ce vs. Nb/Th (a), $(Th/Ta)_P$ vs. $(La/Nb)_P$ (b), SiO_2 vs. $^{87}Sr/^{86}Sr(t)$ (c), and SiO_2 vs. $\varepsilon_{Nd}(t)$ (d) for the basalts in the Sichuan Basin (The fields of PM, N-MORB and E-MORB are from Sun and McDonough, 1989; SCLM are from McDonough, 1990; UC (upper crust), MC (middle crust) and LC (lower crust) are from Rudnick and Gao, 2003; Kerguelen alkaline basalts are from http://georoc.mpch-mainz.gwdg.de/georoc/Entry.html.)

Fig. 10. Plots of Mg# vs. CaO/Al_2O_3 (a), Eu_N/Eu^* vs. Th+U (b), and Eu_N/Eu^* vs. $\sum REE$ (c) for the basalts in the Sichuan Basin (sources of geochemical data from other regions in the ELIP as for Fig. 5; the sample 20LMD05 is assumed as the initial melt of fractional crystallization, mineral fractionation vectors are calculated using Rayleigh fractionation law, and partition coefficients are from McKenzie and O'Nions, 1991).

Pl-plagioclase, Cpx-clinopyroxene and Opx-orthopyroxene.

Fig. 11. Diagrams of Nb/Yb vs. Th/Yb (a), and Ti/Yb vs. Nb/Th (b) for the basalts in the Sichuan Basin (sources of geochemical data from other regions in the ELIP as for Fig. 5. (a) MORB-OIB array, subduction component adding models are from Pearce, 2008. The arrow in the Figure represents the trend of adding subduction component. (b) SCLM are from McDonough, 1990; UC, MC and LC are from Rudnick et al., 2003; Hawaiian OIB mean was obtained from Feigenson et al., 1996; Kerguelen alkaline

basalts are from http://georoc.mpch-mainz.gwdg.de/georoc/Entry.html; Sangxiu Formation basalts were obtained from Zhu et al., 2007).

Fig. 12. Plots of $\varepsilon_{Nd}(t)$ vs. $(La/Yb)_N$ (a), Yb vs. La/Yb (b), Th/La vs. Nb/U (c), and $^{206}Pb/^{204}Pb$ vs. $\varepsilon_{Nd}(t)$ (d) for the basalts in the Sichuan Basin (sources of geochemical data from other regions in the ELIP as for Fig. 5).

Fig. 13. Diagrams of $(La/Sm)_N$ vs. $(Tb/Yb)_N$ (a), and Sm/Yb vs. La/Sm (b) for the basalts in the Sichuan Basin (sources of geochemical data from other regions in the ELIP as for Fig. 5; (b) batch melting trends for garnet and spinel lherzolite were obtained from Lassiter and Depaolo, 1997).

Fig. 14. Stratigraphic variation of the representative lava successions in the ELIP (modified after Xiao et al., 2004; Xu et al., 2001, 2014).

Fig. 15. Evolution model of EILP during the Middle Permian. (The framework for the plumbing system of ELIP associated with the Emeishan mantle plume was modified from Feng et al. (2022) and Liu et al. (2021b). The boundaries of the inner-intermediate-outer zones in the ELIP was defined by He et al. (2003) and Xiao et al. (2004). LQF, HYF and QYF represent the Longquanshan fault, Huayingshan fault and Longquanshan fault, respectively. LT and HT represent low-Ti basalts and high-Ti basalts, respectively. The NE (northeastward) arrows show the direction of movement of the South China Block (Liu et al., 2021b).)

a. During the early-Guadalupian (~269 Ma), Western Yangtze Block experienced Ailaoshan slab (Paleotethys Ocean) eastward subduction, and the adjacent Emeishan mantle plume was modified by the recycled lithospheric fragments. b. In the first stage of end-Guadalupian (260~257 Ma), lithosphere mantle melted and formed the low-Ti basalts (LT) in the inner zone. c. In the second stage of end-Guadalupian (260~257 Ma), the mantle plume melted and formed the high-Ti basalts (HT) in the inner-intermediate-outer zones, with high-Ti basalts overlying low-Ti basalts in the inner zone.

1056 Table 1 Zircon U-Pb dating results of the Emeishan large igneous province

Locality		Rock type	Analytical method	Age/Ma	Reference
Inner Zone	Dali-Jiangwei	acid volcanic rock	ID-TIMS zircon U-Pb	258.9±0.5	Xu et al. (2013)
	Midu-Jinbaoshan	wehrlite	Shrimp zircon U-Pb	260.6±3.5	Tao et al. (2009)
		hornblendite	Shrimp zircon U-Pb	260.7±5.6	
	Binchuan	acid tuff	ID-TIMS zircon U-Pb	259.1±0.5	Zhong et al. (2014)
		basalt	Shrimp zircon U-Pb	256.2±1.4	Li et al. (2016a)
	Panxi-Daheishan	syenite	ID-TIMS zircon U-Pb	259.1±0.5	Shellnutt et al. (2012)
	Panxi-Baima	granite	ID-TIMS zircon U-Pb	259.2±0.4	
	Panxi-Huangcao	syenite	ID-TIMS zircon U-Pb	258.9±0.7	
	Panxi-Cida	granite	ID-TIMS zircon U-Pb	258.4±0.6	
	Panxi-Maomaogou	syenite	Shrimp zircon U-Pb	261.6 ± 4.4	Xu et al. (2008)
	Panxi-Miyi	syenite	Shrimp zircon U-Pb	259.8 ± 3.5	
	Panxi-Salian	diorite	Shrimp zircon U-Pb	260.4 ± 3.6	
	Panxi-Taihe	granite	Shrimp zircon U-Pb	261.4 ± 2.3	
	Panxi-Hongge	gabbro	Shrimp zircon U-Pb	259.3±1.3	Zhong and Zhu (2006)
		gabbro	Shrimp zircon U-Pb	259.3 ± 1.3	
	Panxi-Binggu	gabbro	Shrimp zircon U-Pb	260.7 ± 0.8	
	Xinjie	gabbro	Shrimp zircon U-Pb	259±3	Zhou et al. (2002)
Intermediate Zone	Guizhou-Weining	boundary clay rock	ID-TIMS zircon U-Pb	258.1±0.6	Xu et al. (2013)
	Panxian-Zhudong	ignimbrite	ID-TIMS zircon U-Pb	258.3±1.4	Zhu (2019)
	Xingyi-Xiongwu	tuff	ID-TIMS zircon U-Pb	258.5±0.9	
	Puan-Louxia	tuff	ID-TIMS zircon U-Pb	258.1±1.1	
	Baimazhai	pyroxenite	Shrimp zircon U-Pb	258.5±3.5	Wang et al. (2006)
Outer Zone	Tubagou	basalt	Shrimp zircon U-Pb	257.3±2.0	Li et al. (2016b)
	Baise-Yangxu	basalt	Shrimp zircon U-Pb	259.1±4.0	Fan et al. (2008)
	Bama-Minan	basalt	Shrimp zircon U-Pb	259.6±5.9	
	Nayong-Xilin-Tianyang Area	basalt	LA-ICP-MS zircon U-Pb	257.0±9.0	Lai et al. (2012)

	Guangyuan-Chaotian	boundary clay rock	ID-TIMS zircon U-Pb	258.6±1.4	Xu et al. (2013)
				259.2±0.3	Zhong et al. (2014)
	Funing	diabase	Shrimp zircon U-Pb	260±3	Zhou et al. (2006)
		diorite	Shrimp zircon U-Pb	258±3	
	Mianhuadi	metagabbro	MC-ICP-MS zircon U-Pb	259.6±0.8	Zhou et al. (2013)

1057

1058 Table 2 Major elements (wt.%) and trace elements ($\times 10^{-6}$) contents for the analysed volcanic rocks in the Sichuan Basin

Samples	ST1-2	ST1-5	YT1-1	YT1-3	YT1-4	YT1-5	YT1-6	YT1-7	ZG2-4	ZG2-5	ZG2-7	ZG2-8	20LMD04	20LMD05	20LC04	20LC06	20XL01	20XL02	20XL02 (replicate)
Locality	ST1 Well		YT1 Well						ZG2 Well				Longmendong		Longchi		Xinlin		
SiO_2	49.64	48.78	48.62	47.55	46.69	47.67	48.67	48.96	46.59	47.64	48.74	45.59	45.99	48.99	45.94	49.08	49.21	48.12	48.32
TiO_2	4.01	3.87	4.06	3.91	4.17	4.19	3.83	3.71	4.01	3.98	4.05	4.14	3.69	3.73	4.08	3.69	4.24	3.82	3.84
Al_2O_3	13.75	13.66	13.69	13.66	13.64	13.82	14.99	14.96	13.07	12.98	13.30	13.70	13.44	13.90	13.91	13.88	13.57	13.08	13.06
$Fe_2O_3^T$	12.92	13.82	13.86	15.65	16.91	16.10	13.41	13.60	18.43	17.46	14.02	16.27	15.44	12.75	15.75	12.40	14.32	14.16	14.23
MnO	0.21	0.17	0.18	0.16	0.17	0.17	0.16	0.16	0.20	0.19	0.20	0.19	0.21	0.16	0.17	0.17	0.18	0.17	0.17
MgO	3.43	3.68	4.92	4.81	4.38	4.47	4.99	5.08	4.69	4.33	4.69	4.89	7.12	5.28	5.24	5.41	4.65	5.06	5.10
CaO	4.88	4.27	6.53	8.26	6.03	7.39	7.22	7.21	6.99	7.87	7.01	7.40	6.79	9.09	7.20	6.75	9.15	8.08	8.13
Na_2O	4.38	3.91	3.82	2.29	3.44	2.39	2.78	2.75	4.32	2.14	2.38	2.34	2.81	1.97	2.47	3.52	2.05	2.78	2.76
K_2O	0.22	0.56	1.96	1.73	2.36	1.98	1.92	1.93	0.85	1.94	2.21	2.03	1.51	1.42	1.17	2.15	0.99	1.83	1.85
P_2O_5	0.45	0.45	0.40	0.40	0.42	0.42	0.40	0.43	0.44	0.43	0.43	0.43	0.37	0.39	0.43	0.39	0.45	0.40	0.40
LOI	5.87	6.04	1.89	1.70	1.33	1.12	1.15	1.21	0.54	0.77	2.59	2.68	2.89	2.03	3.03	1.99	1.38	2.25	2.24
Total	99.76	99.20	99.94	100.1	99.56	99.70	99.51	99.99	100.1	99.71	99.61	99.66	100.2	99.71	99.37	99.41	100.1	99.75	100.12
Mg#	34.45	34.49	41.29	37.85	33.92	35.47	42.42	42.53	33.53	32.93	39.85	37.33	47.74	45.09	39.72	46.36	39.15	41.42	39.12
La	45.2	45.1	47.9	46.8	47.1	49.4	45.2	45.8	49.5	48.7	44.2	44.8	37.4	47.2	43.3	44.3	48.4	42.0	41.9
Ce	96.3	95.6	98.3	97.5	99.4	103	93.6	95.6	99.1	101	95.0	97.6	85.9	104	98.0	101	106	94.9	93.4
Pr	12.4	12.2	12.8	12.7	12.9	13.0	11.8	12.4	12.9	13.4	12.8	12.8	11.3	13.2	12.8	13.1	13.8	12.5	12.3
Nd	52.6	51.9	52.1	52.0	52.9	52.7	49.5	50.4	51.4	56.0	52.8	54.0	48.7	54.3	53.4	53.7	56.8	52.8	51.5
Sm	11.7	11.0	11.0	10.6	10.6	10.6	9.41	9.91	9.99	11.6	10.6	11.4	10.8	11.5	11.4	11.6	12.0	11.3	10.7
Eu	3.00	2.82	2.97	3.06	3.01	2.98	2.87	2.95	2.94	3.01	2.96	3.04	2.84	3.08	3.06	3.02	3.30	3.11	3.03
Gd	9.72	9.91	9.55	9.83	9.58	9.51	9.05	9.25	9.67	10.3	9.80	10.3	9.48	10.0	9.69	9.69	10.4	9.64	9.46
Tb	1.36	1.31	1.26	1.28	1.26	1.27	1.13	1.22	1.29	1.33	1.33	1.39	1.32	1.41	1.35	1.41	1.43	1.34	1.31
Dy	8.07	7.36	7.47	7.50	7.80	7.51	6.90	7.02	7.90	8.13	7.83	8.02	7.28	7.65	7.47	7.79	7.91	7.64	7.38
Ho	1.45	1.26	1.29	1.26	1.30	1.35	1.16	1.15	1.37	1.35	1.29	1.39	1.31	1.40	1.33	1.44	1.42	1.35	1.28

Er	3.61	3.36	3.45	3.41	3.42	3.38	3.12	3.08	3.51	3.59	3.51	3.61	3.36	3.61	3.49	3.70	3.55	3.47	3.44
Tm	0.47	0.46	0.44	0.45	0.46	0.46	0.41	0.44	0.50	0.49	0.50	0.51	0.45	0.47	0.46	0.48	0.47	0.47	0.45
Yb	2.93	2.73	2.73	2.70	2.77	2.69	2.48	2.53	2.93	2.75	2.86	2.98	2.74	2.91	2.80	2.97	2.84	2.81	2.73
Lu	0.38	0.36	0.36	0.37	0.37	0.35	0.35	0.36	0.40	0.40	0.39	0.41	0.39	0.40	0.40	0.42	0.40	0.39	0.38
V	355	346	369	366	351	342	307	298	403	388	379	389	382	348	382	329	388	389	375
Cr	345	437	406	76.1	81.6	73.0	346	332	123	111	459	543	197	302	222	271	337	184	166
Co	48.4	45.6	47.5	45.8	46.1	45.3	49.9	50.6	43.3	46.7	49.9	57.8	48.1	41.4	48.7	40.1	46.6	44.9	43.6
Ni	226	265	257	139	158	131	247	246	302	257	255	293	136	172	132	163	195	120	107
Cu	254	284	284	249	304	266	259	267	364	541	193	412	257	241	234	64.4	247	332	326
Zn	128	124	141	133	134	131	116	118	150	123	140	146	136	120	145	120	142	136	132
Ga	25.8	23.1	26.2	25.8	25.2	25.7	25.4	25.5	24.5	25.7	25.4	26.5	27.9	25.5	27.3	23.5	26.0	26.6	25.7
Rb	3.82	13.3	43.4	38.5	52.1	45.7	53.5	53.1	22.6	65.1	70.6	68.9	58.5	38.8	46.9	70.3	23.1	59.7	58.6
Sr	882	870	830	580	1027	639	661	672	457	484	742	785	451	511	448	569	586	546	539
Y	38.3	36.9	36.5	36.0	36.2	35.4	32.7	33.6	37.1	37.0	36.7	37.7	34.4	36.9	35.4	37.6	37.2	36.1	35.0
Zr	365	350	350	348	360	349	327	324	366	352	356	377	304	349	352	353	370	341	335
Nb	40.8	40.4	42.0	42.2	41.8	43.3	42.0	40.2	43.0	39.4	41.8	44.3	33.3	39.0	39.9	38.7	41.9	37.1	36.3
Ba	239	424	1306	405	1621	524	472	498	239	741	1065	1003	627	479	578	697	407	510	490
Hf	9.47	8.78	8.81	8.56	8.79	8.66	7.74	7.91	8.65	8.50	8.55	9.19	7.74	8.96	8.96	9.22	9.51	8.76	8.67
Ta	2.38	2.38	2.54	2.52	2.55	2.58	2.48	2.52	2.56	2.34	2.57	2.83	2.20	2.57	2.62	2.57	2.69	2.46	2.38
Pb	8.48	8.92	7.42	7.74	12.4	8.94	6.61	5.97	5.63	7.64	6.95	8.15	6.54	11.9	7.80	7.64	6.64	8.62	8.95
Th	7.12	6.90	6.84	6.77	7.03	6.97	6.70	6.63	6.58	6.61	6.57	6.81	7.21	8.12	6.49	8.35	6.97	6.47	6.25
U	1.60	1.58	1.69	1.60	1.74	1.69	1.52	1.58	1.55	1.48	1.49	1.68	1.52	1.82	1.50	1.76	1.65	1.47	1.46

LOI: weight loss on ignition to 1000 ℃. Mg# = $Mg^{2+}/(Mg^{2+}+Fe^{2+})$ in atomic ratio, assuming 15% of total iron oxide is ferric.

Table 3 Sr-Nd-Pb isotope ratios for the analysed volcanic rocks in the Sichuan Basin

Sample	ST1-5	YT1-1	YT1-3	YT1-6	YT1-7	ZG2-5	ZG2-7	ZG2-8	20LMD05	20LC06	20XL01
Locality	ST1 Well	YT1 Well				ZG2 Well			Longmendong	Longchi	Xinlin
Rb($\times10^{-6}$)	13.3	43.4	38.5	53.5	53.1	65.1	70.6	68.9	38.8	70.3	23.1
Sr($\times10^{-6}$)	870	830	580	661	672	484	742	785	511	569	586
$^{87}Rb/^{86}Sr$	0.044372	0.151194	0.192215	0.234105	0.228342	0.389072	0.275352	0.254148	0.219834	0.357378	0.113896
$^{87}Sr/^{86}Sr$	0.706884	0.707491	0.707355	0.706681	0.706694	0.706661	0.707085	0.707075	0.706865	0.707546	0.705942
$^{2}\sigma$	0.000008	0.000007	0.00001	0.000008	0.000008	0.000008	0.000006	0.000007	0.000007	0.00001	0.000009
$^{87}Sr/^{86}Sr(t)$	0.706721	0.706935	0.706648	0.705820	0.705854	0.705230	0.706072	0.706140	0.706057	0.706232	0.705523
Sm($\times10^{-6}$)	11.0	11.0	10.6	9.41	9.91	11.6	10.6	11.4	11.5	11.6	12.0
Nd($\times10^{-6}$)	51.9	52.1	52.0	49.5	50.4	56.0	52.8	54.0	54.3	53.7	56.8
$^{147}Sm/^{144}Nd$	0.128166	0.127908	0.123307	0.114987	0.118988	0.125756	0.121209	0.128019	0.128721	0.130854	0.127975
$^{143}Nd/^{144}Nd$	0.512530	0.512533	0.512526	0.512528	0.512528	0.512567	0.512570	0.512573	0.512507	0.512507	0.512561
$^{2}\sigma$	0.000005	0.000008	0.000005	0.000006	0.000005	0.000004	0.000006	0.000013	0.000004	0.000004	0.000008
$^{143}Nd/^{144}Nd(t)$	0.512313	0.512317	0.512317	0.512333	0.512327	0.512354	0.512365	0.512356	0.512289	0.512286	0.512344
$\varepsilon_{Nd}(t)$	0.16	0.22	0.24	0.55	0.42	0.96	1.17	1.00	-0.31	-0.38	0.77
T_{DM}(Ma)	1106	1098	1054	962	1002	1012	958	1028	1154	1184	1049
$f_{Sm/Nd}$	-0.35	-0.35	-0.37	-0.42	-0.40	-0.36	-0.38	-0.35	-0.35	-0.33	-0.35
$^{206}Pb/^{204}Pb$	18.715	18.751	18.728	18.757	18.789	18.800	18.888	18.867	18.789	18.881	18.899
$^{2}\sigma$	0.001	0.001	0.001	0.001	0.001	0.001	0.001	0.001	0.000	0.001	0.000
$^{207}Pb/^{204}Pb$	15.609	15.613	15.612	15.611	15.613	15.617	15.620	15.621	15.626	15.629	15.614
$^{2}\sigma$	0.001	0.001	0.001	0.001	0.001	0.001	0.001	0.001	0.000	0.001	0.000
$^{208}Pb/^{204}Pb$	39.236	39.292	39.271	39.310	39.357	39.276	39.356	39.316	39.432	39.628	39.349
$^{2}\sigma$	0.002	0.002	0.002	0.002	0.002	0.002	0.001	0.002	0.001	0.002	0.001
$^{206}Pb/^{204}Pb(t)$	18.251	18.154	18.185	18.156	18.097	18.293	18.323	18.325	18.388	18.272	18.245
$^{207}Pb/^{204}Pb(t)$	15.585	15.582	15.584	15.580	15.578	15.592	15.591	15.593	15.606	15.598	15.581
$^{208}Pb/^{204}Pb(t)$	38.572	38.500	38.520	38.440	38.403	38.533	38.542	38.597	38.845	38.685	38.446

Notes:

1. $^{87}Rb/^{86}Sr$ and $^{147}Sm/^{144}Nd$ ratios are calculated using Rb, Sr, Sm and Nd contents by ICP-MS and measured $^{87}Sr/^{86}Sr$ and $^{143}Nd/^{144}Nd$ ratios by MC-ICP-MS.
2. In T_{DM} calculation, ratios of $(^{143}Nd/^{144}Nd)_{DM}$ and $(^{147}Sm/^{144}Nd)_{DM}$ took values of 0.51315 and 0.225, respectively.
3. In $\varepsilon_{Nd}(t)$ calculations, ratios of $(^{87}Sr/^{86}Sr)_{CHUR}$, $(^{87}Rb/^{86}Sr)_{CHUR}$, $(^{143}Nd/^{144}Nd)_{CHUR}$ and $(^{147}Sm/^{144}Nd)_{CHUR}$ are 0.7045, 0.0847, 0.512638 and 0.1967, respectively, while t = 258.5 Ma.

Table 4 Distribution of the Emeishan basalts in the ELIP

Zone	Locality	Rock type	Reference
Inner zone	Dali	High-Ti basalts, low Ti basalts	Hanski et al. (2010)
	Lijiang	High-Ti basalts, low Ti basalts	Song et al. (2001), Zhang et al. (2006)
	Binchuan	High-Ti basalts, low Ti basalts	Song et al. (2001), Xiao et al. (2004), Xu et al. (2007), Xu et al. (2001)
	Ertan	High-Ti basalts, low Ti basalts	Song et al. (2001), Xu et al. (2001)
	Jianchuan	High-Ti basalts, low Ti basalts	Song et al. (2001)
	Pingchuan	Low Ti basalts	Xu et al. (2014)
	Miyi	High-Ti basalts	Xu et al. (2014)
	Kangsi	High-Ti basalts	He et al. (2010)
	Wanmachang	High-Ti basalts	He et al. (2010)
	Shuidiqiao	High-Ti basalts	He et al. (2010)
	Longzhoushan	High-Ti basalts	Xu et al. (2007)
	Yongsheng	High-Ti basalts, low Ti basalts	Hao et al. (2004)
Intermediate zone	Dongchuan	High-Ti basalts	Song et al. (2008), Xu et al. (2001)
	Qingyin	High-Ti basalts	Xu et al. (2014)
	Qiaojia	High-Ti basalts	Xu et al. (2014)
	Weining	High-Ti basalts	Xu et al. (2014)
	Duge	High-Ti basalts	Xu et al. (2014)
	Zhaotong	High-Ti basalts	Li et al. (2017c)
Outer zone	Zhijin	High-Ti basalts	Lai et al. (2012), Xu et al. (2007)
	Jinding	High-Ti basalts	Xu et al. (2007)
	Tubagou	High-Ti basalts	Li et al. (2016b)
	Baise	High-Ti basalts	Fan et al. (2008)
	Bama	High-Ti basalts	Fan et al. (2008), Lai et al. (2012), Liu et al. (2017)
	Tianyang	High-Ti basalts	Fan et al. (2008), Liu et al. (2017)
	Sichuan Basin	High-Ti basalts	This study

Figure 1

Click here to access/download;Figure;fig.1.pdf

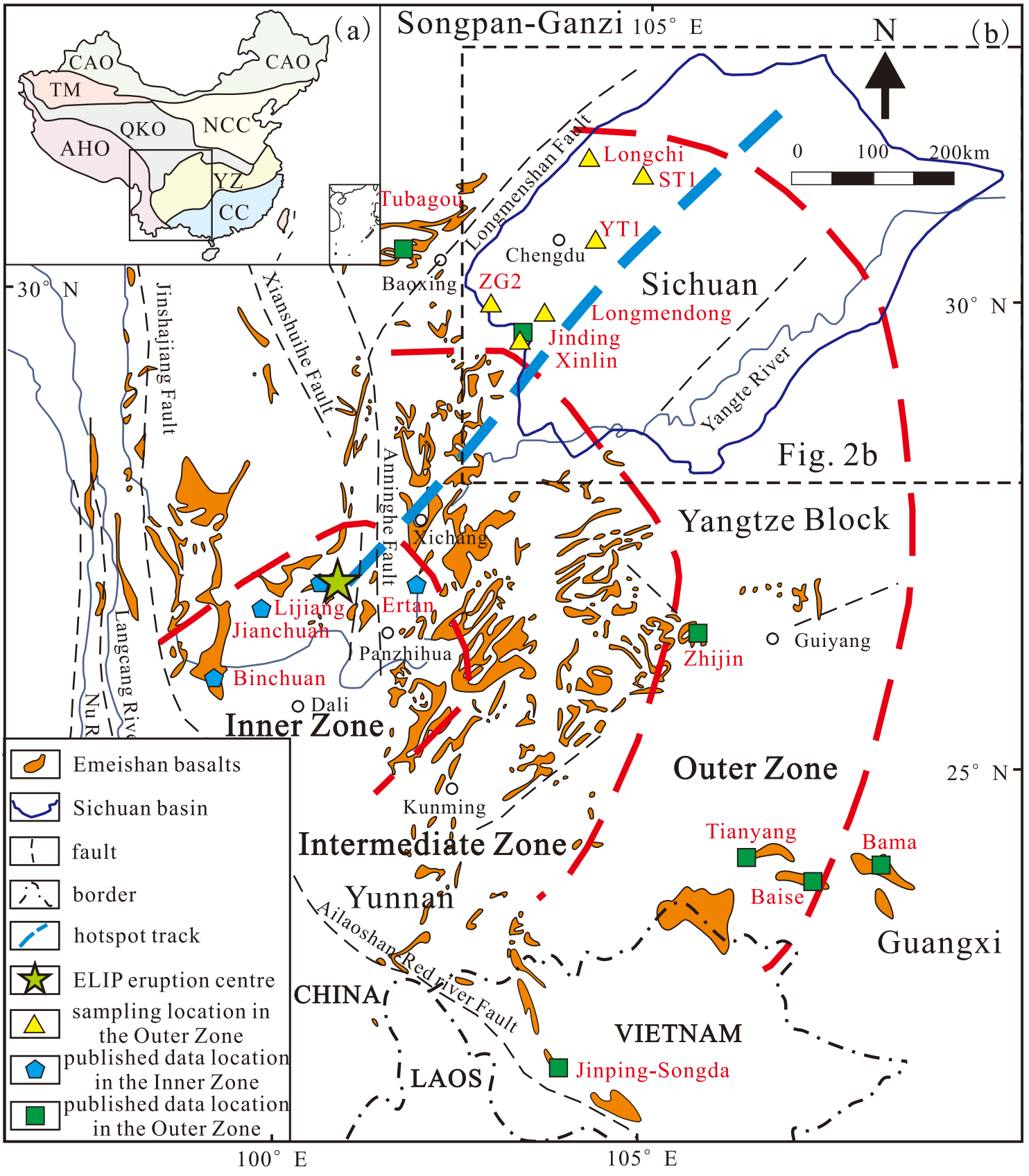

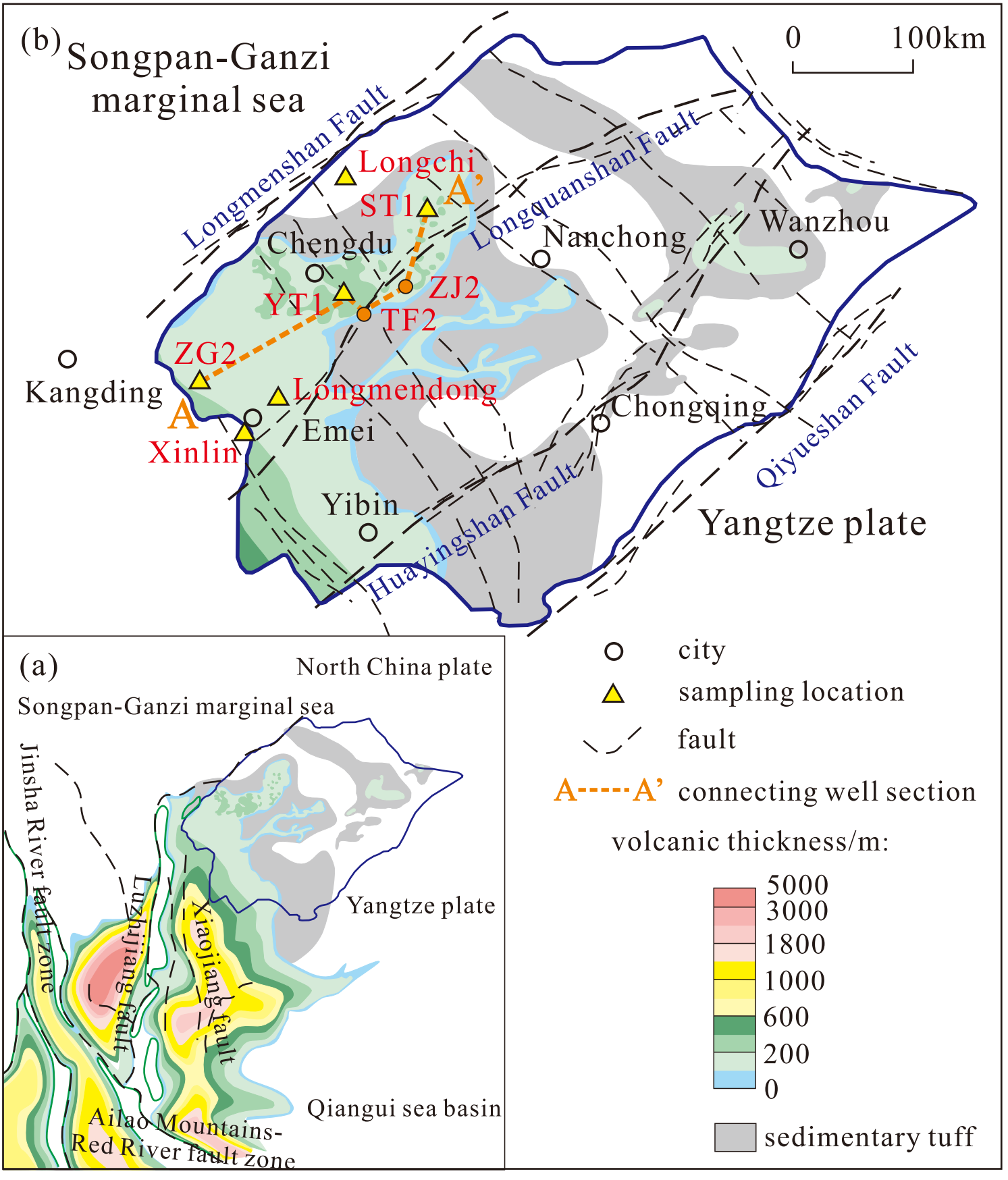

Figure 3

Click here to access/download;Figure;fig.3.pdf

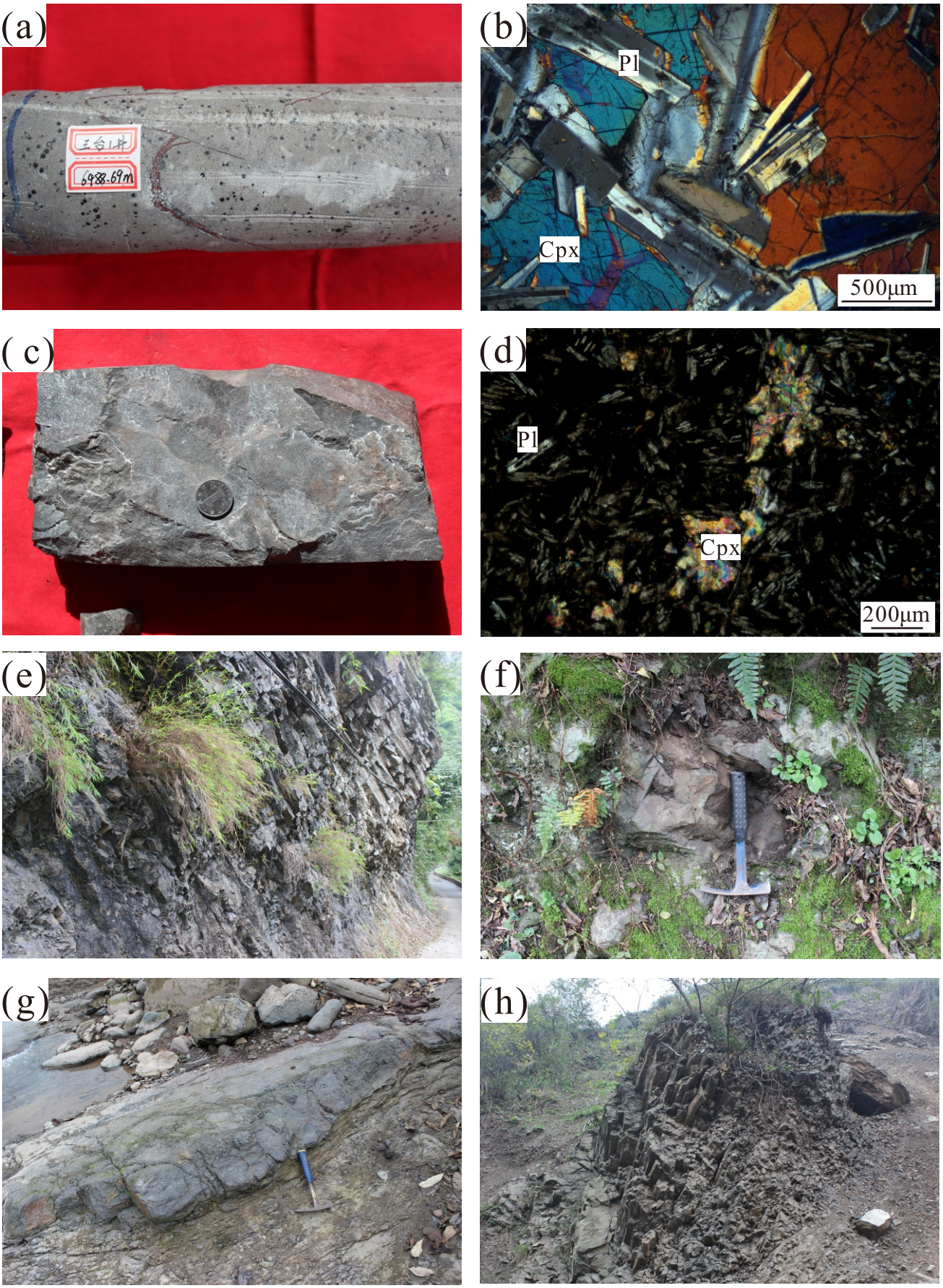

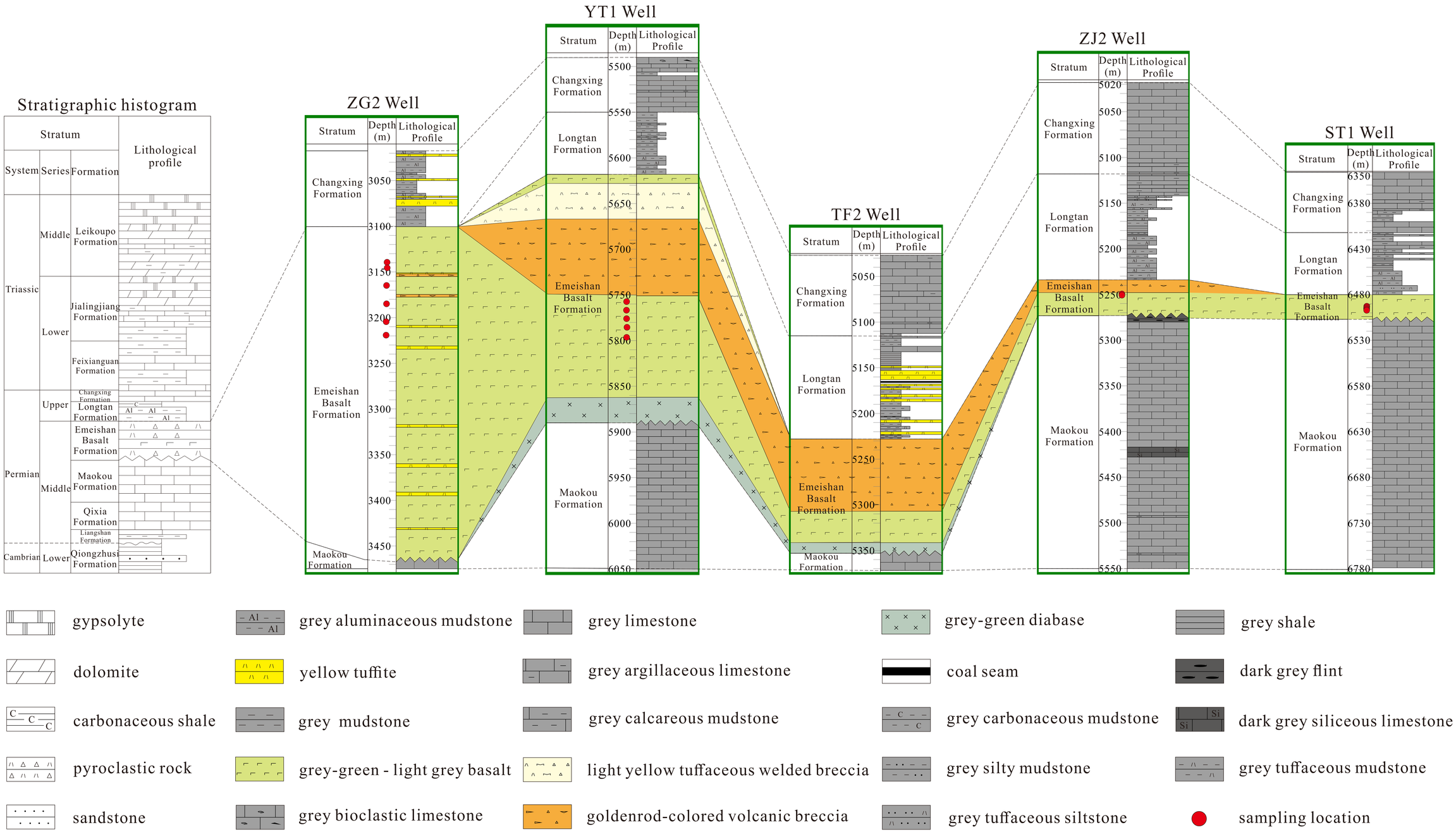

Figure 5

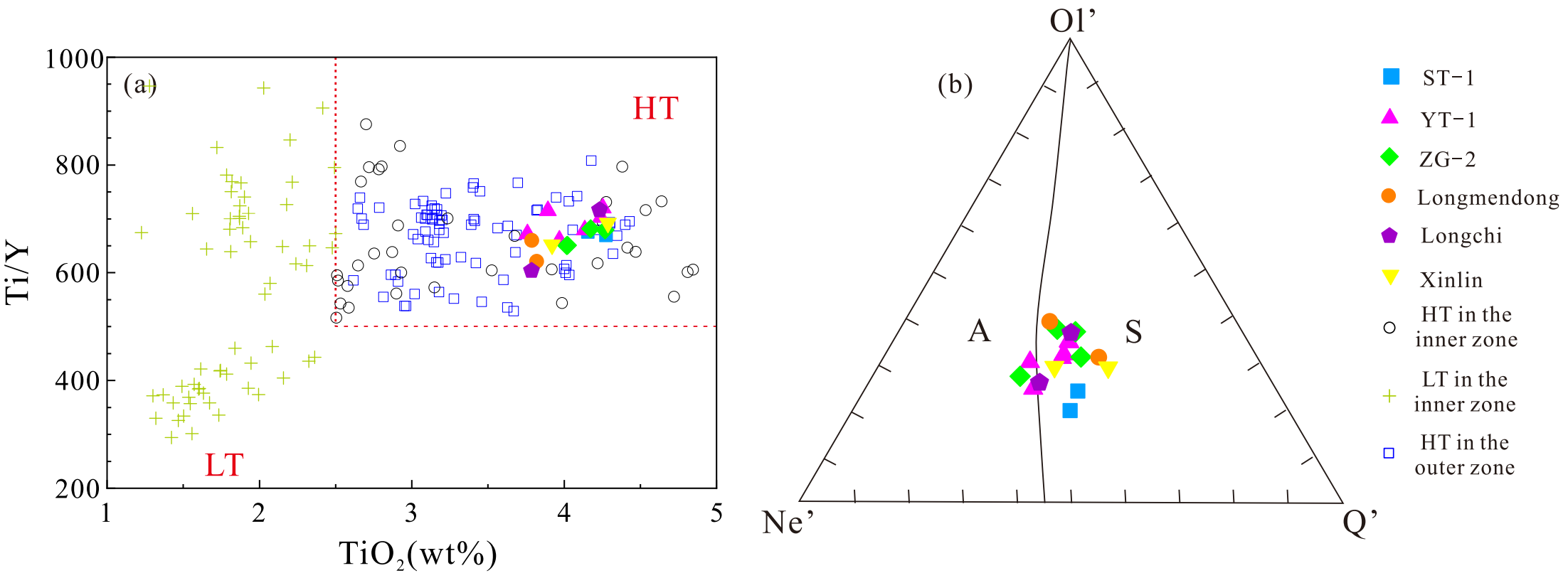

Figure 6

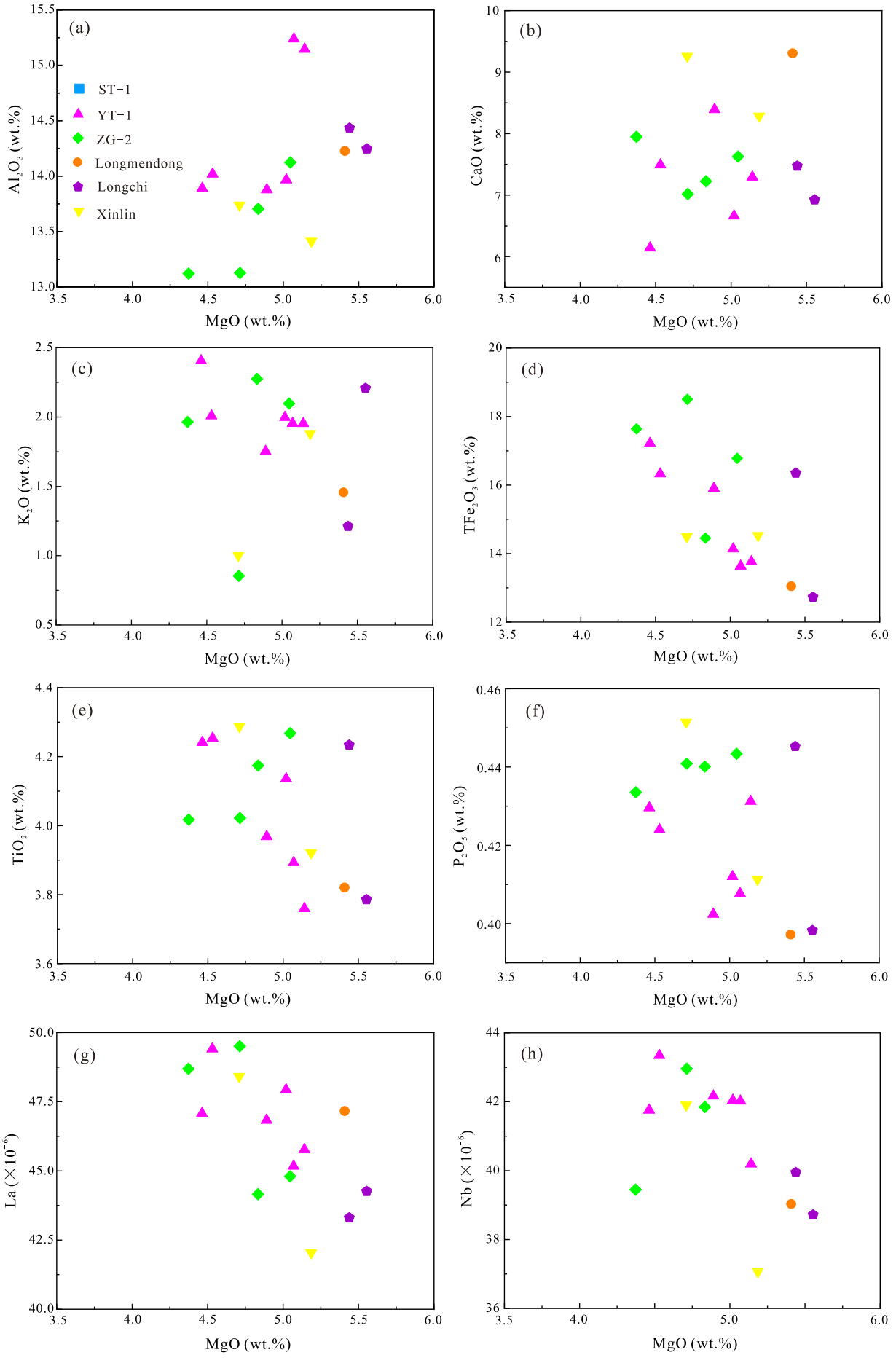

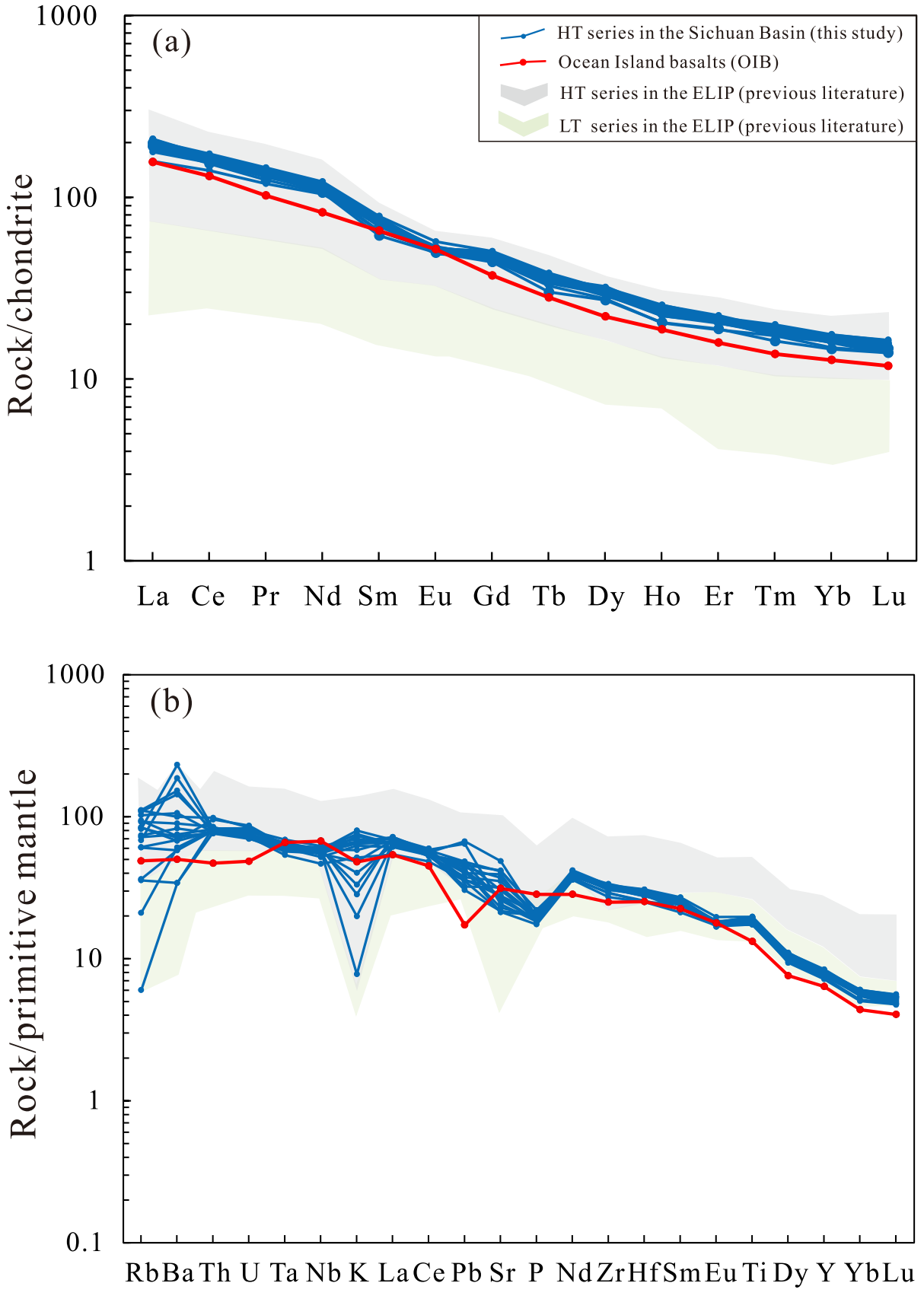

Figure 8

Click here to access/download;Figure;fig.8.pdf

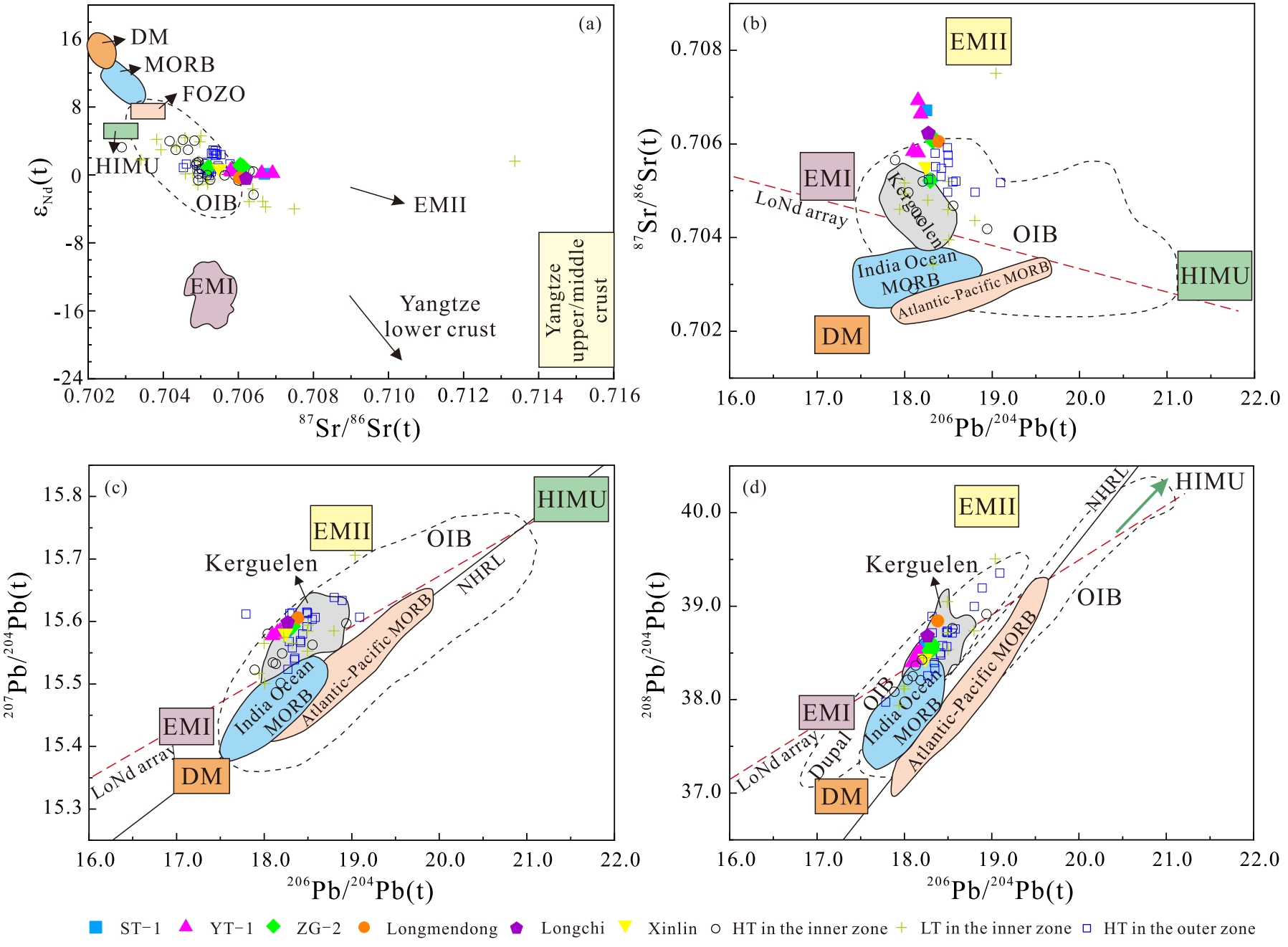

Figure 9

Click here to access/download;Figure;fig.9.pdf

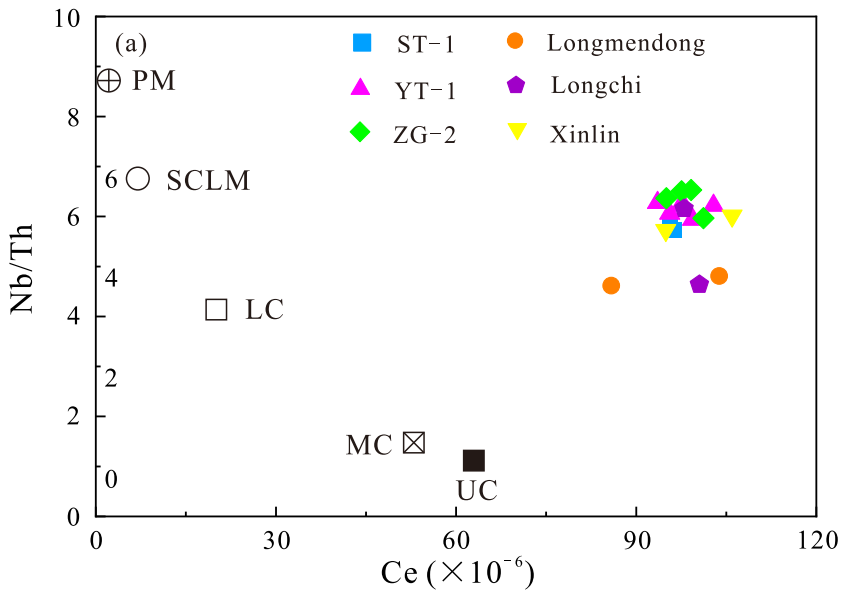

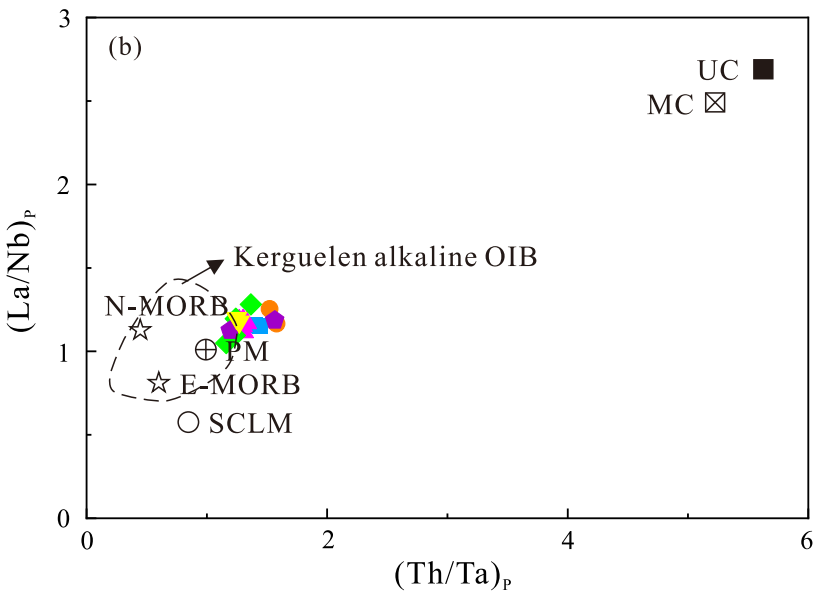

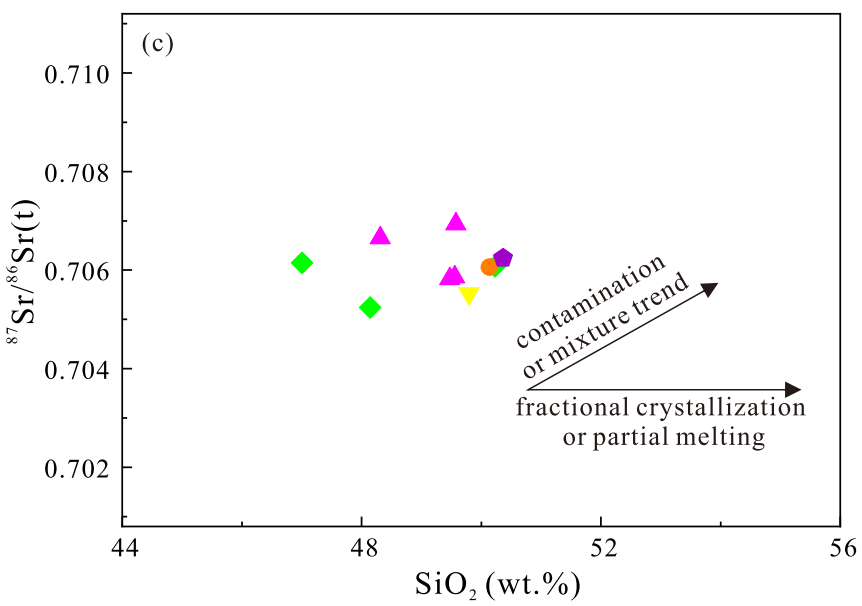

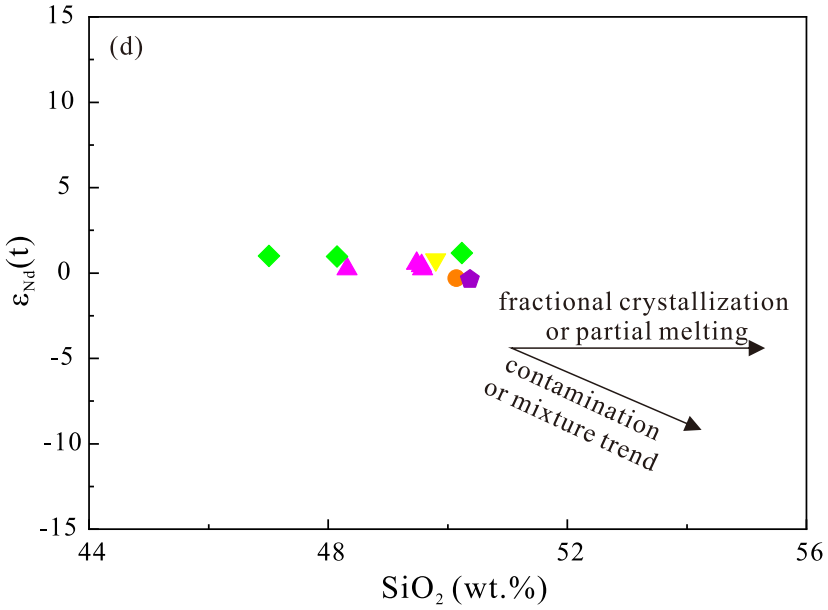

Figure 10

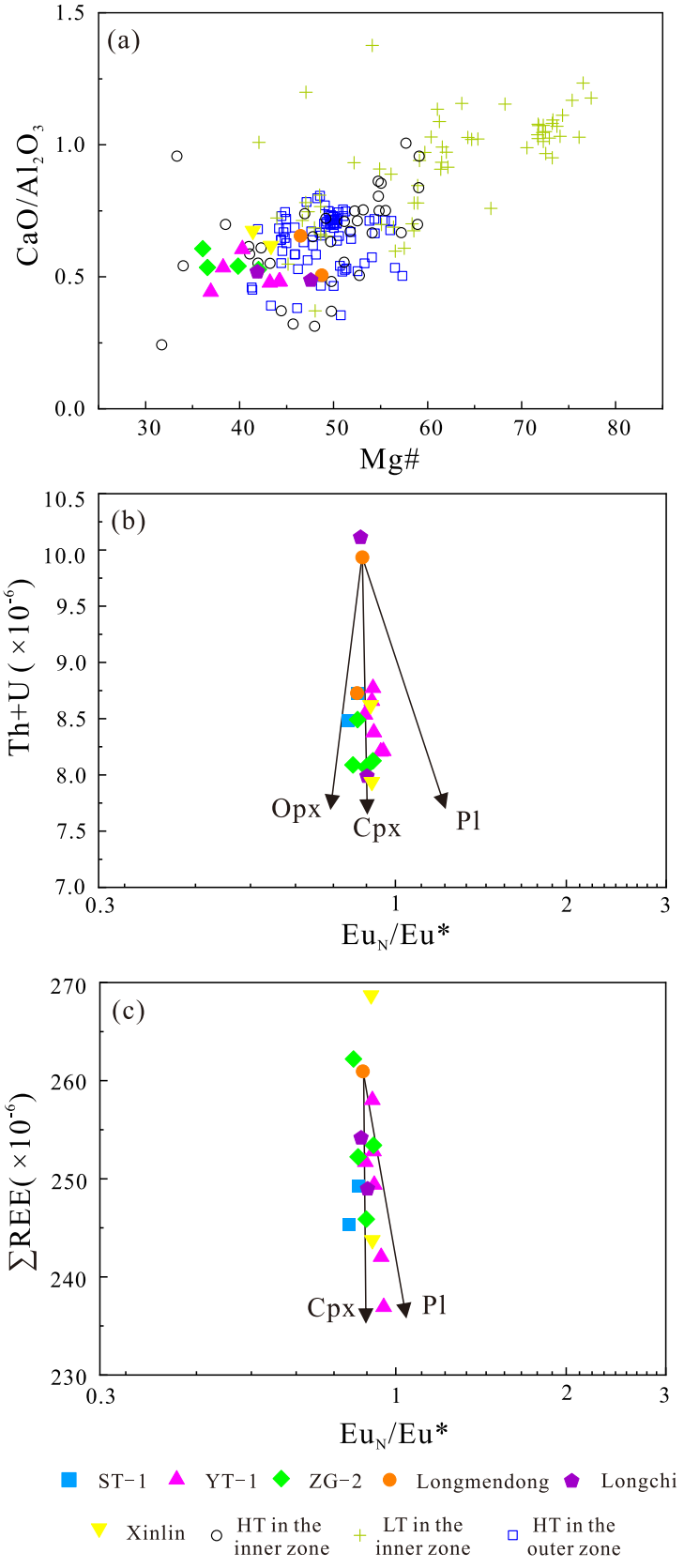

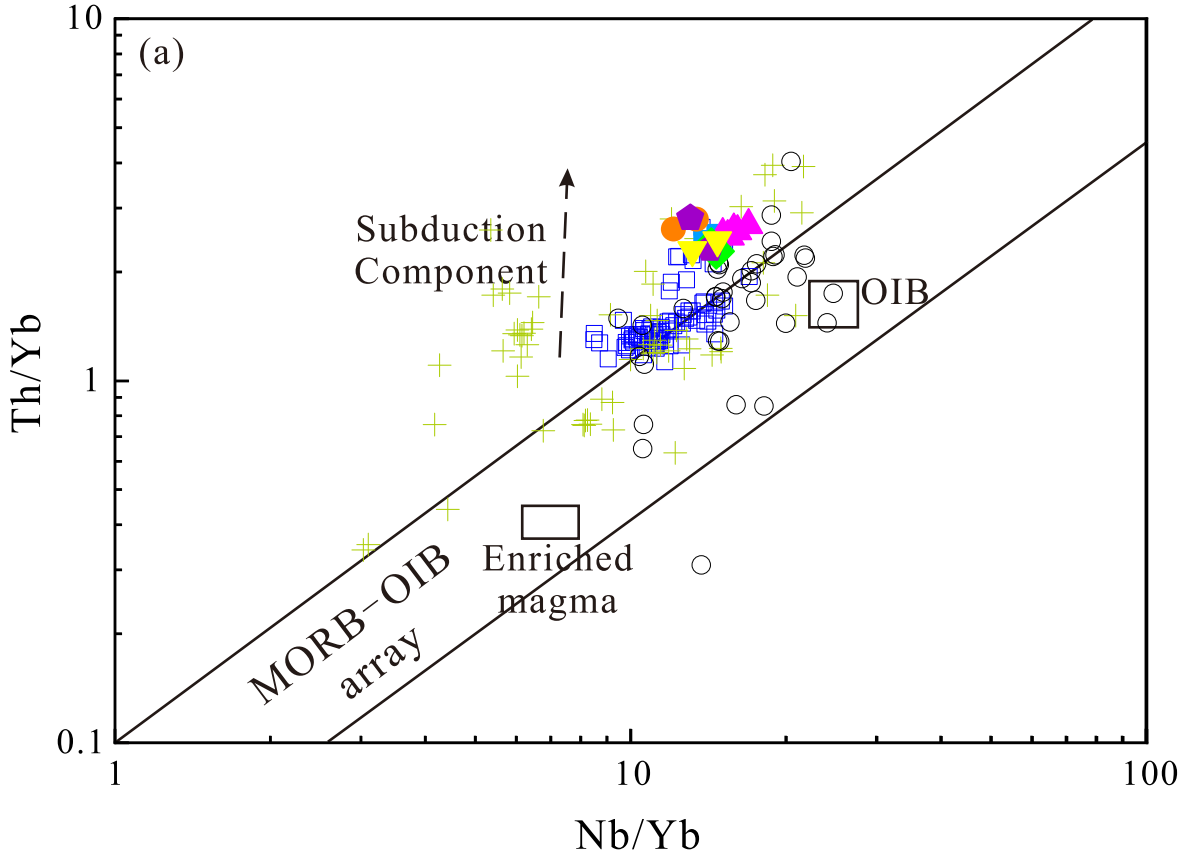

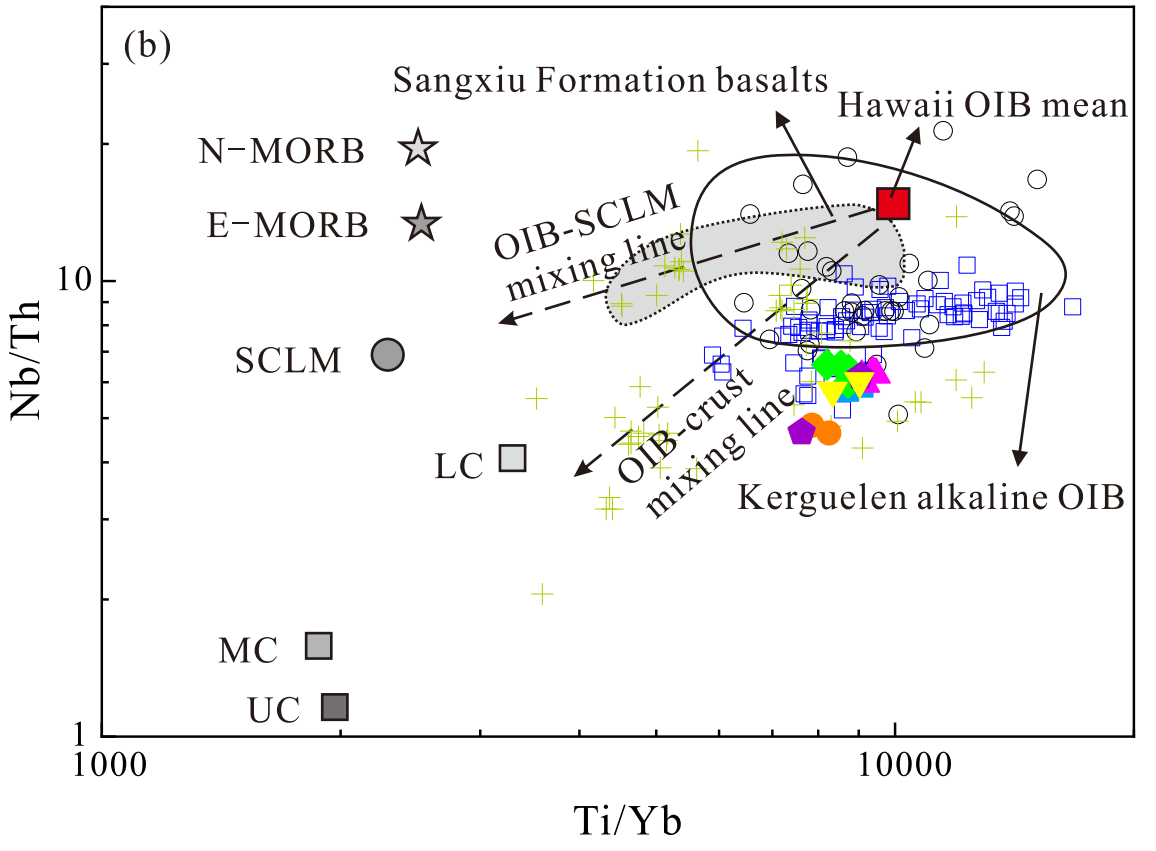

ST–1 YT–1 ZG–2 Longmendong Longchi

Xinlin HT in the inner zone LT in the inner zone HT in the outer zone

Figure 12

Click here to access/download;Figure;fig.12.pdf

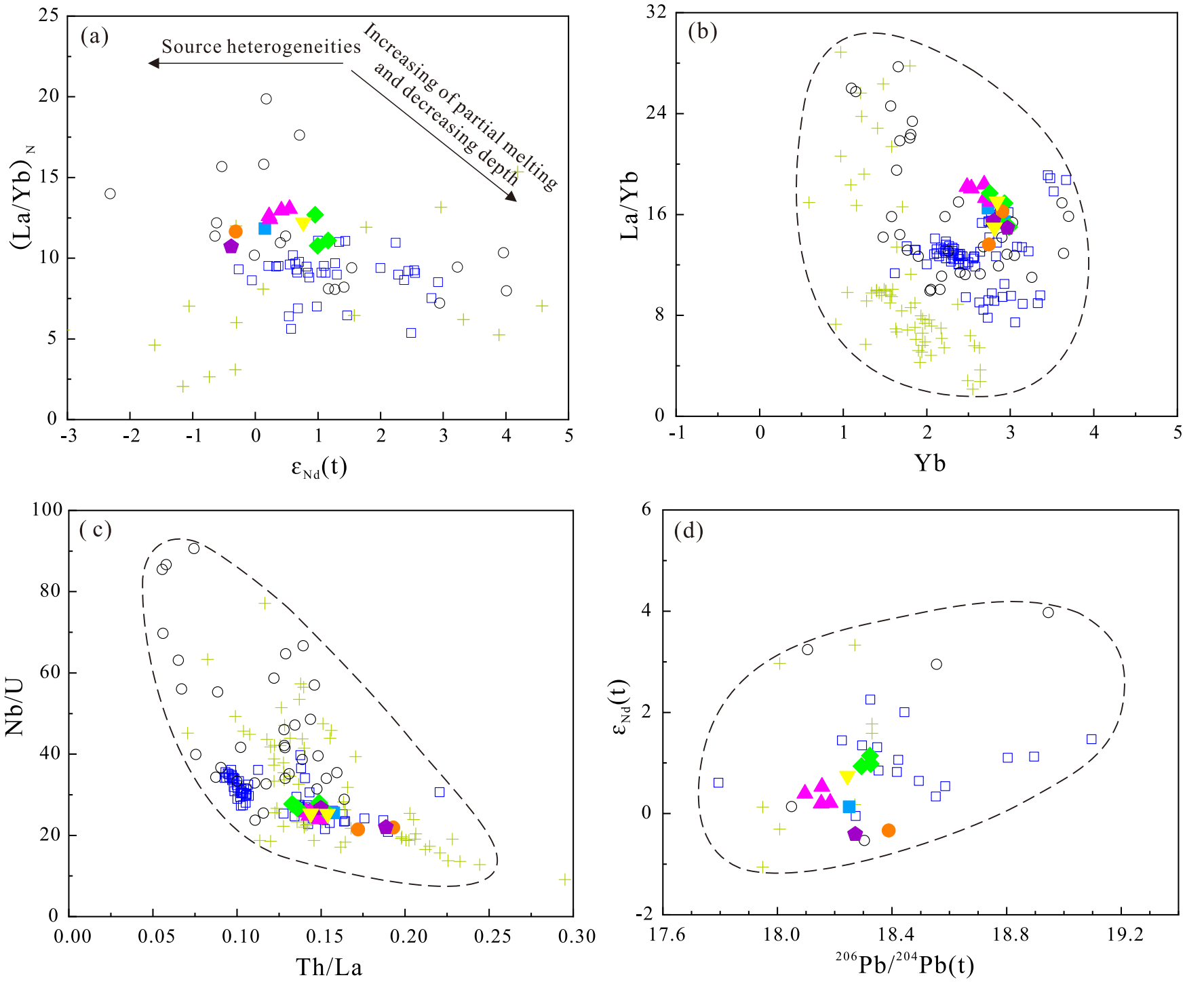

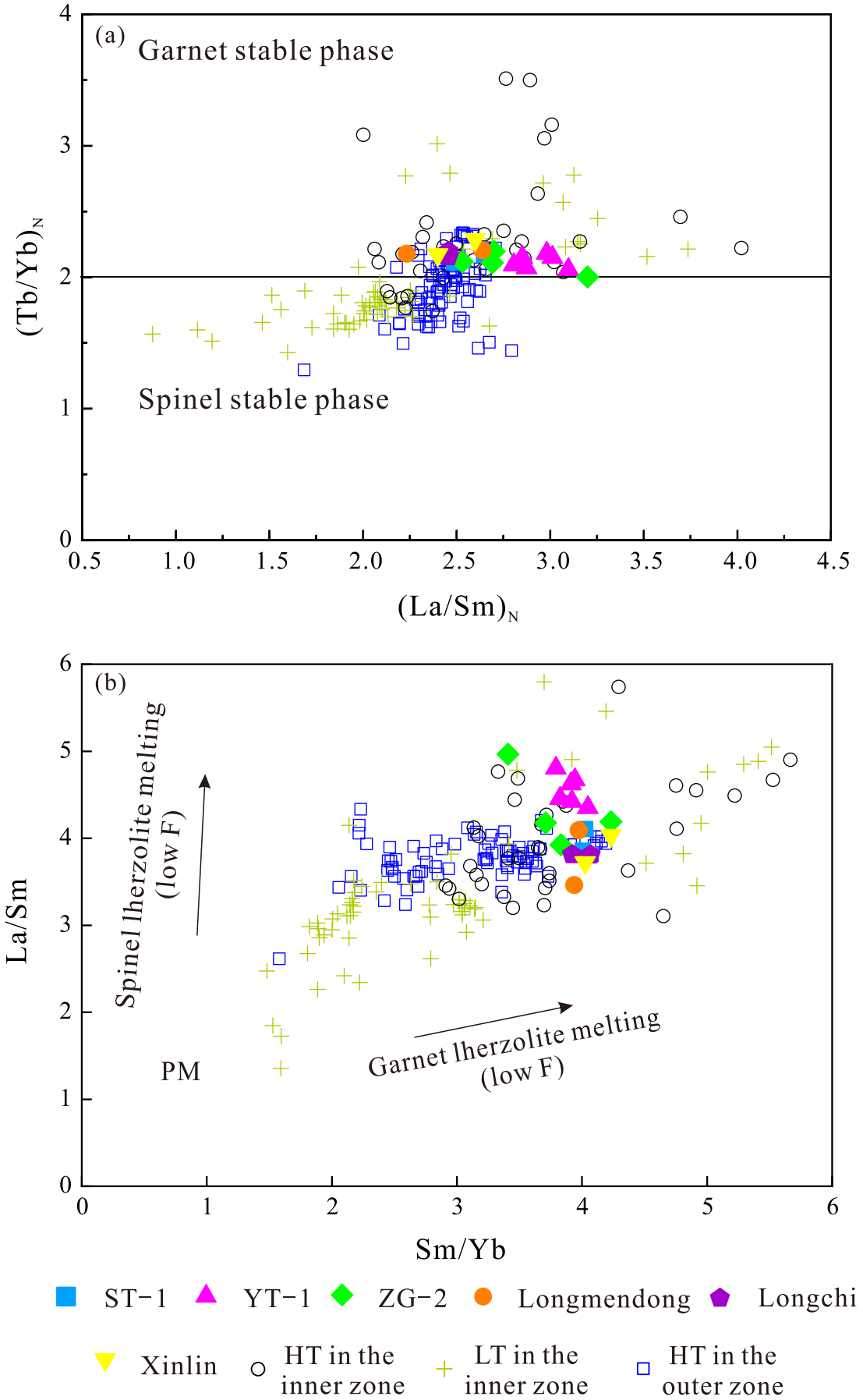

Figure 14

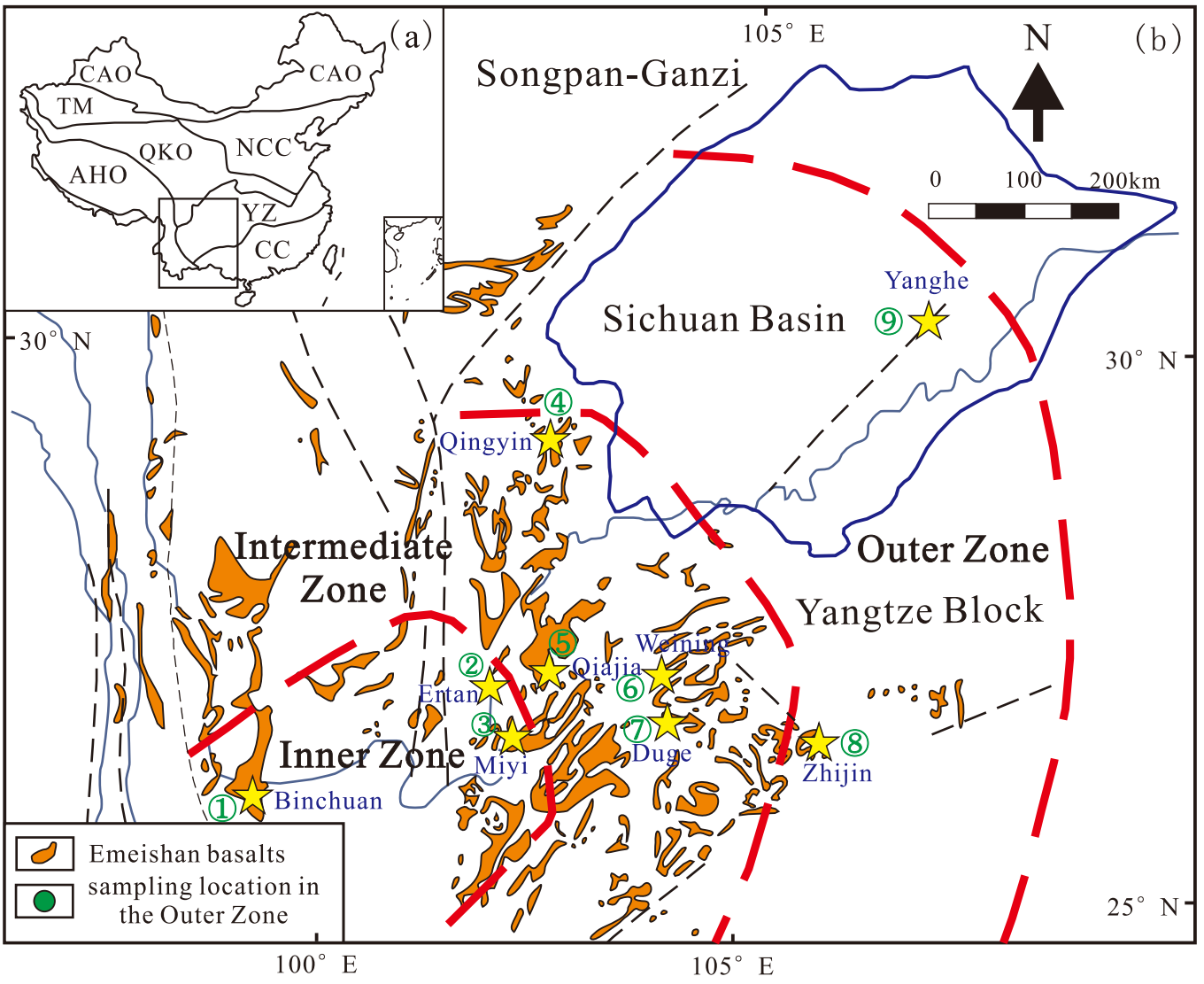

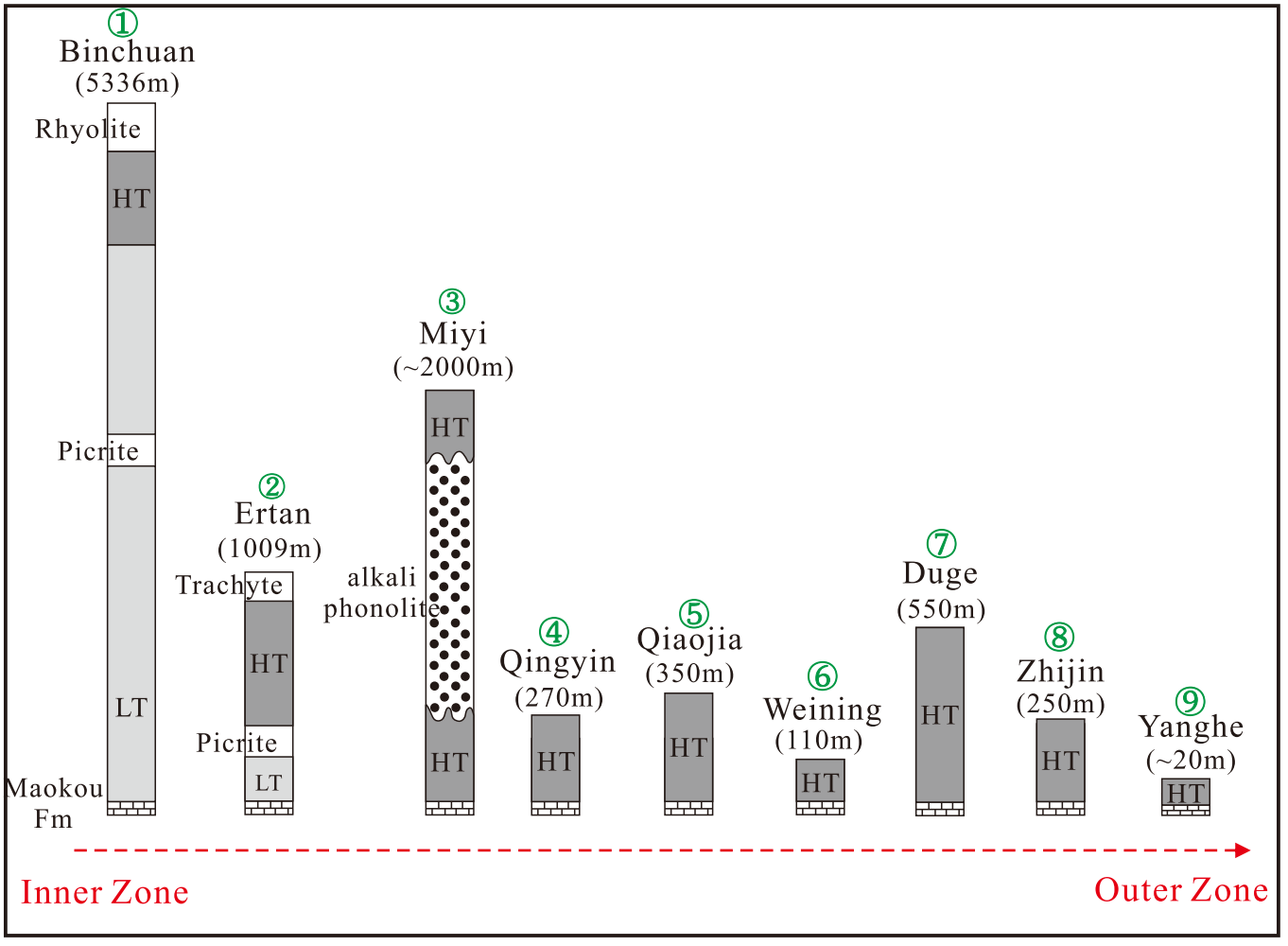

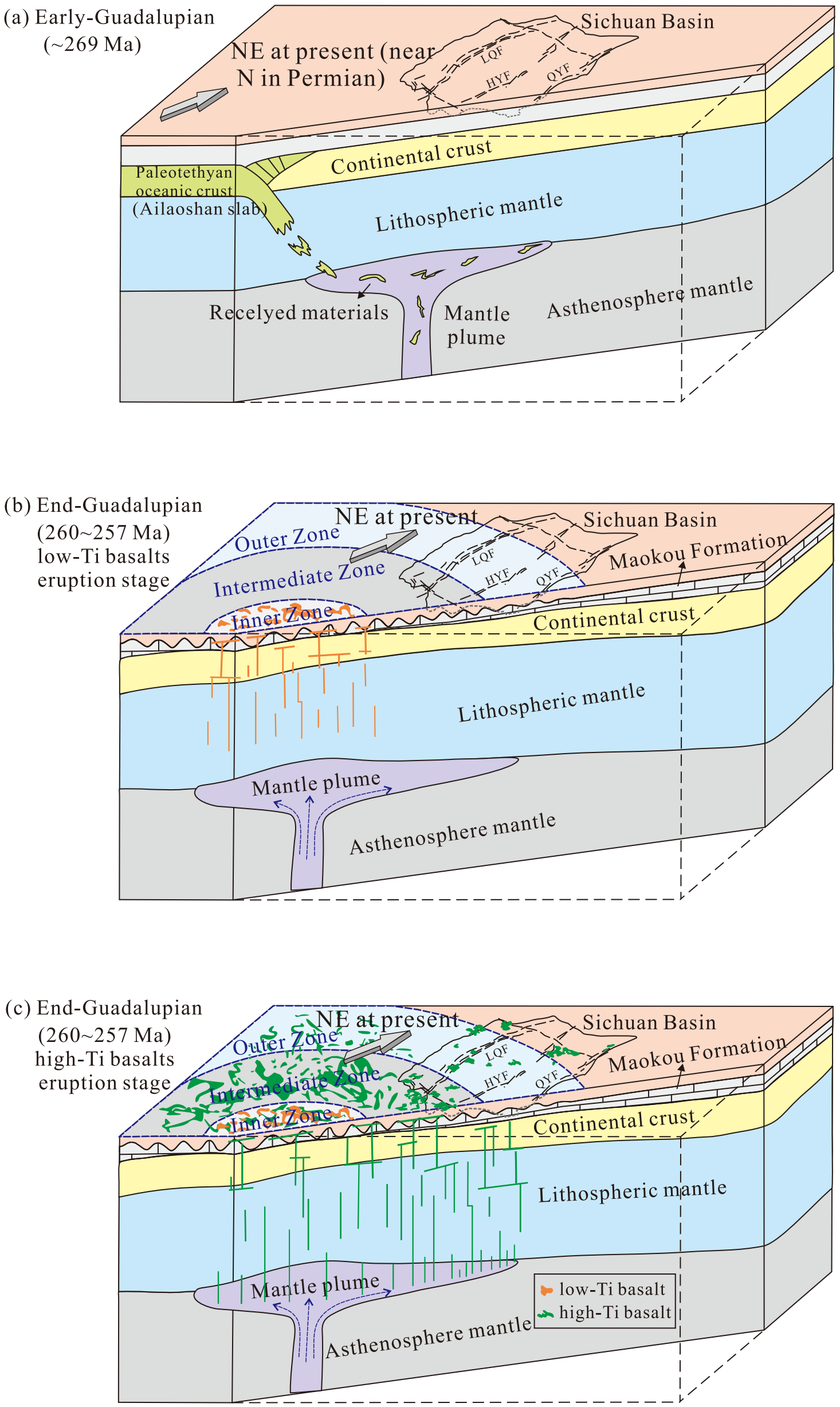

Table 1 Zircon U-Pb dating results of the Emeishan large igneous province

Locality		Rock type	Analytical method	Age/Ma	Reference
Inner Zone	Dali-Jiangwei	acid volcanic rock	ID-TIMS zircon U-Pb	258.9±0.5	Xu et al. (2013)
	Midu-Jinbaoshan	wehrlite	Shrimp zircon U-Pb	260.6±3.5	Tao et al. (2009)
		hornblendite	Shrimp zircon U-Pb	260.7±5.6	
	Binchuan	acid tuff	ID-TIMS zircon U-Pb	259.1±0.5	Zhong et al. (2014)
		basalt	Shrimp zircon U-Pb	256.2±1.4	Li et al. (2016a)
	Panxi-Daheishan	syenite	ID-TIMS zircon U-Pb	259.1±0.5	Shellnutt et al. (2012)
	Panxi-Baima	granite	ID-TIMS zircon U-Pb	259.2±0.4	
	Panxi-Huangcao	syenite	ID-TIMS zircon U-Pb	258.9±0.7	
	Panxi-Cida	granite	ID-TIMS zircon U-Pb	258.4±0.6	
	Panxi-Maomaogou	syenite	Shrimp zircon U-Pb	261.6 ± 4.4	Xu et al. (2008)
	Panxi-Miyi	syenite	Shrimp zircon U-Pb	259.8 ± 3.5	
	Panxi-Salian	diorite	Shrimp zircon U-Pb	260.4 ± 3.6	
	Panxi-Taihe	granite	Shrimp zircon U-Pb	261.4 ± 2.3	
	Panxi-Hongge	gabbro	Shrimp zircon U-Pb	259.3±1.3	Zhong and Zhu (2006)
		gabbro	Shrimp zircon U-Pb	259.3 ± 1.3	
	Panxi-Binggu	gabbro	Shrimp zircon U-Pb	260.7 ± 0.8	
	Panxi-Panzhihua	gabbro	Shrimp zircon U-Pb	263±3	Zhou et al. (2005)
		Picrate dyke	LA-ICP-MS zircon U-Pb	261.4±4.6	Hou et al. (2013)
		Ultramafic dyke	Shrimp zircon U-Pb	262±3	Guo et al. (2004)
	Xinjie	gabbro	Shrimp zircon U-Pb	259±3	Zhou et al. (2002)

	Limahe	gabbro	Shrimp zircon U-Pb	263±3	Zhou et al. (2008)
	Zhubu	diorite	Shrimp zircon U-Pb	261 ± 2	
Intermediate Zone	Guizhou-Weining	boundary clay rock	ID-TIMS zircon U-Pb	258.1±0.6	Xu et al. (2013)
	Panxian-Zhudong	ignimbrite	ID-TIMS zircon U-Pb	258.3±1.4	Zhu (2019)
	Xingyi-Xiongwu	tuff	ID-TIMS zircon U-Pb	258.5±0.9	
	Puan-Louxia	tuff	ID-TIMS zircon U-Pb	258.1±1.1	
	Baimazhai	pyroxenite	Shrimp zircon U-Pb	258.5±3.5	Wang et al. (2006)
Outer Zone	Tubagou	basalt	Shrimp zircon U-Pb	257.3±2.0	Li et al. (2016b)
	Baise-Yangxu	basalt	Shrimp zircon U-Pb	259.1±4.0	Fan et al. (2008)
				253.7±6.1	Fan et al. (2004)
	Bama-Minan	basalt	Shrimp zircon U-Pb	259.6±5.9	Fan et al. (2008)
	Nayong-Xilin-Tianyang Area	basalt	LA-ICP-MS zircon U-Pb	257.0±9.0	Lai et al. (2012)
	Guangyuan-Chaotian	boundary clay rock	ID-TIMS zircon U-Pb	258.6±1.4	Xu et al. (2013)
				259.2±0.3	Zhong et al. (2014)
	Funing	diabase	Shrimp zircon U-Pb	260±3	Zhou et al. (2006)
		diorite	Shrimp zircon U-Pb	258±3	
	Mianhuadi	metagabbro	MC-ICP-MS zircon U-Pb	259.6±0.8	Zhou et al. (2013)

Table 2 Major elements (wt.%) and trace elements ($\times 10^{-6}$) contents for the analysed volcanic rocks in the Sichuan Basin

Samples	ST1-2	ST1-5	YT1-1	YT1-3	YT1-4	YT1-5	YT1-6	YT1-7	ZG2-4	ZG2-5	ZG2-7	ZG2-8	20LMD04	20LMD05	20LC04	20LC06	20XL01	20XL02	20XL02 (replicate)
Locality	ST1 Well		YT1 Well						ZG2 Well				Longmendong		Longchi		Xinlin		
SiO_2	49.64	48.78	48.62	47.55	46.69	47.67	48.67	48.96	46.59	47.64	48.74	45.59	45.99	48.99	45.94	49.08	49.21	48.12	48.32
TiO_2	4.01	3.87	4.06	3.91	4.17	4.19	3.83	3.71	4.01	3.98	4.05	4.14	3.69	3.73	4.08	3.69	4.24	3.82	3.84
Al_2O_3	13.75	13.66	13.69	13.66	13.64	13.82	14.99	14.96	13.07	12.98	13.30	13.70	13.44	13.90	13.91	13.88	13.57	13.08	13.06
$Fe_2O_3^T$	12.92	13.82	13.86	15.65	16.91	16.10	13.41	13.60	18.43	17.46	14.02	16.27	15.44	12.75	15.75	12.40	14.32	14.16	14.23
MnO	0.21	0.17	0.18	0.16	0.17	0.17	0.16	0.16	0.20	0.19	0.20	0.19	0.21	0.16	0.17	0.17	0.18	0.17	0.17
MgO	3.43	3.68	4.92	4.81	4.38	4.47	4.99	5.08	4.69	4.33	4.69	4.89	7.12	5.28	5.24	5.41	4.65	5.06	5.10
CaO	4.88	4.27	6.53	8.26	6.03	7.39	7.22	7.21	6.99	7.87	7.01	7.40	6.79	9.09	7.20	6.75	9.15	8.08	8.13
Na_2O	4.38	3.91	3.82	2.29	3.44	2.39	2.78	2.75	4.32	2.14	2.38	2.34	2.81	1.97	2.47	3.52	2.05	2.78	2.76
K_2O	0.22	0.56	1.96	1.73	2.36	1.98	1.92	1.93	0.85	1.94	2.21	2.03	1.51	1.42	1.17	2.15	0.99	1.83	1.85
P_2O_5	0.45	0.45	0.40	0.40	0.42	0.42	0.40	0.43	0.44	0.43	0.43	0.43	0.37	0.39	0.43	0.39	0.45	0.40	0.40
LOI	5.87	6.04	1.89	1.70	1.33	1.12	1.15	1.21	0.54	0.77	2.59	2.68	2.89	2.03	3.03	1.99	1.38	2.25	2.24
Total	99.76	99.20	99.94	100.1	99.56	99.70	99.51	99.99	100.1	99.71	99.61	99.66	100.2	99.71	99.37	99.41	100.1	99.75	100.12
Mg#	34.45	34.49	41.29	37.85	33.92	35.47	42.42	42.53	33.53	32.93	39.85	37.33	47.74	45.09	39.72	46.36	39.15	41.42	39.12
La	45.2	45.1	47.9	46.8	47.1	49.4	45.2	45.8	49.5	48.7	44.2	44.8	37.4	47.2	43.3	44.3	48.4	42.0	41.9
Ce	96.3	95.6	98.3	97.5	99.4	103	93.6	95.6	99.1	101	95.0	97.6	85.9	104	98.0	101	106	94.9	93.4
Pr	12.4	12.2	12.8	12.7	12.9	13.0	11.8	12.4	12.9	13.4	12.8	12.8	11.3	13.2	12.8	13.1	13.8	12.5	12.3
Nd	52.6	51.9	52.1	52.0	52.9	52.7	49.5	50.4	51.4	56.0	52.8	54.0	48.7	54.3	53.4	53.7	56.8	52.8	51.5
Sm	11.7	11.0	11.0	10.6	10.6	10.6	9.41	9.91	9.99	11.6	10.6	11.4	10.8	11.5	11.4	11.6	12.0	11.3	10.7
Eu	3.00	2.82	2.97	3.06	3.01	2.98	2.87	2.95	2.94	3.01	2.96	3.04	2.84	3.08	3.06	3.02	3.30	3.11	3.03
Gd	9.72	9.91	9.55	9.83	9.58	9.51	9.05	9.25	9.67	10.3	9.80	10.3	9.48	10.0	9.69	9.69	10.4	9.64	9.46
Tb	1.36	1.31	1.26	1.28	1.26	1.27	1.13	1.22	1.29	1.33	1.33	1.39	1.32	1.41	1.35	1.41	1.43	1.34	1.31
Dy	8.07	7.36	7.47	7.50	7.80	7.51	6.90	7.02	7.90	8.13	7.83	8.02	7.28	7.65	7.47	7.79	7.91	7.64	7.38
Ho	1.45	1.26	1.29	1.26	1.30	1.35	1.16	1.15	1.37	1.35	1.29	1.39	1.31	1.40	1.33	1.44	1.42	1.35	1.28

Er	3.61	3.36	3.45	3.41	3.42	3.38	3.12	3.08	3.51	3.59	3.51	3.61	3.36	3.61	3.49	3.70	3.55	3.47	3.44
Tm	0.47	0.46	0.44	0.45	0.46	0.46	0.41	0.44	0.50	0.49	0.50	0.51	0.45	0.47	0.46	0.48	0.47	0.47	0.45
Yb	2.93	2.73	2.73	2.70	2.77	2.69	2.48	2.53	2.93	2.75	2.86	2.98	2.74	2.91	2.80	2.97	2.84	2.81	2.73
Lu	0.38	0.36	0.36	0.37	0.37	0.35	0.35	0.36	0.40	0.40	0.39	0.41	0.39	0.40	0.40	0.42	0.40	0.39	0.38
V	355	346	369	366	351	342	307	298	403	388	379	389	382	348	382	329	388	389	375
Cr	345	437	406	76.1	81.6	73.0	346	332	123	111	459	543	197	302	222	271	337	184	166
Co	48.4	45.6	47.5	45.8	46.1	45.3	49.9	50.6	43.3	46.7	49.9	57.8	48.1	41.4	48.7	40.1	46.6	44.9	43.6
Ni	226	265	257	139	158	131	247	246	302	257	255	293	136	172	132	163	195	120	107
Cu	254	284	284	249	304	266	259	267	364	541	193	412	257	241	234	64.4	247	332	326
Zn	128	124	141	133	134	131	116	118	150	123	140	146	136	120	145	120	142	136	132
Ga	25.8	23.1	26.2	25.8	25.2	25.7	25.4	25.5	24.5	25.7	25.4	26.5	27.9	25.5	27.3	23.5	26.0	26.6	25.7
Rb	3.82	13.3	43.4	38.5	52.1	45.7	53.5	53.1	22.6	65.1	70.6	68.9	58.5	38.8	46.9	70.3	23.1	59.7	58.6
Sr	882	870	830	580	1027	639	661	672	457	484	742	785	451	511	448	569	586	546	539
Y	38.3	36.9	36.5	36.0	36.2	35.4	32.7	33.6	37.1	37.0	36.7	37.7	34.4	36.9	35.4	37.6	37.2	36.1	35.0
Zr	365	350	350	348	360	349	327	324	366	352	356	377	304	349	352	353	370	341	335
Nb	40.8	40.4	42.0	42.2	41.8	43.3	42.0	40.2	43.0	39.4	41.8	44.3	33.3	39.0	39.9	38.7	41.9	37.1	36.3
Ba	239	424	1306	405	1621	524	472	498	239	741	1065	1003	627	479	578	697	407	510	490
Hf	9.47	8.78	8.81	8.56	8.79	8.66	7.74	7.91	8.65	8.50	8.55	9.19	7.74	8.96	8.96	9.22	9.51	8.76	8.67
Ta	2.38	2.38	2.54	2.52	2.55	2.58	2.48	2.52	2.56	2.34	2.57	2.83	2.20	2.57	2.62	2.57	2.69	2.46	2.38
Pb	8.48	8.92	7.42	7.74	12.4	8.94	6.61	5.97	5.63	7.64	6.95	8.15	6.54	11.9	7.80	7.64	6.64	8.62	8.95
Th	7.12	6.90	6.84	6.77	7.03	6.97	6.70	6.63	6.58	6.61	6.57	6.81	7.21	8.12	6.49	8.35	6.97	6.47	6.25
U	1.60	1.58	1.69	1.60	1.74	1.69	1.52	1.58	1.55	1.48	1.49	1.68	1.52	1.82	1.50	1.76	1.65	1.47	1.46

LOI: weight loss on ignition to 1000 ℃. Mg# = $Mg^{2+}/(Mg^{2+}+Fe^{2+})$ in atomic ratio, assuming 15% of total iron oxide is ferric.

Table 3 Sr-Nd-Pb isotope ratios for the analysed volcanic rocks in the Sichuan Basin

Sample	ST1-5	YT1-1	YT1-3	YT1-6	YT1-7	ZG2-5	ZG2-7	ZG2-8	20LMD05	20LC06	20XL01
Locality	ST1 Well	YT1 Well				ZG2 Well			Longmendong	Longchi	Xinlin
Rb($\times10^{-6}$)	13.3	43.4	38.5	53.5	53.1	65.1	70.6	68.9	38.8	70.3	23.1
Sr($\times10^{-6}$)	870	830	580	661	672	484	742	785	511	569	586
$^{87}Rb/^{86}Sr$	0.044372	0.151194	0.192215	0.234105	0.228342	0.389072	0.275352	0.254148	0.219834	0.357378	0.113896
$^{87}Sr/^{86}Sr$	0.706884	0.707491	0.707355	0.706681	0.706694	0.706661	0.707085	0.707075	0.706865	0.707546	0.705942
$^{2}\sigma$	0.000008	0.000007	0.00001	0.000008	0.000008	0.000008	0.000006	0.000007	0.000007	0.00001	0.000009
$^{87}Sr/^{86}Sr(t)$	0.706721	0.706935	0.706648	0.705820	0.705854	0.705230	0.706072	0.706140	0.706057	0.706232	0.705523
Sm($\times10^{-6}$)	11.0	11.0	10.6	9.41	9.91	11.6	10.6	11.4	11.5	11.6	12.0
Nd($\times10^{-6}$)	51.9	52.1	52.0	49.5	50.4	56.0	52.8	54.0	54.3	53.7	56.8
$^{147}Sm/^{144}Nd$	0.128166	0.127908	0.123307	0.114987	0.118988	0.125756	0.121209	0.128019	0.128721	0.130854	0.127975
$^{143}Nd/^{144}Nd$	0.512530	0.512533	0.512526	0.512528	0.512528	0.512567	0.512570	0.512573	0.512507	0.512507	0.512561
$^{2}\sigma$	0.000005	0.000008	0.000005	0.000006	0.000005	0.000004	0.000006	0.000013	0.000004	0.000004	0.000008
$^{143}Nd/^{144}Nd(t)$	0.512313	0.512317	0.512317	0.512333	0.512327	0.512354	0.512365	0.512356	0.512289	0.512286	0.512344
$\varepsilon_{Nd}(t)$	0.16	0.22	0.24	0.55	0.42	0.96	1.17	1.00	-0.31	-0.38	0.77
T_{DM}(Ma)	1106	1098	1054	962	1002	1012	958	1028	1154	1184	1049
$f_{Sm/Nd}$	-0.35	-0.35	-0.37	-0.42	-0.40	-0.36	-0.38	-0.35	-0.35	-0.33	-0.35
$^{206}Pb/^{204}Pb$	18.715	18.751	18.728	18.757	18.789	18.800	18.888	18.867	18.789	18.881	18.899
$^{2}\sigma$	0.001	0.001	0.001	0.001	0.001	0.001	0.001	0.001	0.000	0.001	0.000
$^{207}Pb/^{204}Pb$	15.609	15.613	15.612	15.611	15.613	15.617	15.620	15.621	15.626	15.629	15.614
$^{2}\sigma$	0.001	0.001	0.001	0.001	0.001	0.001	0.001	0.001	0.000	0.001	0.000
$^{208}Pb/^{204}Pb$	39.236	39.292	39.271	39.310	39.357	39.276	39.356	39.316	39.432	39.628	39.349
$^{2}\sigma$	0.002	0.002	0.002	0.002	0.002	0.002	0.001	0.002	0.001	0.002	0.001
$^{206}Pb/^{204}Pb(t)$	18.251	18.154	18.185	18.156	18.097	18.293	18.323	18.325	18.388	18.272	18.245

$^{207}Pb/^{204}Pb(t)$	15.585	15.582	15.584	15.580	15.578	15.592	15.591	15.593	15.606	15.598	15.581
$^{208}Pb/^{204}Pb(t)$	38.572	38.500	38.520	38.440	38.403	38.533	38.542	38.597	38.845	38.685	38.446

Notes:

1. $^{87}Rb/^{86}Sr$ and $^{147}Sm/^{144}Nd$ ratios are calculated using Rb, Sr, Sm and Nd contents by ICP-MS and measured $^{87}Sr/^{86}Sr$ and $^{143}Nd/^{144}Nd$ ratios by MC-ICP-MS.

2. In T_{DM} calculation, ratios of $(^{143}Nd/^{144}Nd)_{DM}$ and $(^{147}Sm/^{144}Nd)_{DM}$ took values of 0.51315 and 0.225, respectively.

3. In $\varepsilon_{Nd}(t)$ calculations, ratios of $(^{87}Sr/^{86}Sr)_{CHUR}$, $(^{87}Rb/^{86}Sr)_{CHUR}$, $(^{143}Nd/^{144}Nd)_{CHUR}$ and $(^{147}Sm/^{144}Nd)_{CHUR}$ are 0.7045, 0.0847, 0.512638 and 0.1967, respectively, while t = 258.5 Ma.

Table 4 Distribution of the Emeishan basalts in the ELIP

Zone	Locality	Rock type	Reference
Inner zone	Dali	High-Ti basalts, low Ti basalts	Hanski et al. (2010)
	Lijiang	High-Ti basalts, low Ti basalts	Song et al. (2001), Zhang et al. (2006)
	Binchuan	High-Ti basalts, low Ti basalts	Song et al. (2001), Xiao et al. (2004), Xu et al. (2007), Xu et al. (2001)
	Ertan	High-Ti basalts, low Ti basalts	Song et al. (2001), Xu et al. (2001)
	Jianchuan	High-Ti basalts, low Ti basalts	Song et al. (2001)
	Pingchuan	Low Ti basalts	Xu et al. (2014)
	Miyi	High-Ti basalts	Xu et al. (2014)
	Kangsi	High-Ti basalts	He et al. (2010)
	Wanmachang	High-Ti basalts	He et al. (2010)
	Shuidiqiao	High-Ti basalts	He et al. (2010)
	Longzhoushan	High-Ti basalts	Xu et al. (2007)
	Yongsheng	High-Ti basalts, low Ti basalts	Hao et al. (2004)
Intermediate zone	Dongchuan	High-Ti basalts	Song et al. (2008), Xu et al. (2001)
	Qingyin	High-Ti basalts	Xu et al. (2014)
	Qiaojia	High-Ti basalts	Xu et al. (2014)
	Weining	High-Ti basalts	Xu et al. (2014)
	Duge	High-Ti basalts	Xu et al. (2014)
	Zhaotong	High-Ti basalts	Li et al. (2017c)
Outer zone	Zhijin	High-Ti basalts	Lai et al. (2012), Xu et al. (2007)
	Jinding	High-Ti basalts	Xu et al. (2007)
	Tubagou	High-Ti basalts	Li et al. (2016b)
	Baise	High-Ti basalts	Fan et al. (2008)
	Bama	High-Ti basalts	Fan et al. (2008), Lai et al. (2012), Liu et al. (2017)
	Tianyang	High-Ti basalts	Fan et al. (2008), Liu et al. (2017)
	Sichuan Basin	High-Ti basalts	This study

International standard samples values of major and trace elements and Sr-Nd-Pb isotopes are listed in it.

No conflict of interest exits in the submission of this manuscript, and manuscript is approved by all authors for publication

I would like to declare on behalf of my co-authors that the work described was original research that has not been published previously, and not under consideration for publication elsewhere, in whole or in part.